

Development of Laser Doping Process at Room Temperature for High Efficiency Crystalline Silicon Solar Cell Fabrication

(高効率結晶シリコン太陽電池作製に向けた室温レーザードーピングプロセスの開発)

Hideki Nishimura

西村 英紀

March 2015

Graduate School of Materials Science

Nara Institute of Science and Technology

Acknowledgements

This work has been done at the Microelectronic Device Science Laboratory, Graduate School of Materials Science, Nara Institute of Science and Technology (NAIST), under the direction of Professor Takashi Fuyuki. This study was partially supported by New Energy and Industrial Technology Development Organization (NEDO) as part of the Ultimate Crystalline Silicon Solar Cells R&D Program.

The author would like to express his deepest appreciation and gratitude to Professor Takashi Fuyuki for his kind advices, continuous supporting, valuable suggestions and encouragements to this study as well as critical reading of this thesis. He is also grateful to his supervisors at NAIST; Professor Jun Ohta, Professor Tsuyoshi Kawai, and Professor Hitoshi Kawaguchi, for their valuable discussions and critical comments for this thesis.

The author sincerely acknowledges to Dr. M. Saif Islam at Integrated Nanodevices and Nanosystems Research (iNano), University of California, Davis for his international supervision, the collaboration work and giving the chance of oversea study to the author at iNano. The author also acknowledges to Dr. Matthew Monari Ombaba, Dr. Dewyani Janardan Patil, Dr. Mark Triplett, Dr. Jin Yong Oh, Mr. Kazim Gurkan Polat, Mr. Ahmed Mayet, and all members in iNano, for the acceptance and guidance for author's stay with useful discussions.

The author is grateful to Associate Professor Yasuaki Ishikawa at NAIST, Professor Seigo Ito at University of Hyogo, and Dr. Shuhei Yoshiba at Japan Science and Technology Agency and Technology, for their fruitful advices and discussions.

The author wishes to thank to Dr. Yoshinori Ikeda and Ms. Yuka Tomizawa at TEIJIN

Corporation, for the collaboration work, supplying samples and useful discussions. The author would like to thank to Mr. Katsuya Tanitsu, Dr. Yu Takahashi at Tokyo Ohka Kogyo Corporation for supplying samples and useful discussions.

The author is indebted to the staffs and researchers in Microelectronic Device Science Laboratory; Dr. Tomoaki Hatayama (now at Sumitomo Electric Industries, Ltd), Dr. Hiroshi Yano, Ms. Ayumi Tani, Ms. Masami Tsuji, and Ms. Kaori Araki, for their experimental and clerical helps, useful advices and heartfelt encouragements.

The author sincerely acknowledges to those who belonged or belongs to PV group in the Microelectronic Device Science Laboratory; Dr. Kenji Hirata (now at SHARP Corporation), Dr. Emi Sugimura (now at Mitsubishi Electric Corporation), Dr. Takashi Suezaki (now at Kaneka Corporation), Mr. Tomohiro Funatani (now at Panasonic Corporation), Mr. Mitsuhiro Hasegawa (now at DENSO), Mr. Tamaki Takayama (now at Fujikura Ltd.), Mr. Shinichiro Tsujii (now at Panasonic Corporation), Mr. Takuya Katagiri (now at SHARP Corporation), Mr. Sohichiro Takamoto (now at Mitsubishi Electric Corporation), Mr. Shota Morisaki (now at Mitsubishi Electric Corporation), Mr. Shigeaki Tanaka (now at TDK Corporation), Mr. Shingo Yumoto (now at Toyota Motor Corporation), Mr. Takanori Okamura (now at Sony Corporation), Mr. Yuki Yamamoto (now at Mitsubishi Electric Corporation), Mr. Keigo Fukunaga (now at Mitsubishi Electric Corporation), Mr. Shigekazu Shimazaki, Mr Ippei Kita, Mr Tsuyoshi Tomimoto, Mr Mitsuaki Manabe, Mr Kazuma Ikeda, Mr Hideki Sakagawa, Mr Shota Tsuduki for their valuable discussions, continuous encouragements, kind helps and excellent time of working together. The author also wishes to thank to Mr. Timothee Moliere, the internship from Universite de Poitiers (now at Université de Paris-Sud) for having useful discussions and good days.

The author would like to thank to Dr. Dai Okamoto (now at AIST), Dr. Hidenori

Koketsu (now at Mitsubishi Electric Corporation), Dr. Yoshihiro Ueoka (now at IDEMITSU KOSAN Co., Ltd.), Mr. Shinya Kotake (now at Nitto Denko Corporation), Mr. Kento Amishima (now at NTT FACILITIES, inc.), Mr. Kenta Shingu (now at Fuji Xerox Co., Ltd.), Mr. Tsuyoshi Araoka (now at Fuji Electric Co., Ltd.), Mr. Ryuji Morishita (now at Mitsubishi Motors Corporation), Mr. Toshimitsu Takaue (now at DENSO) and all other members in Microelectronic Device Science Laboratory for sharing good time of research work.

Finally, the author really thanks his parents and his sisters for their understanding, continuous support and heartfelt encouragement.

March, 2015

Hideki Nishimura

Abstract

This thesis aims to apply laser doping (LD) to textured surfaces at room temperature to fabricate high-efficiency solar cells. To achieve this purpose, the influence of surface formation on the quality of LD-generated emitters was evaluated first. Furthermore, textured surfaces were double-doped to improve emitter quality. Next, the substrate wettability was modified from hydrophobic to hydrophilic using chemical processes to reinforce the interface between phosphor-silicate glass (PSG) and substrate. Finally, the LD process was applied to new precursor layers, including a silicon nanoparticle and a polyboron film (PBF). A high-efficiency solar cell structure acting as a selective emitter was generated by LD-enabled local doping of PBF.

In Chapter 2, the influence of surface formation on emitter property after LD was investigated, and the ability of double-scan LD to increase doping homogeneity using textured samples was evaluated. First, surface improvements were attempted by additional pre-LD etching. Surface voids observed after LD were considered to originate from the existence of a void at the PSG–silicon interface. Because of additional etching, improved surfaces after LD exhibited enhanced photovoltaic characteristics, such as open-circuit voltage (V_{oc}), short-circuit current density (J_{sc}), and fill factor (FF). Second, LD was applied to textured substrates and surface formation improvements were attempted by a double laser scan. Irregular rough surfaces were formed after a single LD scan while surface formation was improved by a double scan. Double-scan LD reduced electric defects and achieved deep doping depths and high surface dopant concentrations. Consequently, this surface

modification ameliorated the current–voltage (I–V) characteristics.

In Chapter 3, Si substrates were chemically transformed into hydrophilic surfaces to reinforce PSG–substrate interfacial adhesion. The difference in chemical states of crystalline silicon surfaces between hydrophobic and hydrophilic provided control over the interface nanostructure. The LD process reduced surface holes and considerably increased doping depth in hydrophilic samples. Moreover, hydrophilic surfaces showed enhanced diode characteristics, especially emitter leak current. These samples exhibited higher V_{oc} and J_{sc} values than their hydrophobic counterparts. These results suggested that the interface nanostructure considerably influenced the electric properties of laser-doped regions.

In Chapter 4, silicon nanoparticle and PBF precursor layers were subjected for the first time to the LD process. PBF was used for formation of locally laser-doped region as a selective emitter for high-efficiency solar cells. Silicon nanoparticles directly absorbed the laser energy and enhanced the reproducibility of the experiment. High photovoltaic characteristics were observed in samples formed using a high energy laser. On the other hand, the organic polymer-based doping precursor PBF improved interface adhesion, enabling a homogeneous introduction of impurities. Textured surfaces mostly remained intact even after LD. Photovoltaic characteristics were improved by combining selective emitter formation using PBF and optimum laser energy. Additional doping by metal contact reduced the reverse saturation current. Consequently, the selective emitter formed by LD showed increased V_{oc} and FF values, boosting solar cell efficiency.

Contents

Acknowledgments

Abstract

Contents

Chapter 1	Introduction	1
1.1	Background	1
1.2	Laser Doping Process	4
1.2.1	Laser Processing for Crystalline Silicon Solar Cell Fabrication	4
1.2.2	Laser Doping Process	7
1.3	Purpose and Outline of this Thesis	10
	References of Chapter 1.	15
Chapter 2	Emitter Quality Improvement after Laser Doping by Surface Structure Control	18
2.1	Introduction	18
2.2	Experimental Procedure	20
2.2.1	Laser Doping Set Up	20
2.2.2	Laser Doping Procedure	22
2.3	Influence of Surface Roughness on Laser Doping	26
2.3.1	Surface Structure Evaluation after Laser Doping	26

Contents

2.3.2	Surface Structure Improvement after Laser Doping	31
2.3.3	Emitter Property Improvement by Surface Structure Control	37
2.3.4	Laser Doping Melt–Recrystallization Mechanism	41
2.4	Reduction of Surface Electric Defects by Double-Scan Laser Doping	44
2.4.1	Double-Scan Laser Doping Procedure	44
2.4.2	Surface Structure and Electric Properties after Double-Scan Laser Doping	46
2.5	Summary	53
	References of Chapter 2.	55
8	Chapter 3 Interface Control by Chemical Surface Modification	57
3.1	Introduction	57
3.2	Experimental Procedure	58
3.2.1	Laser Doping Set Up	58
3.2.2	Sample Preparation	58
3.3	Emitter Quality Improvement by Chemical Modification	64
3.3.1	Surface Structure Improvement after Laser Doping	64
3.3.2	Emitter Property Improvement by Control of Interface Chemical State	70
3.4	Summary	80
	References of Chapter 3.	81

Chapter 4 Local Impurity Doping and High-Efficiency Structures using Novel	82
Precursor Layers	
4.1 Introduction	82
4.2 Experimental Procedures	83
4.2.1 Laser Doping Procedure using Silicon Nanoparticles	84
4.2.2 Selective Emitter Fabrication using Polyboron Films	86
4.3 Laser Doping using Silicon Nanoparticles	88
4.4 Selective Emitter Formation by Laser Doping using Textured	96
Substrates	106
4.5 Summary	108
References of Chapter 4.	
Chapter 5 Summary and Outlook	112
5.1 Summary	112
5.2 Outlook	116
Appendix A	117
List of publications	122
About Author	137

List of abbreviations and symbols

Experimental techniques

ARC	Anti-Reflection Coating
BSF	Back Surface Field
LD	Laser Doping
TD	Thermal Diffusion
SPM	Sulfuric Acid / Hydrogen Peroxide Mixture clean in RCA cleaning
APM	Ammonium / Hydrogen Peroxide Mixture clean in RCA cleaning
HPM	Hydrochloric Acid / Hydrogen Peroxide Mixture clean in RCA cleaning
PV	Photovoltaics (Solar generation system)
SE	Selective Emitter (structure)
IBC	Interdigitated Back-Contact (solar cell)
PERL	Passivated Emitter with Rear Locally Diffused (solar cell)
LSI	Large-Scale Integration
CW	Continuous Wave
TEM	Transverse Electromagnetic
CMP	Chemical Mechanical Planarization
DPSS	Diode pumped solid-state (laser)
SoD	Spin-on-Dopant

Materials

(c-)Si	(Monocrystalline) silicon
mc-Si	Multicrystalline silicon
a-Si(:H)	(Hydrogenated) amorphous silicon
SiO ₂	Silicon (di) oxide
SiN(:H)	(Hydrogenated) silicon nitride
Cz	Czochralski
SOG-Si	Solar grade silicon
TEOS	Tetra eth-oxy silane
BSG	Boro-silicate glass
PSG	Phosphor-silicate glass
PBF	Poly boron film
Ag	Silver
Al	Aluminum
B	Boron
P	Phosphorus
CO ₂	Carbon dioxide
SO _x	Sulfur oxide
NO _x	Nitrogen oxide
CIS	Copper indium selenide
CdTe	Cadmium telluride
Nd ³⁺ :YVO ₄	Neodymium-doped yttrium orthovanadate
HF	Hydrofluoric acid
H ₂ SO ₄	Sulfuric acid

HCl	Hydrochloric acid
NH ₃	Ammonia
H ₂ O ₂	Hydrogen peroxide
CH ₃ CO ₂ C ₂ H ₅	Ethyl acetate
HNO ₃	Nitric acid
CH ₃ COOH	Acetic acid
BRL	Boron rich layer

Measurements

SEM	Scanning Electron Microscopy
SIMS	Secondary Ion Mass Spectroscopy
Ra	Arithmetic average of absolute values
EBIC	Electron Beam Induced Current
UV	Ultra-violet (in wavelength)
QSSPC	Quasi steady states photo conductance decay

Symbols

AM	Air Mass
<i>Eff</i>	Conversion efficiency
<i>F.F.</i>	Fill factor
<i>I</i>	Current
<i>I_{sc}</i>	Short circuit current

I_m	Current at maximum power point
J	Current density
J_0	Saturation current density
J_{sc}	Short circuit current density
J_m	Current density at maximum power point
P_{light}	Power of incident light
P_{max}	Maximum output power
R_s	Series Resistance
R_p	Parallel Resistance
V	Applied voltage
V_{oc}	Open circuit voltage
V_m	Voltage at maximum power point
η	Conversion efficiency
Ω	Ohm
pFF	Pseud fill factor
FF_0	Ideal fill factor

Chapter 1

Introduction

1.1 Background

Chronic and unavoidable issues related to energy supply have been continually plaguing society worldwide. Since the industrial revolution, our civilization has been sustained by fossil fuels and nuclear energy. Transportation, electricity, and industries rely on energy sources, such as oil, coal, or nuclear resources, which exist in limited quantities. These resources are extracted from earth but this extraction has become increasingly difficult with the decreasing amount of fossil fuel beneath the Earth's surface. For example, reserve–production ratio of oil amounts to approximately 53 years,¹⁾ suggesting that the exhaustion of all fossil fuels will occur in the near future. Furthermore, the consumption of these resources poses additional environmental issues. Burning materials, such as oil and coal, generates several pollution gasses, such as CO₂, SO_x, and NO_x, which cause acid rain, abnormal climate trends, and ecosystem destruction related to global warming. On the other hand, nuclear energy produces radioactive waste, which require over 10,000 years to lose their radioactivity.²⁾ Moreover, nuclear plants are vulnerable to disasters, as exemplified by the

Fukushima Daiichi nuclear plant accident. Therefore, alternative energy supply systems are highly desirable.

Almost all current technology depends on computing and electrification. Most importantly, future energy systems rely on the development of electricity sources. Electricity has typically been generated by thermal power plants. New electrical generation systems are expected to combine various complementary energy sources. A promising source, solar energy is unlimited from the perspective of energy consumption. The energy of solar radiation reaching the Earth's surface approximates 9×10^{13} kW,³⁾ which is 5000-fold higher than human energy consumption, making it highly attractive. The number of solar energy conversion systems has greatly increased in recent years. Figure 1.1 shows cumulative solar cells installations worldwide.⁴⁾ The global photovoltaic installation reached 136 GW in 2013. However, a 10-fold increase in photovoltaic installation is necessary to cover a large part of the global electricity generation. Such an increase requires low-cost production of solar generation systems. The cost per generated electric power equaled 37 yen/kWh in 2013,⁵⁾ exceeding that of other conventional electricity generation systems. The target cost recommended by the New Energy and Industrial Development Organization in its "PV Roadmap 2030⁺" amounted to 14 and 7 yen/kWh in 2010 and 2030, respectively, for solar cell production. Therefore, further technological developments are necessary to reduce the cost of solar cell systems.

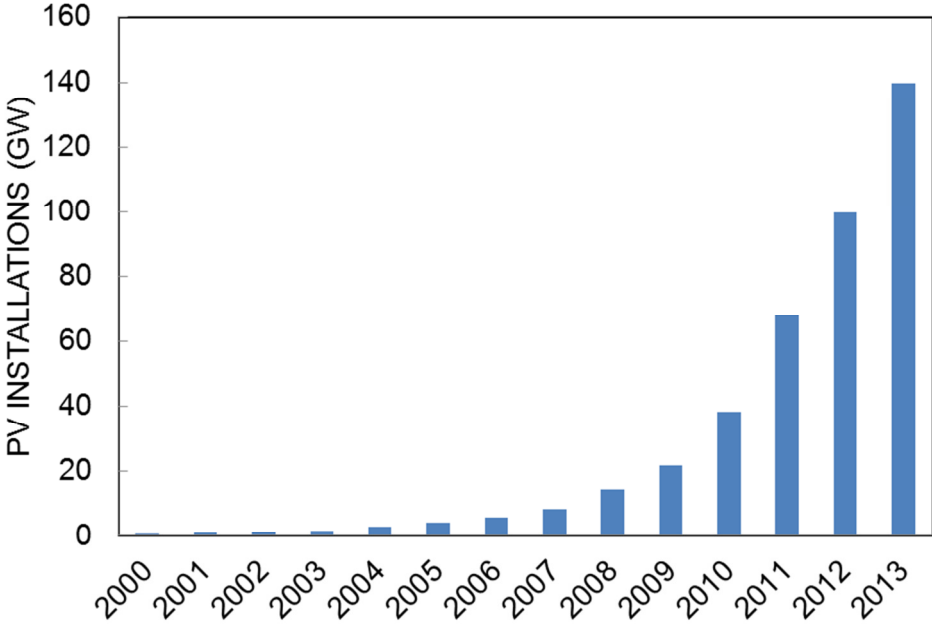


Figure 1.1 The world cumulative photovoltaic (PV) installations after 2000

1.2 Laser Doping Process

1.2.1 Laser Processing for Fabrication of Crystalline Silicon Solar cell

Solar cell development currently relies on various components, such as composite,⁶⁾ organic,⁷⁾ and organic–inorganic hybrid materials,⁸⁾ which are expected to be useful for numerous solar cell applications. However, crystalline silicon (c-Si) solar cells prevail at the production stage. As shown in Figure 1.2, Si-based solar cells exceed 90% of the overall solar cell production.⁹⁾ This predominance of silicon results from several facts. First, the second most abundant element in the Earth’s crust after oxygen¹⁰⁾ is silicon, which is also the most prevalent material in solar cell substrates. It is easily dug as a silica stone but requires high electric power to convert to its pure crystalline form. However, various studies and efforts have gradually lowered energy costs.¹¹⁾ Second, c-Si device fabrication processes have been developed for many years. The first wafer-based c-Si solar cell was produced in 1954.¹²⁾ Since the invention of Si devices, c-Si wafers have been implemented in all electronic components, making Si transistor fabrication processes very easy to transpose to their c-Si solar cell fabrication equivalents. The application of conventional c-Si device fabrication processes to solar cell production has boosted the number of installed photovoltaic systems, as mentioned

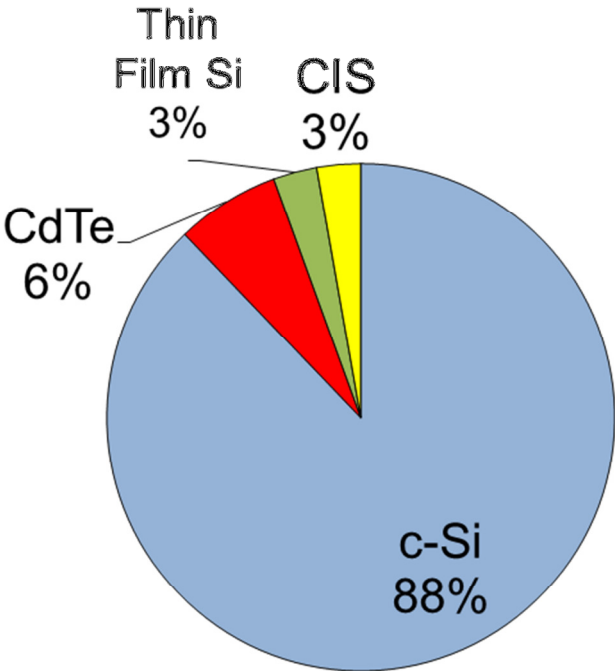


Figure 1.2 Solar cells produced in 2013 according to the type of materials⁹⁾

above. However, this rapid growth of the solar cell industry results from political pressure and a certain global movement, making it easy to influence. The cost per watt of the output power is an important criterion for achieving a sustainable prevalence of solar generation system. This cost per watt has recently dramatically decreased but remains higher than that of thermal power plants. Cost reduction is necessary for further progress.

The fabrication cost of photovoltaic modules encompasses cell material expenses, module material expenses, and process cost. Photovoltaic production costs approximately 176 yen/W overall.¹³⁾ Cell material expenses are reduced by the growth of new silicon materials, such as high-quality multicrystalline¹⁴⁾ and monocrystalline-like silicon.¹⁵⁾ Module material expenses are decreased by mass production or business efforts while process cost is lowered by technical development. In particular, cell efficiency enhancements dramatically reduce actual costs from the perspective of cost per watt. However, manufacturing complex structures requires several additional methods, such as high temperature, vacuum, and wet chemical processes,¹⁶⁾ which generate higher costs than conventional cell processes and consequently cannot lower cell process costs. Hence, laser processing has attracted significant attention because it exhibits a highly controllable process area at high speed using simple equipment. Laser grooved buried contact, the first laser processing approach for crystalline silicon solar cell fabrication, was proposed by M. A. Green et al. in 1984.¹⁷⁾ It reduced series resistances of solar cells by formation of three-dimensional structure of front metallization with grooving of substrate by laser. Lasers operate under ambient atmosphere and at room

Chapter 1. Introduction

temperature without any vacuum or thermal equipment. They are found in many solar cell fabrication processes without requiring additional equipment and chemical steps. Many processes, such as laser edge isolation,¹⁸⁾ laser-based foil-metallization,¹⁹⁾ laser texturing,²⁰⁾ and laser contact opening,²¹⁾ have been developed recently (Fig. 1.3). Furthermore, these processes are applicable to thinner substrates, which are required to reduce solar cell thickness, and thus wafer material expenses amount to approximately 30% of the total module production cost. However, thinner substrates decrease yields because of thermally and chemically induced transformation and breakage. Therefore, laser processing can facilitate the production of thinner solar cells because it avoids thermal and chemical processes. Another important laser processing application, laser doping (LD), the main topic of this thesis, generates impurity-doped regions on c-Si surfaces. The resulting impurity doping profiles determine the electric property of solar cells and provide high-efficiency cell structures.

1.2.2 Laser Doping Process

LD was developed by J. M. Fairfield and G. H. Schwuttke in 1968.²²⁾ Because it works under ambient atmosphere at room temperature, LD facilitates low cost and high-throughput processing during c-Si solar cell fabrication, offering an attractive alternative to conventional methods.²³⁾ In this approach, only the irradiated area is heated and impurities diffuse in the substrate without thermal damage. Laser irradiation is controlled at the micron

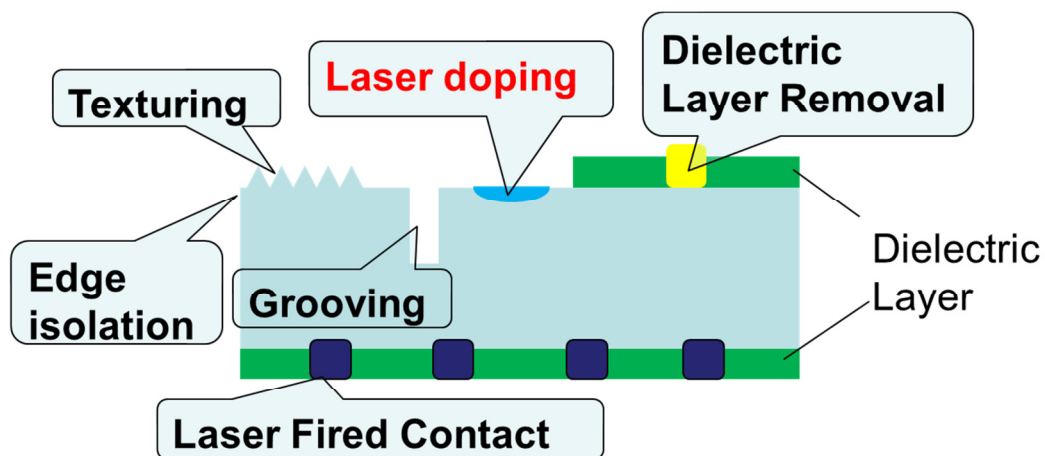


Figure 1.3 Laser processing during c-Si solar cell fabrication

Chapter 1. Introduction

scale and high speed using a transfer sample stage or an optical system. Doping depth profiles are tuned by changing the laser output power.²⁴⁾ Impurities diffuse in the liquid phase during melting–recrystallization, causing doping layers to form very quickly. Monocrystalline silicon solar cells fabricated by LD have shown efficiencies reaching 18.9%.²⁵⁾ Moreover, LD easily produces two-dimensional structures necessary for high-efficiency c-Si solar cells, such as selective emitters (SEs)²⁶⁾ and interdigitated back-contact²⁷⁾ solar cells. The fabrication of these structures by conventional furnace processing requires costly and time-consuming photolithography. In contrast, LD readily forms a selective doping area, giving high-efficiency solar cells at low cost and high throughput without needing photolithography. To manufacture these structures, LD is performed on textured surfaces. It has previously been applied to textured surfaces using a gas source or vacuum process to improve reproducibility.²⁸⁾ However, the spin-on dopant (SoD) layer, which acts as a cost-reducing doping precursor in industrial processes, may cause aggravated interface adherence between precursor and textured surface. Therefore, doping mechanisms involving LD-processed textured surfaces and SoD as a doping precursor remain unclear.

1.3 Purpose and Outline of this Thesis

Crystalline silicon solar cells require cost-effective manufacturing approaches and high conversion efficiency. LD exhibits many advantages applicable to high-efficiency solar cell structures such as passivated emitter with rear locally diffused (PERL) cells. Its implementation in the fabrication of these devices hinges on the evaluation of its adaptability to textured structures. A textured surface structure is formed on the c-Si substrate to increase incident light absorption. This surface structure (1) reduces the surface reflection of incident light, (2) expands the light path length in the c-Si substrate, and (3) reduces transmission loss (Fig. 1.4).²⁹⁾

This thesis aims to develop a LD process for textured Si substrates. Experiments focus on applying LD to textured surfaces and understanding the related melt-recrystallization mechanism. Passivation, anti-reflection coating (ARC) using SiO_x or SiN_x , and any other process designed to improve cell efficiency are not conducted in this study. Nonetheless, this study will enable to improve efficiency in solar cells fabricated through these processes. Doping precursor layers are deposited by spin coating, a single-step low-cost technique that provides uniform films at room temperature.

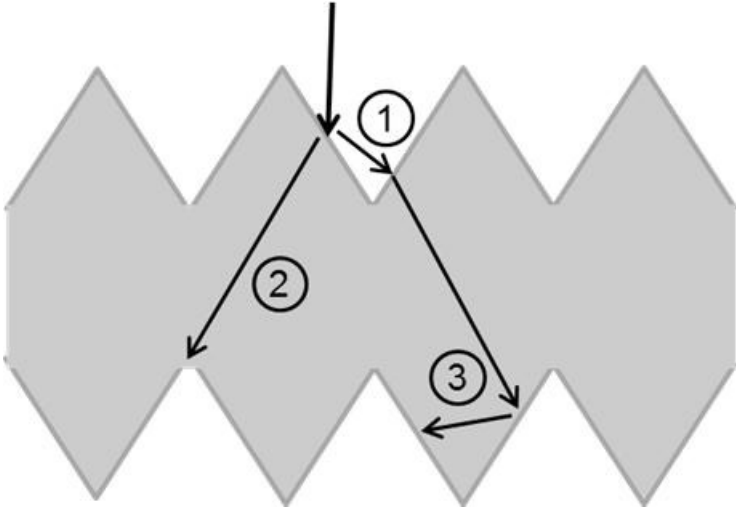


Figure 1.4 Schematic model of optical management on a textured surface. ① Reduction of surface reflection of incident light, ② expansion of light path length in c-Si substrate, and ③ reduction of transmission loss

Specifically, dopant materials dispersed in organic solvents are spread on surfaces by spinning before solvent evaporation, and a precursor layer is formed by low temperature heating or prebake (<200 °C). Spin coating is necessary for future industrial applications of LD. However, its combination with LD for the production of solar cells with textured surfaces raises several issues, making the influence of this combination on the electric characteristics of impurity-doped areas of textured surfaces worth investigating. This thesis assesses and attempts to resolve these problems.

Chapter 1 describes research background, purpose, and contents.

Chapter 2 investigates the influence of surface unevenness on emitter properties after LD, and shows that double-scan LD improves the doping homogeneity of textured samples. The LD process is considered to follow the melt–recrystallization mechanism. When phosphorus silicate glass (PSG) acts as a doping precursor, the incident laser light (wavelength: 532 or 355 nm) penetrates the precursor before being absorbed by the Si substrate. The absorbed laser energy is converted into heat, melting the substrate and creating thermal conduction from the molten silicon to PSG. This causes impurities to spread into the substrate via liquid phase diffusion.³⁰⁾ This mechanism suggests that the PSG–substrate interface plays an important role in the LD process. Voids may appear on substrates exhibiting surface roughness. Therefore, PSG is deposited on surfaces presenting different configurations, and the influence of the PSG–substrate interface on the LD process is evaluated. In addition, interface adhesion is improved by double-scan LD. The first scan

Chapter 1. Introduction

enhances interface adhesion by melting the substrate and PSG, which may contribute to homogeneous dopant introduction during the second laser scan. Surface appearance after LD and electric properties are evaluated along with phosphorus doping profiles and current–voltage (I–V) characteristics. The melt–recrystallization process associated with laser irradiation-induced impurity doping is discussed.

In Chapter 3, the hydrophobic Si substrate is chemically modified into a hydrophilic surface. The PSG–substrate interface significantly influences LD processes, making it important to control. The wettability of textured surfaces is changed from hydrophobic to hydrophilic to reinforce the interface adhesion between PSG and substrate. The influence of interface adhesion on the LD process is evaluated. Surface formation after LD, doping profiles, and photovoltaic characteristics are analyzed.

Chapter 4 deals the application of silicon nanoparticles and a poly boron film (PBF) as precursor layers in the LD process. A selective emitter is produced by local LD involving PBF. The strengthening of the PSG–substrate interface adhesion improves the electric characteristics of LD-generated impurity-doped areas (Chapter 3). Therefore, stronger interfaces may provide better control over crystal defects and inhomogeneous introduction of dopant impurities during LD. Interface conditions that are more suitable for LD are achieved using new precursor layers and LD mechanisms are discussed. Silicon nanoparticles absorb laser energy and are sintered to the substrate after melt–recrystallization. Therefore, Si nanoparticles may cancel the influence of interface adhesion and enhance repeatability. On the

other hand, an organic polymer-based doping precursor, such as PBF, improves interface adhesion. Strong interface adhesion may promote the homogeneous introduction of impurities and result in high-quality doped areas. In addition to interface adhesion, surface formation after LD, doping profiles, and photovoltaic characteristics are evaluated.

Chapter 5 summarizes the main findings of this research and discusses future outlook.

References of Chapter 1

- 1) BP: “BP Statistical Review of World Energy June 2014” (2014), p. 6.
- 2) Nuclear Regulation Authority: About ensuring safety about plutonium,

<http://www.nsr.go.jp/archive/nsc/hakusyo/hakusyo13/111.htm> (in Japanese).
- 3) K. Yamada and H. Komiyama: Photovoltaic Engineering (2009), p. 8.
- 4) International Energy Agency Photovoltaic Power Systems Programs (IEA-PVPS):

“TRENDS 2014 IN PHOTOVOLTAIC APPLICATIONS” (2014).
- 5) New Energy and Industrial Development Organization (NEDO): “NEDO PV Challenges”

(2014), <http://www.nedo.go.jp/content/100573590.pdf> (in Japanese).
- 6) P. Lam, J. Wu, M. Tang, Q. Jiang, S. Hatch, R. Beanland, J. Wilson, R. Allison, and H. Liu:

Sol. Energy Mater. Sol. Cells **126** (2014), p. 83.
- 7) H. W. Chen, Y. D. Chiang, C. W. Kung, N. Sakai, M. Ikegami, Y. Yamauchi, K. C. W. Wu,

T. Miyasaka, and K. C. Ho: Journal of Power Sources **245** (2014), p. 411.
- 8) M. A. Green: Proc. of 29th European Photovoltaic Solar Energy Conf. (2014), p. 1489.
- 9) RTS Corporation: “Information of Solar Power Generation April to June 2013” (2013),

p. 17. (in Japanese).
- 10) JOGMEC: “Flow of Mineral Resources Material, Silicon” (2013), p. 322 (in Japanese).
- 11) M. Konagai and Y. Ueda: Solar Cell Technology Handbook (Ohmsha, Tokyo, 2013) 1st

ed., p. 38 (in Japanese).

- 12) D. M. Chapin, S. Fuller, and G. L. Pearson: *J. Appl. Phys.* **25** (1954), p. 676.
- 13) JST: “PV Power Systems: Quantitative Technology Scenarios, and Science and Technology Roadmap based on Elemental Technology Structure” (2014), p. 4. (in Japanese).
- 14) S. Joonwichien, I. Takahashi, S. Matsushima, and N. Usami: *Proc. of 28th European Photovoltaic Solar Energy Conf.* (2013), p. 911.
- 15) A. Jouini, D. Ponthenier, H. Lignier, N. Enjalbert, B. Marie, B. Drevet, E. Pihan, C. Cayron, T. Lafford, and D. Camel: *Prog. Photovolt: Res. Appl.* **20** (2012), p. 735.
- 16) N. Stem and M. Cid: *Solid-State Electronics* **48** (2004), p. 197.
- 17) M. A. Green, A. W. Blakers, S. R. Wenham, S. Narayanan, M. R. Willson, M. Taouk, and T. Szpitalak: *Proc. 18th IEEE PVSC* (1985), p. 61.
- 18) C. Chan, M. Abbott, B. Hallam, M. Juhl, D. Lin, Z. Li, Y. Li, J. Rodriguez, and S. Wenham: *Sol. Energy Mater. Sol. Cells* **132** (2015), p. 535.
- 19) M. Graf, J. Nekarda, D. Eberlein, N. Wöhrle, R. Preu, R. Böhme, and T. Grosse: *Proc. of 29th European Photovoltaic Solar Energy Conf.* (2014), p. 532.
- 20) K. R. Kim, T. H. Kim, H. A. Park, S. Y. Kim, S. H. Cho, J. Yi, and B. D. Choi: *Applied Surface Science* **264** (2013), p. 404.
- 21) Z. Du, N. Palin, J. Chena, M. Hong, and B. Hoex: *Energy Procedia* **25** (2012), p. 19.
- 22) J. Fairfield and G. H. Schwuttke: *Solid State Electronics* **11** (1968), p. 1175.
- 23) T. Akane, T. Nii, and S. Matumoto, *Jpn. J. Appl. Phys.* **31** (1992), p. 4437.

Chapter 1. Introduction

- 24) K. Hirata, A. Ogane, T. Saitoh, A. Kitiyanan, E. Sugimura, and T. Fuyuki, Proc. 24th European Photovoltaic Solar Energy Conf. (2009), p. 1708.
- 25) S. J. Eisele, T. C. Roder, J. R. Kohler, and J. H. Werner: Appl. Phys. Lett. **95** (2009), p. 133501.
- 26) U. Jäger, M. Okanovic, M. Hörtheis, A. Grohe, and R. Preu: Proc. 24th European Photovoltaic Solar Energy Conf., 2009, p. 1740.
- 27) M. Dahlinger, B. B. Bachi, T. C. Roder, J. R. Kohler, R. Z. Gottwick, and J. H. Werner: Energy Procedia **38** (2013), p. 250.
- 28) G. Polain, D. Blanc, A. Focsa, J. Giber, E. Fourmond, B. B. Bachi, B. Semmache, Y. Pellegrin, and M. Lemiti: Energy Procedia **27** (2012), p. 455.
- 29) A. Luque, and S. Hegedus: Handbook of Photovoltaic Science and Engineering (Wiley, Chichester, 2011) 21nd ed., p. 277.
- 30) G. Poulain, D. Blanc, B. Semmache, Y. Pellegrini, M. Letimi: Energy Procedia **8** (2011), p. 587.

Chapter 2

Emitter Quality Improvement after Laser Doping by Surface Structure Control

2.1 Introduction

Previous studies on LD have addressed smooth surfaces¹⁾ but solar cell efficiency enhancement requires textured surfaces. In these previous experiments, LD use on samples showing as-cut surfaces altered surface structures, generating many voids on these surfaces. In addition, the resulting samples exhibited significantly lower solar cell efficiency than those with smooth surfaces.²⁾ An as-cut surface displays unevenness compared to its smooth counterpart polished by chemical mechanical planarization (CMP, Fig. 2.1), affecting the LD process because of the generation of voids at the interface between doping precursor and substrate. As-cut wafers are usually utilized for solar cell fabrication to reduce production costs, while CMP-treated wafers are typically used for large-scale integration. A previous application of LD to multi crystalline silicon (mc-Si) solar cells resulted in photovoltaic characteristics. However, LD-processed mc-Si substrates showed lower electric performance than LD-processed monocrystalline silicon because they presented as-cut surfaces.

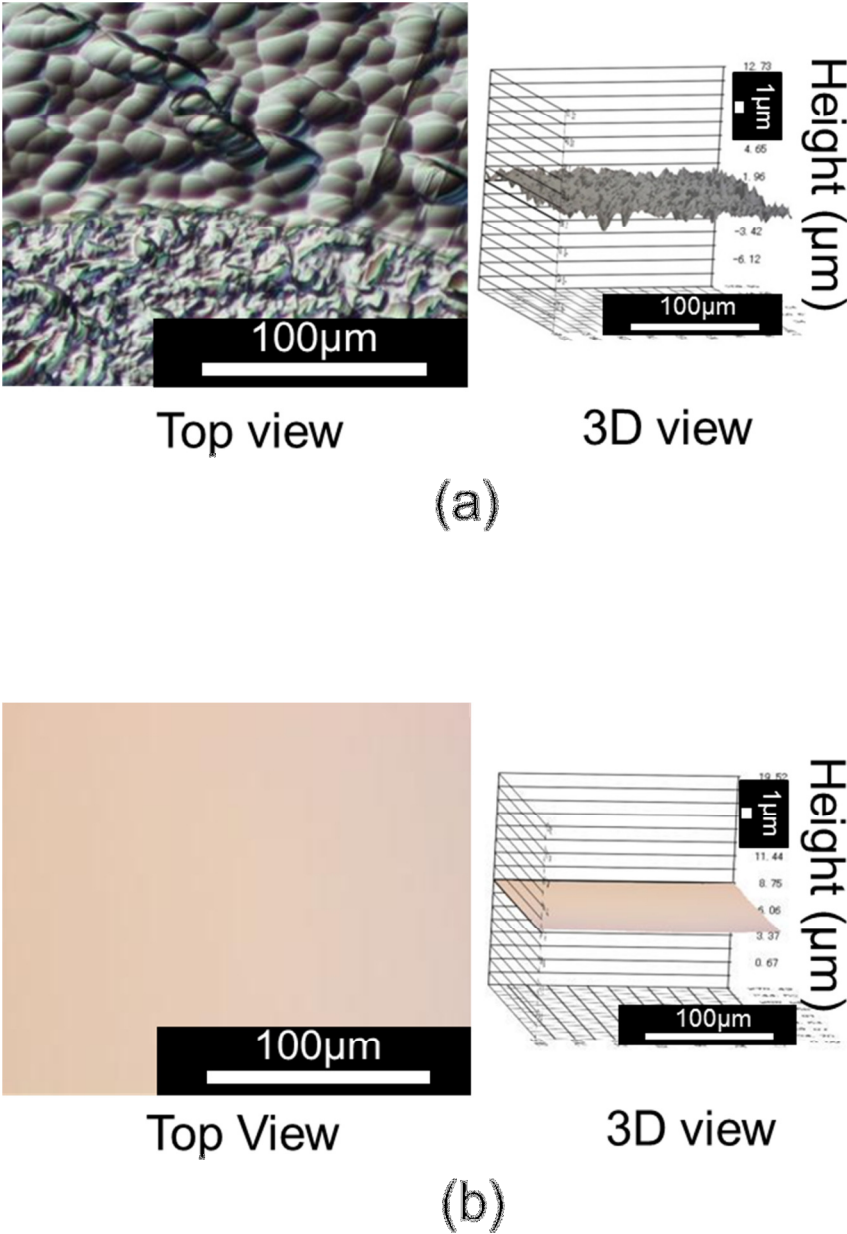


Figure 2.1 Surface morphology of Si wafers. (a) As-cut surface and (b) CMP-treated smooth surface

In this chapter, the influence of surface structure on LD-generated emitter quality was evaluated. Double-scan LD was applied to textured surfaces to improve emitter quality. LD was performed using a 532 nm continuous wave (CW) laser on mc-Si substrates to produce emitters. mc-Si surface structures were modified by chemical etching, and their relationship with the electric properties of the LD-processed surfaces was analyzed. Moreover, LD-treated textured surface structures were evaluated. The minority carrier inhomogeneity was improved by double-scan LD using the 532 nm CW laser. Surface topography, doping profiles, and electric characteristics were assessed.

2.2 Experimental Procedure

2.2.1 Laser Doping Set Up

The laser system (Fig. 2.2) consisted of a 532 nm CW Nd³⁺:YVO₄ laser (Coherent, Verdi/V-5), a mechanical shutter operated using a Model F116 controller (SURUGA SEIKI), reflective mirrors, and a collective lens (Nikon, CF plan, 5×/0.35, working distance: 20.5 mm). Samples were scanned on an x–y stage equipped with a controller unit (SHOT T-202, SIGMA KOKI) connected to a personal computer. The laser spot was a circle and displayed a Gaussian distribution (TEM₀₀-mode).³⁾

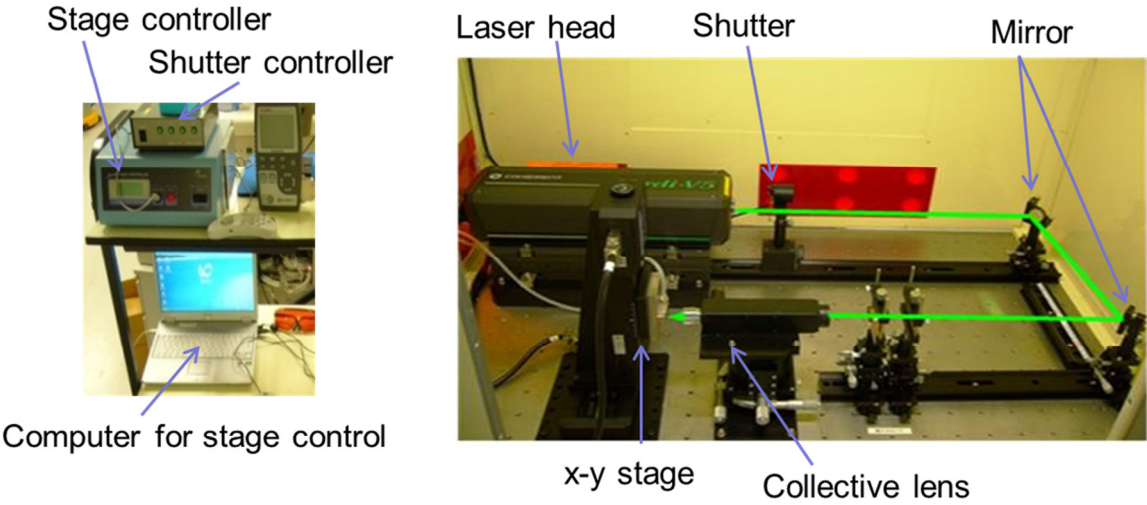


Figure 2.2 Laser system of LD, (left) stage control system and (right) overview of laser system

2.2.2 Laser Doping Procedure

Monocrystalline silicon wafers were used as substrates to investigate the origin of surface structure changes (Section 2.3.1), and mc-Si wafers were utilized to evaluate the effect of chemical modification (Sections 2.3.2–2.3.4). These wafers were cut into 1.1 cm × 1.1 cm squares, subjected to RCA cleaning (Table 2.1), and etched using an acidic solution with HF (55%) and HNO₃ (60%) and CH₃COOH (99%) in a ratio of 2:15:5 to remove cutting-saw damage. Next, the dopant precursor was deposited on substrate surfaces by spin coating (Table 2.2), and samples were subsequently baked on a hotplate at 100 °C for 15 min to give PSG as a solid-phase diffusion layer. The entire PSG-coated sample surface was exposed to CW laser irradiation at room temperature in air to form the emitter (Fig. 2.3). Laser conditions were previously optimized for monocrystalline silicon solar cells.⁴⁾ The output power was maintained at 5 W, and the laser spot diameter was condensed to 12 μm on the sample surface. The doped area was formed by moving the x–y stage during laser irradiation. An xy-translation in the x-direction moved the stage from one sample edge to the other at a scanning speed of 6 cm/s before shifting it by 6 μm in the y-direction. This cycle was repeated and the remaining PSG was removed by HF cleaning. To evaluate the p–n junction properties, metal contacts were deposited by thermal evaporation. Ti/Ag and Al electrodes acted as front side grid and back contacts, respectively. Photovoltaic properties were measured using a solar simulator. Surface structures were examined by scanning

Chapter 2. Emitter Quality Improvement after Laser Doping by Surface Structure Control

electron microscopy (SEM), while surface minority carriers were observed by electron beam induced current (EBIC) analysis.

Table 2.1 RCA cleaning procedure

Process	Chemicals	Conditions
1. SPM1	H ₂ SO ₄ (97%)	80 °C 5min
2. SPM2	H ₂ SO ₄ (97%):H ₂ O ₂ = 1:1	80 °C 10min
3. Rinse	Deionized water	20 °C
4. HF	HF (5%)	25 °C 3min
5. Rinse	Deionized water	20 °C
6. APM	NH ₃ (27%):H ₂ O:H ₂ O ₂ = 1:5:1	80 °C 5min
7. Rinse	Deionized water	20 °C
8. HF	HF (5%)	25 °C 3min
9. Rinse	Deionized water	20 °C
10. HPM	HCl (27%):H ₂ O:H ₂ O ₂ = 1:5:1	80 °C 5min
11. Rinse	Deionized water	20 °C
12. HF	HF (5%)	25 °C 3min
13. Rinse	Deionized water	20 °C
14. Dry		N ₂ gun blow

Table 2.2 Spin-coating conditions and phosphorus silica glass precursor composition

Layer	Chemical	Spin coat
PSG	OCD-T-1(P-59250)	3000 rpm
	CH ₃ CO ₂ C ₂ H ₅ : TOK., LTD	20 s

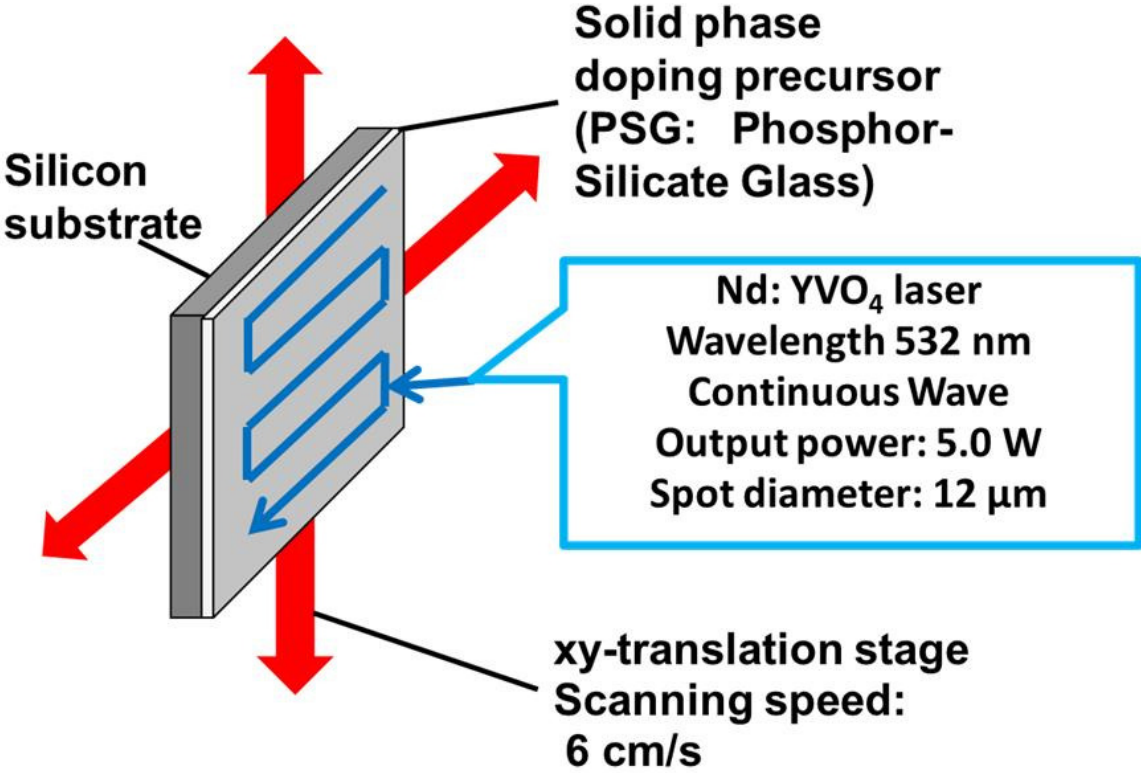


Figure 2.3 Laser conditions and schematic viewing of laser doping

2.3 Influence of Surface Roughness on Laser Doping

The influence of surface structure on emitter properties was investigated. First, LD-processed monocrystalline silicon substrate structures were evaluated by SEM. Next, emitter properties of mc-Si substrates were evaluated by SEM–EBIC and I–V measurements in the dark and under illumination.

2.3.1 Surface Structure Evaluation after Laser Doping

The origin of voids on LD-processed substrate surfaces was investigated using monocrystalline silicon surfaces presenting different coatings. Substrates consisted in 300- μm -thick p-type, Czochralski (Cz), (100)-oriented monocrystalline silicon wafers exhibiting a resistivity of 0.1–2 Ωcm . The PSG layer was formed by spin coating and subsequent prebake using a hotplate. Therefore, interface adhesion between PSG and substrate may be aggravated during PSG formation. During the emitter fabrication by LD, PSG characteristics, such as composition and PSG–substrate interface, may affect structural changes in substrate surfaces. Here, the Cz monocrystalline silicon substrates were polished by CMP on one side. Four samples (**1–4**, Fig. 2.4) were produced through different approaches (Fig. 2.5). In sample **1**, PSG was formed on the smooth surface by prebake only

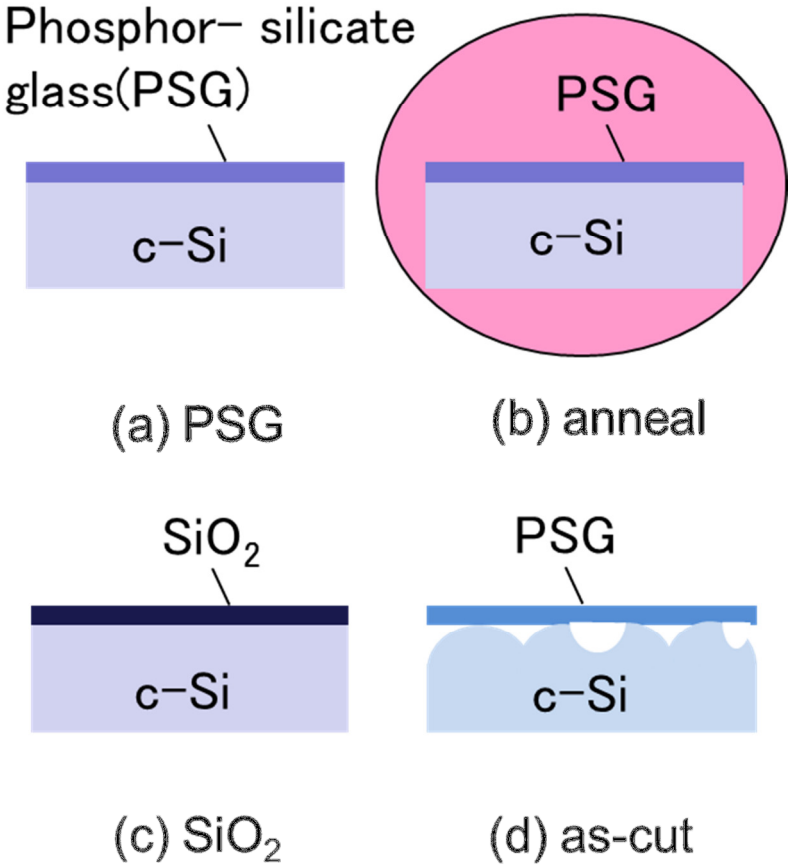


Figure 2.4 Schematic representation of surface structures, (a) spin-coated and prebaked PSG on a smooth surface; (b) spin-coated, prebaked, and annealed PSG; (c) spin-coated and prebaked SiO₂ on a smooth surface; and (d) spin-coated and prebaked PSG on an as-cut surface

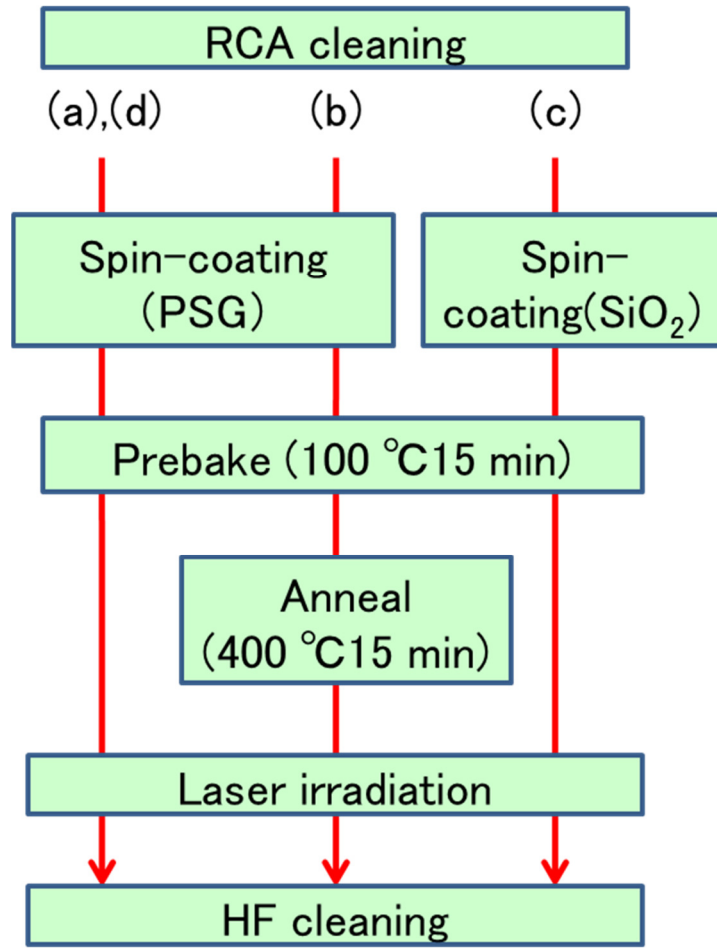


Figure 2.5 Sample preparations for surface structure evaluation

Table 2.3 Spin-coating conditions and SiO₂ precursor composition

Layer	Chemical	Spin coat
SiO ₂	OCD-T-2(Si-59000)	3000 rpm
	CH ₃ CO ₂ C ₂ H ₅ : TOK., LTD	20 sec

Chapter 2. Emitter Quality Improvement after Laser Doping by Surface Structure Control

(Fig. 2.4a). In sample **2**, the formed PSG layer was subjected to additional annealing at 400 °C for 60 min in a furnace after prebake to enhance its rigidity. In sample **3**, PSG was replaced by SiO₂ (Table 2.3). In sample **4**, PSG was generated on the as-cut surface by the same method as for sample **1** to evaluate the influence of surface structure. All samples were exposed to laser irradiation, as described in Section 2.2, and their surfaces were examined by SEM.

Figure 2.6 shows superficial SEM images of laser irradiated monocrystalline silicon substrates **1–4**. These images correspond to top (left) and tilted views (right). When PSG was formed by prebake only, the smooth surface became slightly rougher on laser irradiation (Fig. 2.6a). Surface structures did not change after laser irradiation for samples **2** and **3** (Figs. 2.6b and c). In laser irradiated sample **2**, the annealed PSG layer strongly adhered to the substrate, suggesting that the generation of a rough surface may enhance adhesion at the PSG–substrate interface. Similarly, the laser irradiated sample **3**, in which the dopant only contained SiO₂, exhibited a flat surface (Fig. 2.6c), indicating that the presence of phosphorus affects surface structure. Nonetheless, surface structure changes observed in Fig. 2.6a were little, implying that surface roughness stems from other reason than the presence of phosphorus. When PSG was formed on the as-cut surface, laser irradiation significantly altered the surface structure (Fig. 2.6d). The top and tilted views showed voids and their rims, respectively, demonstrating that as-cut surfaces formed by wafer cutting promoted the appearance of voids during the laser-induced melt–recrystallization process.

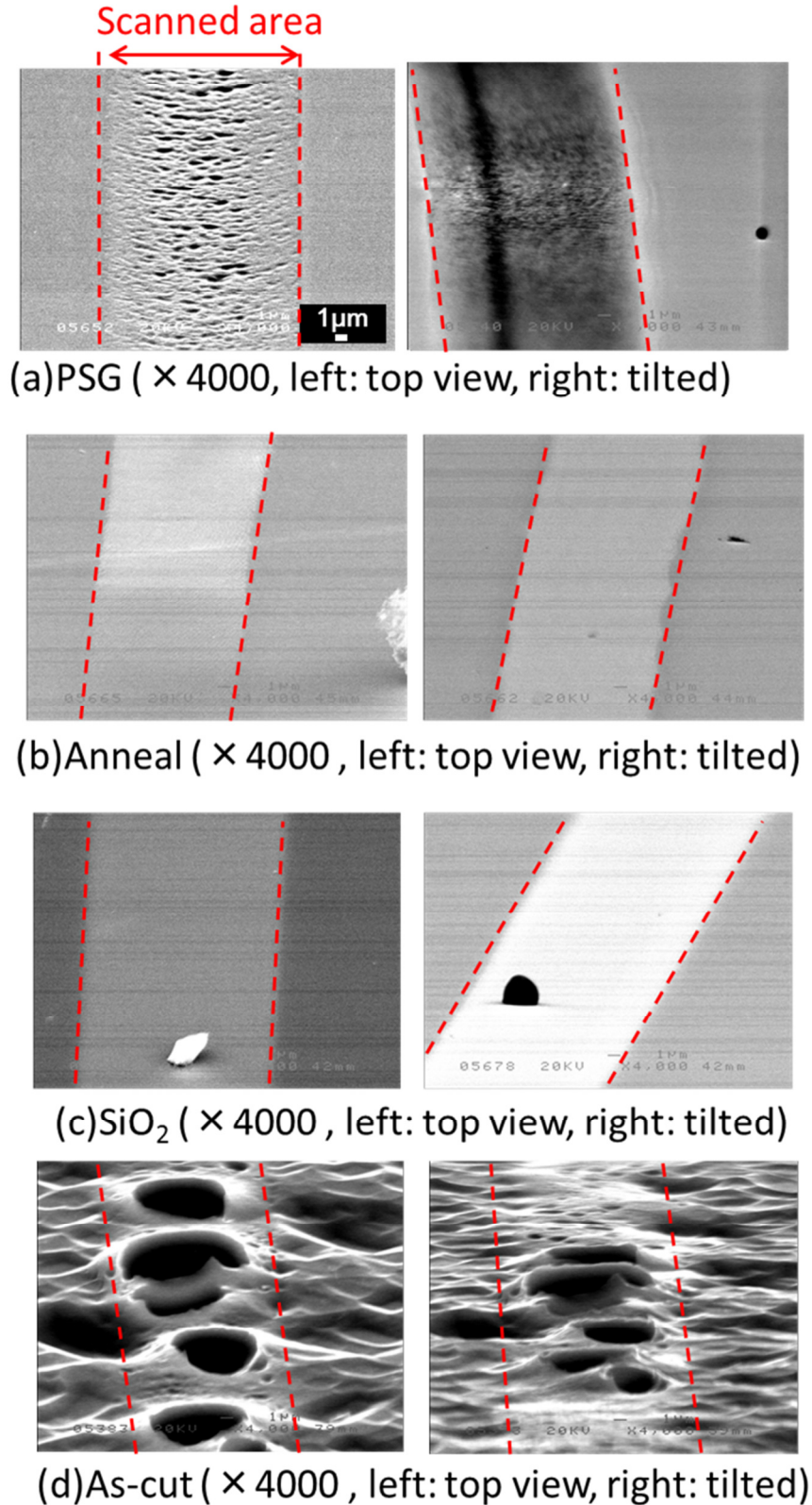


Figure 2.6 Surface morphologies after LD using (a) standard PSG, (b) annealed PSG, (c) SiO₂ formed on a smooth surface, and (d) standard PSG formed on an as-cut surface.

2.3.2 Surface Structure Improvement after Laser Doping

Surface structure improvements were assessed using 300- μm -thick p-type cast-grown mc-Si wafers exhibiting a resistivity of 0.78 Ωcm . Experimental procedures are shown in Fig. 2.7. After RCA cleaning, front and back surfaces of mc-Si substrates were etched by approximately 25 μm using a 2:15:5 HF (55%)/HNO₃ (60%)/CH₃COOH (99%) mixture to remove any cutting-saw damage. This typical damage removal process maintains the surface roughness. Therefore, the resulting surfaces were called “as-cut.” In this experiment, the LD-processed surface was improved by additional chemical etching. In this additional step, front and back surfaces of mc-Si substrates were planarized by approximately 50 μm using a 1:10 HF (55%)/HNO₃ (60%) mixture.⁵⁾ Surface structures and electric properties of as-cut and planarized samples were compared.

Figure 2.8 shows three-dimensional images of (left) as-cut and (right) planarized mc-Si sample surfaces before laser irradiation. As-cut mc-Si substrates exhibited rough surfaces because of saw damage. In contrast, additional etching significantly decreased the surface roughness. The arithmetic average of absolute values (Ra) was calculated to quantitatively describe the surface roughness. As-cut and planarized samples displayed Ra values of 0.40 and 0.11 μm , respectively.

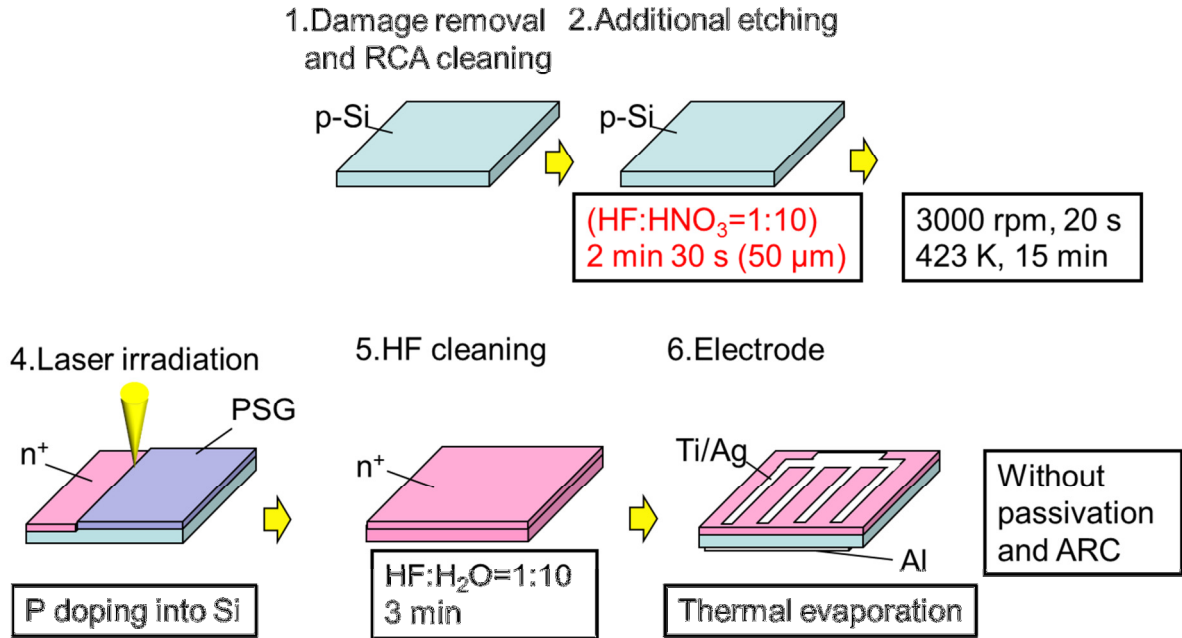


Figure 2.7 Schematic representation of the LD process including additional etching

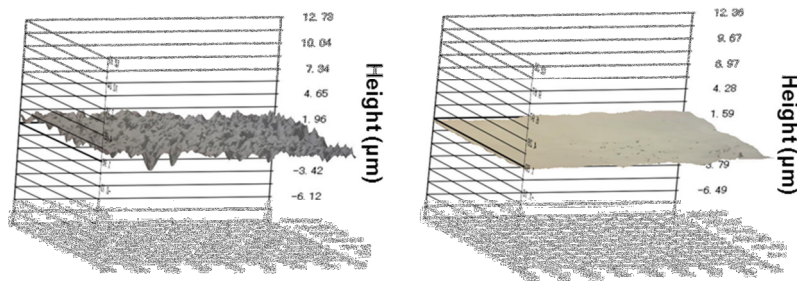
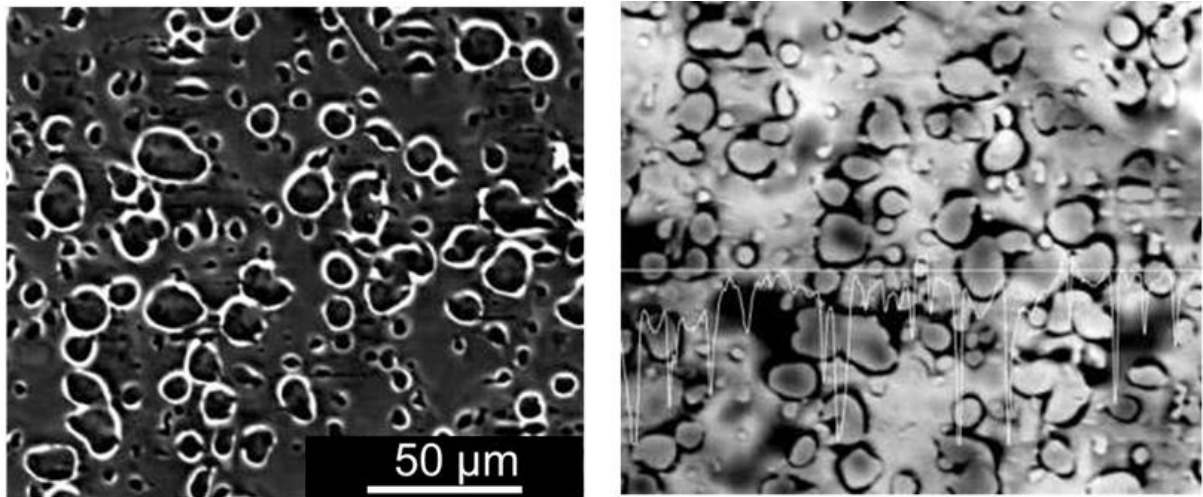


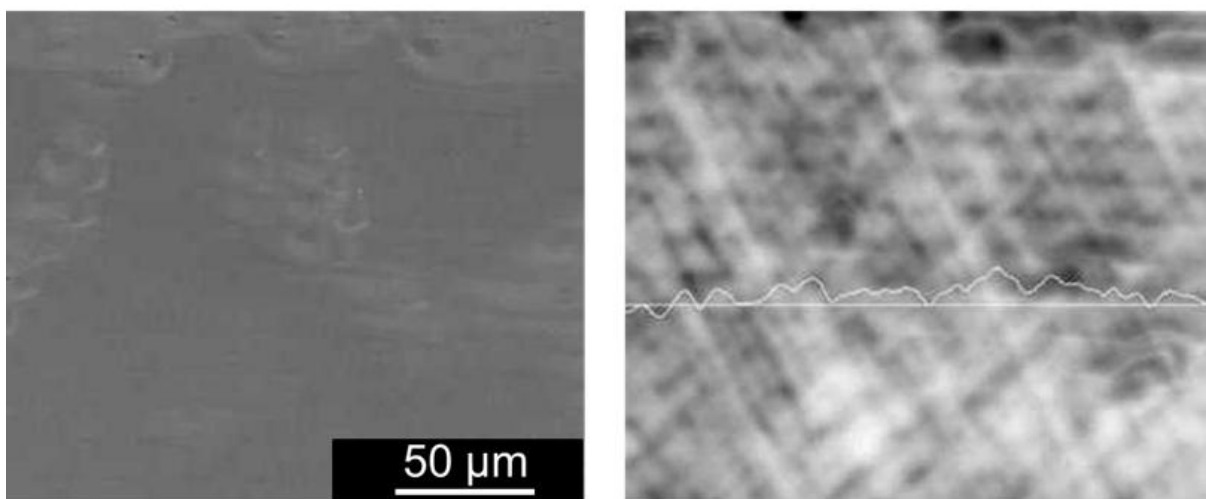
Figure 2.8 Surface morphologies of samples with as-cut and planarized surfaces

Chapter 2. Emitter Quality Improvement after Laser Doping by Surface Structure Control

Different as-cut and planarized surface structures were processed by LD. Figure 2.9 shows (left) SEM and (right) EBIC images of the resulting silicon surfaces. Fig. 2.9a and Fig. 2.9b show the samples after LD with and without additional etching, respectively. As shown, as-cut sample surfaces displayed numerous voids after LD (Fig. 2.9a), which may derive from void formation at the PSG–substrate interface. On the other hand, planarized samples presented smooth surfaces (Fig. 2.9b). The surface electric property of the LD-processed mc-Si substrate was obtained by EBIC analysis. In this technique (Fig. 2.10), charge carriers generated by the microscope electron beam are collected by an electric field within the specimen and detected as a current in an external circuit. When employed as an SEM video signal, this collected current image reveals inhomogeneity in the electrical properties of the specimen.⁶⁾ As-cut sample images showed a black area at the edges of surface voids (Fig.2.9a). These EBIC measurements were conducted using an electron accelerating voltage of 20 kV, and minority carriers were excited to a maximum depth of 4.7 μm .⁷⁾ Phosphorus doping depths ranged from 1.5 to 3 μm , which is lower than the electron penetration depth. Therefore, these measurements analyzed electric property for the entire doped region but did not provide bulk properties. The black area observed in Fig. 2.9a was attributed to electric defects that prevent the collection of minority carriers excited by the electron beam in the doped region, suggesting that surface voids become minority carrier recombination centers. Therefore, this surface structure reduces the open circuit voltage (V_{oc}) and the short circuit current density (J_{sc}). Even worse, it may prevent contact with metal electrodes. This surface structure needs to



(a)As-cut (left: SEM, right: EBIC)



(b)Additional etching (left: SEM, right: EBIC)

Figure 2.9 SEM surface morphologies and EBIC electrical characteristics of (a) as-cut and (b) planarized substrates after LD

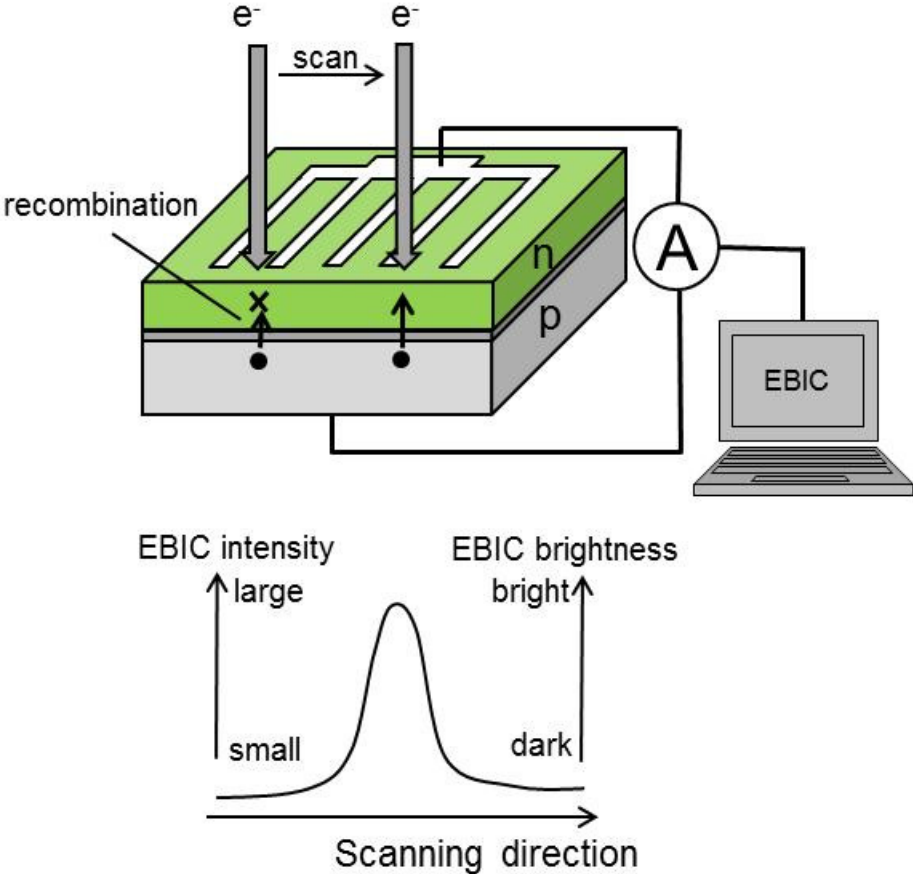


Figure 2.10 Schematic representation of EBIC measurements

be modified to improve photovoltaic characteristics for solar cell fabrication. Planarized samples showed a homogeneous surface electric property (Fig. 2.9b), demonstrating that the decrease in surface voids enhance the electronic properties of laser-doped emitters.

2.3.3 Emitter Property Improvement by Surface Structure Control

Dark I–V characteristics of LD-processed mc-Si solar cells using as-cut surfaces were compared with those using planarized surfaces (Fig. 2.11). Solar cells typically exhibit series and shunt resistances. In dark I–V measurements, high series resistance limits the current increase in the forward bias high-voltage region. A low parallel resistance increases the current in the forward bias low-voltage region and the reverse bias saturation current.⁸⁾ Therefore, higher series resistance and lower parallel resistance aggravate J_{sc} and V_{oc} , respectively. Planarized samples showed lower reverse bias saturation current and low-voltage forward bias current but higher high-voltage forward bias current than as-cut samples with surface. These findings suggest that we achieved improvement of sheet resistance and parallel resistance.

Photovoltaic properties were investigated through illuminated I–V measurements. The solar cell efficiency is defined as the ratio of the photovoltaically generated electric output of the cell to the incident luminous power. It is written as follows:

$$\eta = \frac{I_m V_m}{P_{light}} = \frac{FF I_{sc} V_{oc}}{P_{light}}, \quad (2.1)$$

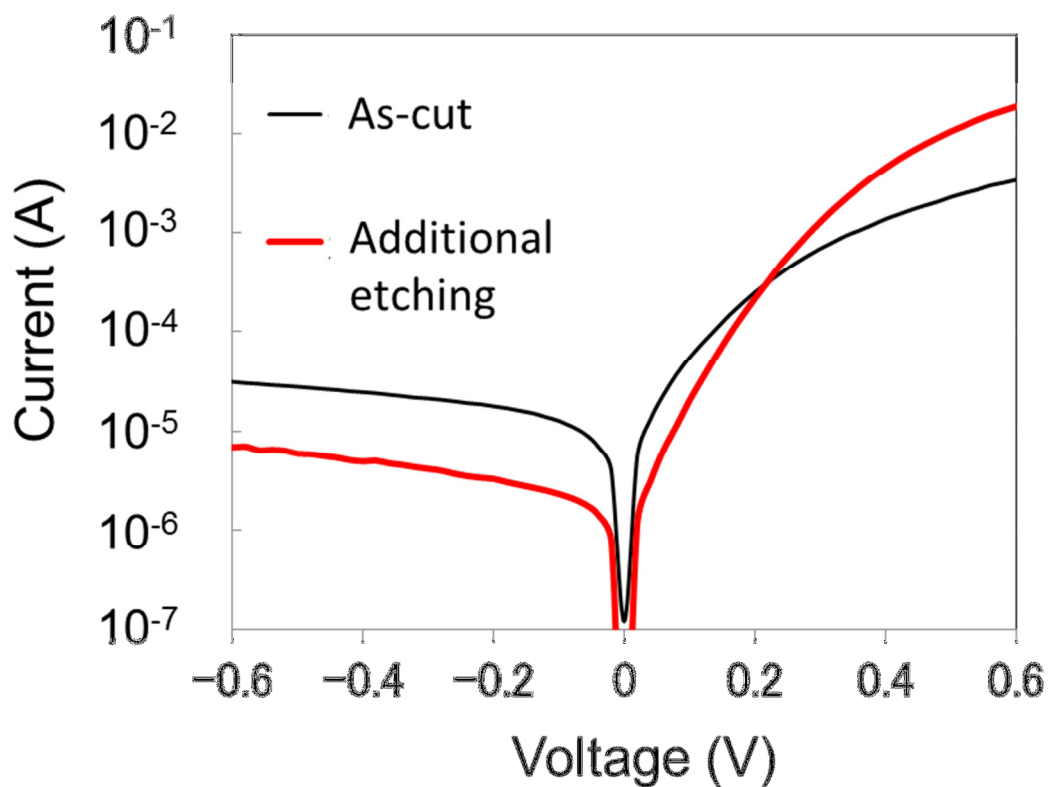


Figure 2.11 Dark I-V characteristics of as-cut and planarized samples

Chapter 2. Emitter Quality Improvement after Laser Doping by Surface Structure Control

where P_{light} is the luminous power and I_m and V_m are the current and voltage at the optimal operating point, respectively. The open circuit voltage V_{oc} is obtained when no current is drawn from the solar cell. The short circuit current I_{sc} is measured if the solar cell is short circuited, i.e., no voltage is detected at the cell. The fill factor (FF) represents the area underneath the I–V characteristic filled by the rectangle $V_m I_m$ relative to the rectangle $V_{oc} I_{sc}$.⁹⁾

Figure 2.12 compares illuminated I–V characteristics of LD-generated mc-Si solar cells displaying as-cut and planarized surfaces. Solar cells involving planarized surfaces presented higher FF, J_{sc} , and V_{oc} values than those with as-cut surfaces, consistent with dark I–V measurements. Photovoltaic characteristics were improved by reducing surface voids, highlighting the importance of surface structure in optimizing these characteristics.

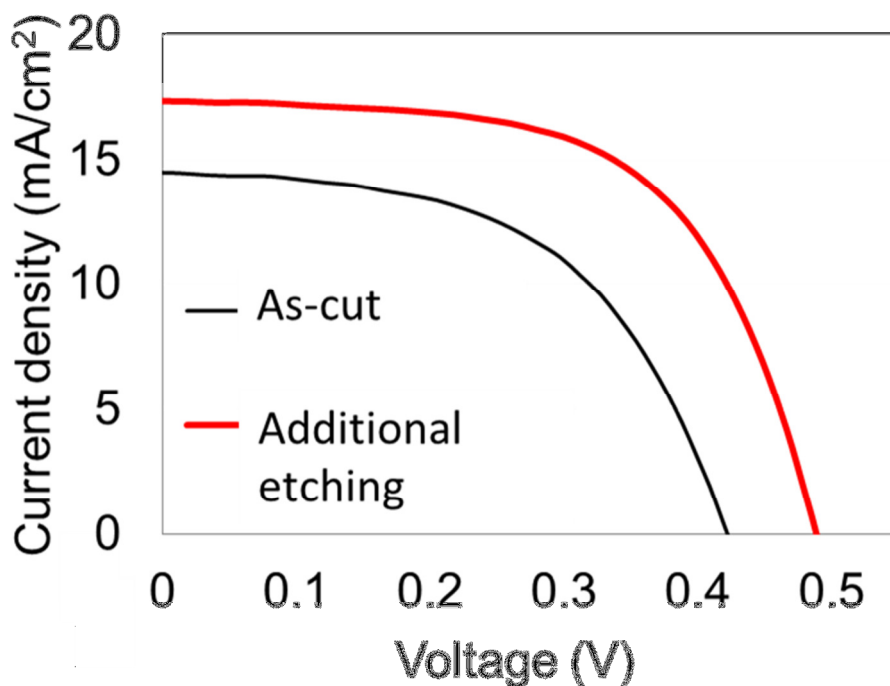


Figure 2.12 Illuminated I–V characteristics of solar cells presenting as-cut and planarized surfaces

Table 2.4. Photovoltaic characteristics obtained from individual I–V curves shown in Figure 2.8

	V_{oc} (mV)	J_{sc} (mA/cm ²)	FF (%)	Eff (%)
As-cut	417	14.5	54.0	3.3
Etching	485	17.3	61.0	5.1

2.3.4 Laser Doping Melt–Recrystallization Mechanism

This section discusses the origin of voids during LD. LD-induced surface structure changes observed for monocrystalline silicon substrates revealed that the presence of phosphorus in PSG and the PSG–substrate interface influence the generation of surface voids by LD. As-cut surface structures dramatically affected these changes and appeared to be the main factor for these surface voids. When LD was applied to smooth substrate surfaces obtained, no surface voids appeared even after melt–recrystallization. The origin of surface voids is discussed below assuming that as-cut surface structure plays a main factor in this phenomenon. Figure 2.13 shows a mechanistic representation for the generation of surface voids. The PSG–substrate interface of as-cut surfaces, in which the dopant precursor contained phosphorus, displayed voids. Air and silica exhibit refractive indices of approximately 1 and 1.46, respectively.¹⁰⁾ The reflectivity locally depends on the presence of voids at the PSG–substrate interface. At the laser wavelength used here (532 nm), it increases with the presence of air at this interface. If it varies locally because of voids, the laser energy transferred to the substrate and the melt depth also change significantly in local areas. In general, molten silicon recrystallizes with epitaxial growth during LD.¹¹⁾ However, locally different laser energy may cause random nucleation. Shallowly melted regions absorb lower laser energy and show higher cooling rate than their deeply melted counterparts. In addition,

nucleation may occur in lower temperature areas in molten silicon.¹²⁾ Therefore, the boundary between deeply and shallowly melted regions may initiate nucleation. Molten silicon recrystallizes along the direction of crystal nuclei. Voids may form according to this mechanism. Random nucleation¹³⁾ and different recrystallization rates¹⁴⁾ in the crystal growth area may generate defects, explaining the appearance of the edges of voids as electric defects by EBIC measurements (Fig. 2.9a).

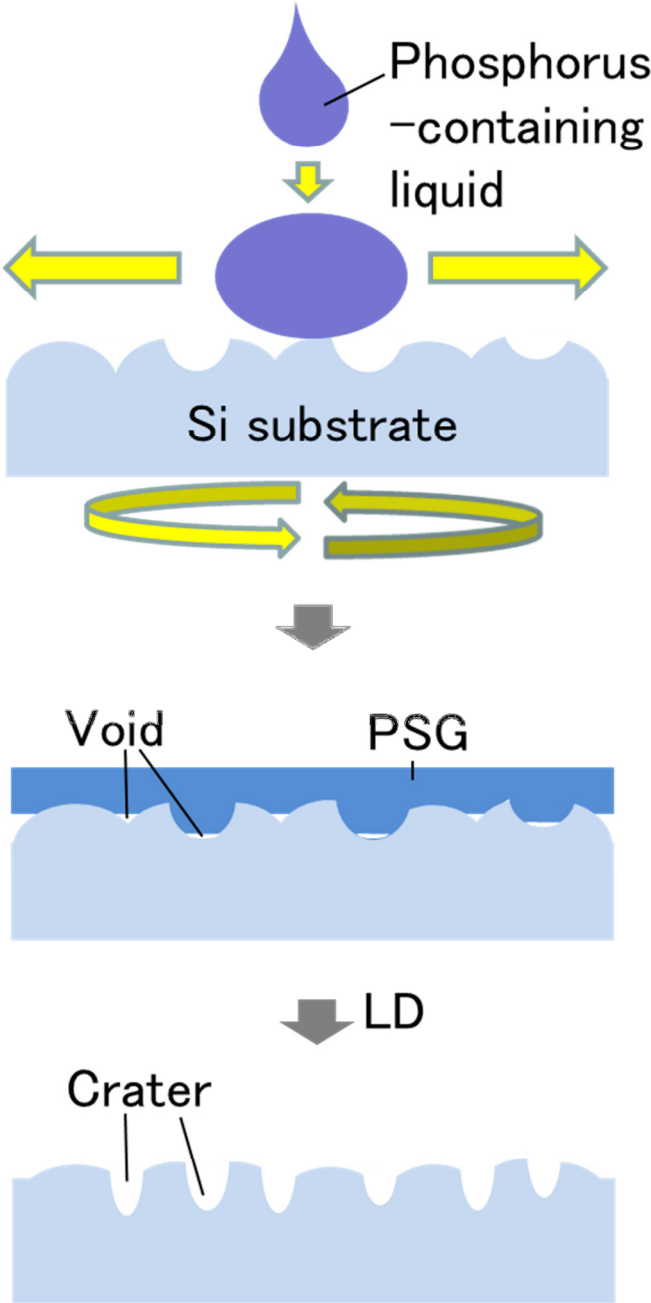


Figure 2.13 Mechanism showing the generation of voids by spin coating

2.4 Reduction of Surface Electric Defects by Double-Scan Laser Doping

2.4.1 Double-Scan Laser Doping Procedure

The double-scan LD procedure was conducted using 180- μm -thick alkali-textured p-type Cz silicon wafers (1.1 cm \times 1.1 cm) presenting a resistivity of 1.5 Ωcm as substrates. After RCA cleaning, the PSG precursor was spin-coated on the substrate and prebaked on a hotplate at 100 $^{\circ}\text{C}$ to obtain the dopant layer. The entire surface of the PSG coated samples was scanned with the 532 nm Nd:YVO₄ CW laser under similar conditions as in Section 2.2.2. Some samples were exposed to laser irradiation again with the remaining PSG to improve the doping homogeneity (Fig. 2.14). Finally, the remaining PSG was removed by HF cleaning, and front (Ti/Ag) and back (Al) side electrodes were deposited on the sample by evaporation. Samples were analyzed by secondary ion mass spectroscopy (SIMS), SEM, EBIC, and illuminated I–V characteristic measurements.

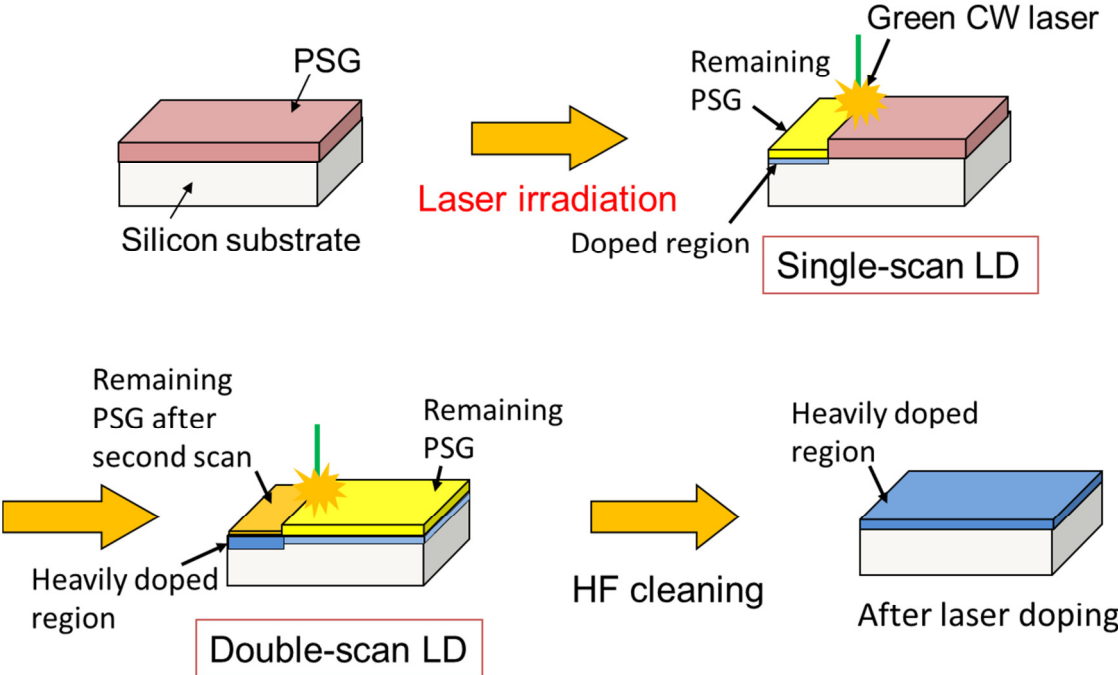


Figure 2.14 Schematic representation of the double-scan LD process

2.4.2 Surface Structure and Electric Properties after Double-Scan Laser Doping

Figure 2.15 shows the alkali-textured surfaces (a) before laser treatment and (b) after single- and (c) double-scan LD. Superficial and cross-sectional images are displayed on the left- and right-hand sides, respectively. The silicon substrate was subjected to a standard texturing process with alkaline solution and presented micron-sized pyramids (Fig. 2.15a). It exhibited irregular rough surface after LD. Many irregular protrusions reaching 10 μm in height appeared in the surface after single-scan LD (Fig. 2.15b). These protrusions resulted from the melt–recrystallization process occurring during this first laser scan. Regions presenting strong PSG–substrate interface adhesion showed deeper melting, while those displaying interfacial voids exhibited shallower melting and formed crystal nuclei. This nucleation mechanism is consistent with the mechanism discussed in Section 2.3.4. The nucleation started at the pyramids and molten silicon in other region aggregated on these crystal nuclei. In solar cell fabrication, these protrusions may prevent metal contact formation and increase series resistance. Figure 2.15c shows that these rough surfaces became smooth after the second laser scan, which caused melt–recrystallization again.

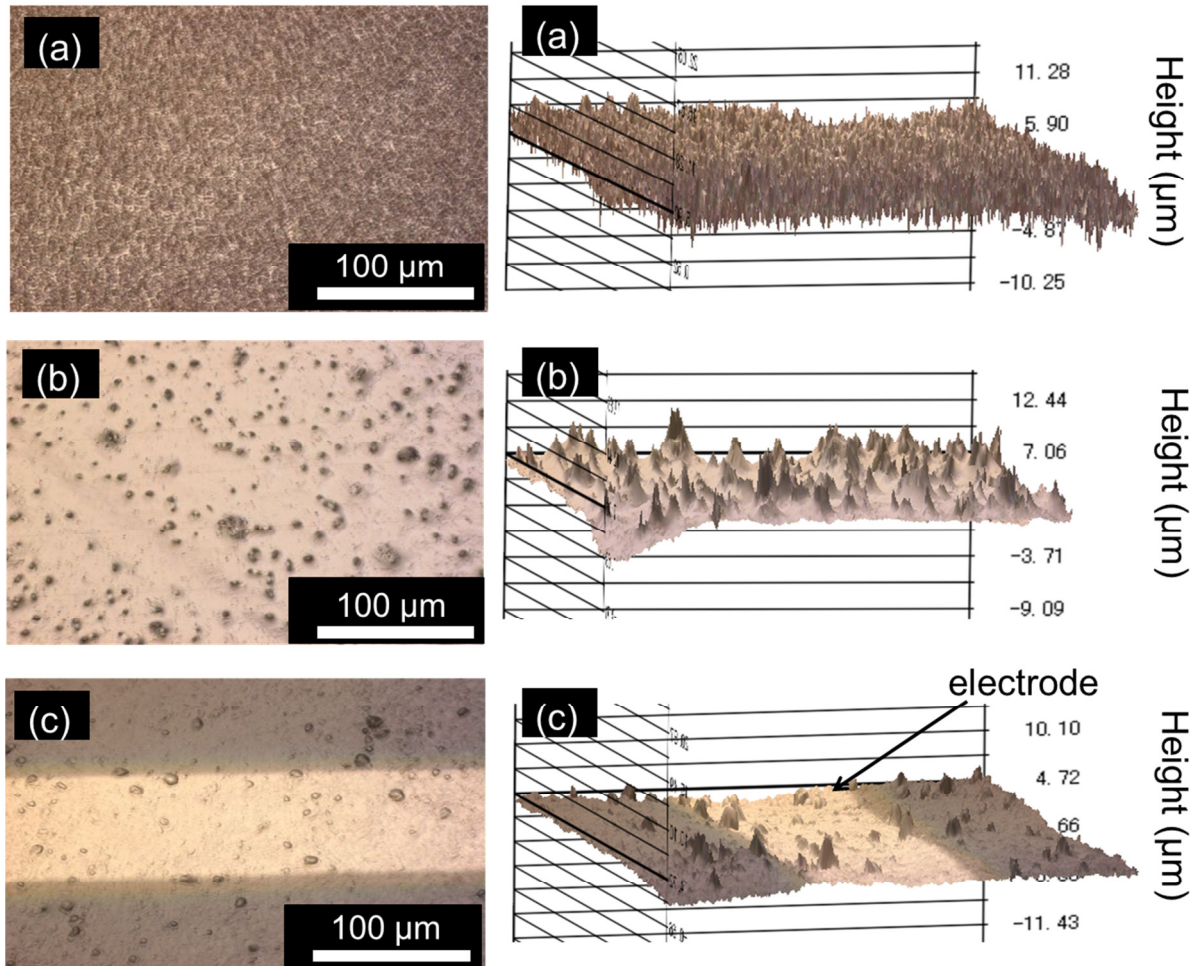


Figure 2.15 Surface appearances of substrates which were alkali-textured (a) before laser scan, (b) after a single laser scan, and (c) after a double laser scan. Superficial and cross-sectional images are shown on the left- and right-hand sides, respectively.

Figure 2.16 compares SEM images of textured silicon surfaces after single (a) and double laser scans (c) as well as their corresponding EBIC measurements (b and d, respectively). Single-scan LD formed a rough surface (Fig. 2.16a) displaying many black areas by EBIC (Fig. 2.16b). These black areas correspond to electronic defects that may collect minority carriers in silicon solar cells, indicating that surface protrusions became minority carrier recombination centers. Double-scan LD formed smoother surfaces than a single-scan LD (Fig. 2.16c) and reduced the black areas (Fig. 2.16d). Figure 2.17 compares EBIC line scans obtained after first (Fig. 2.16b) and second laser scans (Fig. 2.16d) and averaged over ten line scans. These lines were randomly drawn in the lateral direction of the EBIC image. The EBIC image intensity increased after the second laser scan, indicating that double-scan LD reduced the number of minority carrier recombination centers.

Dopant profiles of samples obtained after single and double laser scans are shown in Fig. 2.18. Samples exhibited more concentrated and deeper dopant profiles after double-scan LD than after a single laser scan. The interface between the dopant precursor and the silicon substrate plays an important role in the LD process. In the first scan, phosphorus atoms dope silicon in an inhomogeneous manner and in small amounts because of low interface adhesion. At the same time, this scan improved the interface by suppressing voids and strengthening adhesion. Consequently, during the second laser scan, the silicon surface melted again and dopant atoms moved to deeper regions at higher concentrations.

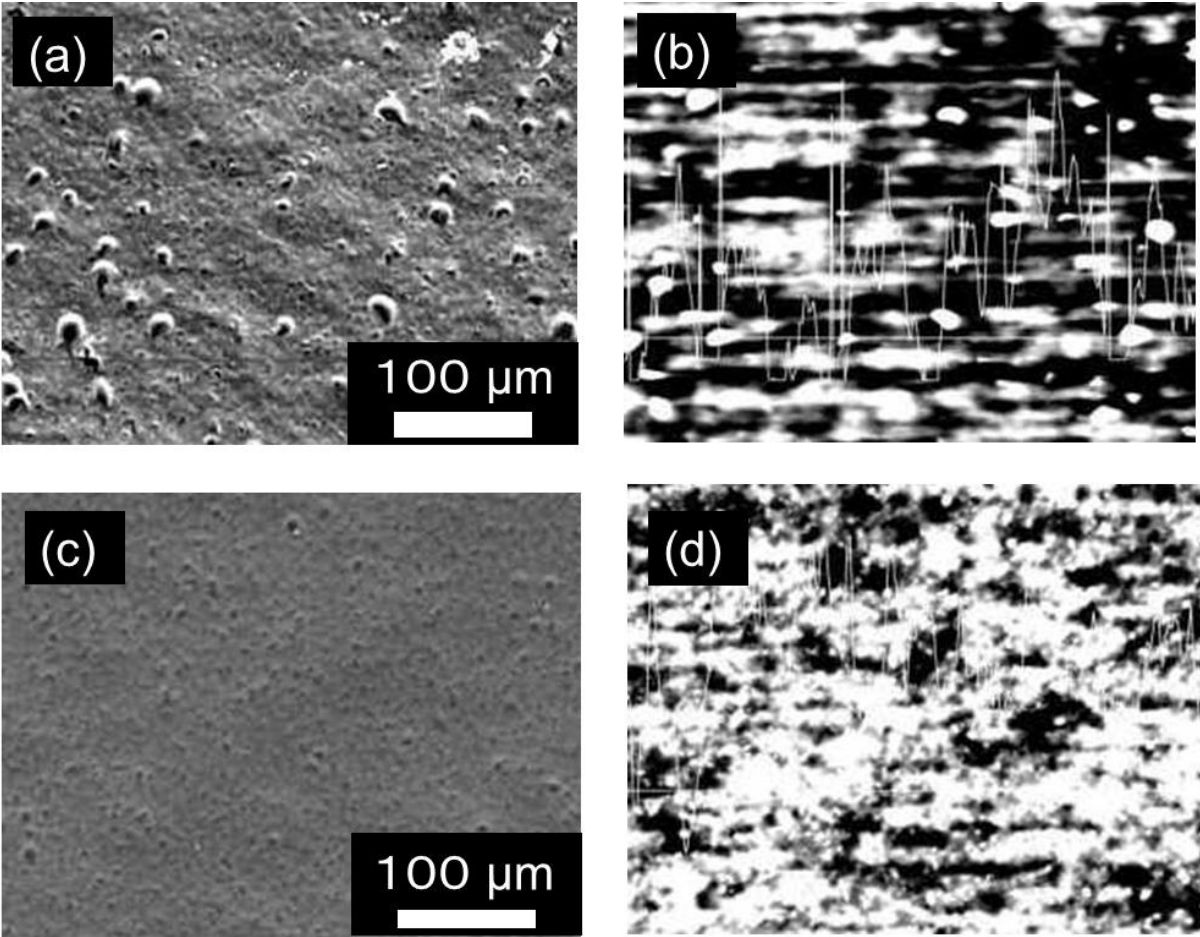


Figure 2.16 SEM surface morphologies and EBIC electrical characteristics after (a) single- and (b) double-scan LD

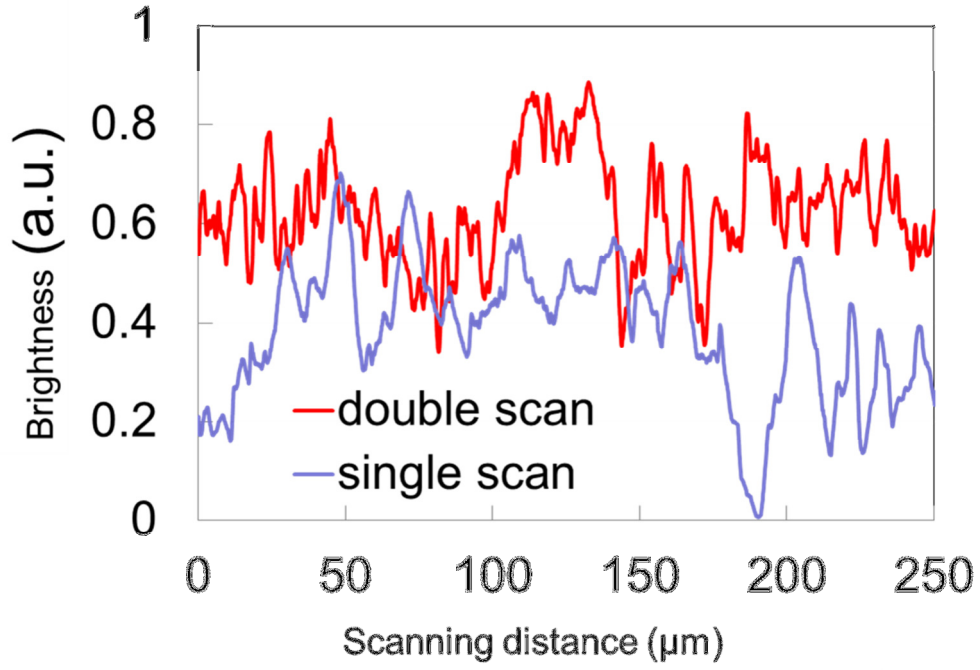


Figure 2.17 EBIC line scans after single- and double-scan LD

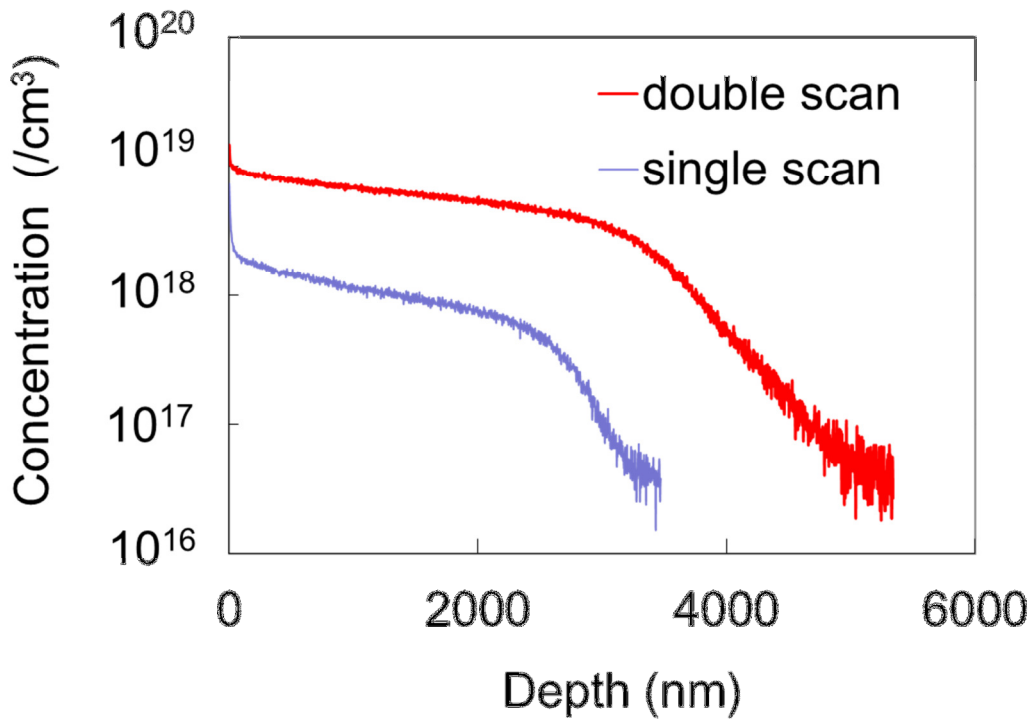


Figure 2.18 Dopant profiles after single- and double-scan LD

Chapter 2. Emitter Quality Improvement after Laser Doping by Surface Structure Control

Illuminated I–V characteristics were measured to evaluate the LD-generated p–n junction (Fig. 2.19). Samples produced by double laser scan displayed higher J_{sc} , V_{oc} , and FF values than those obtained after a single laser scan. The double laser scan reduced the number of minority carrier recombination centers, as shown by EBIC images, increasing J_{sc} and V_{oc} . Furthermore, it homogenized the surface and improved contact with metal electrodes. Therefore, the resulting samples exhibited lower series resistance and higher FF. Despite an increase, J_{sc} and V_{oc} values remained low. Laser conditions will be optimized in future studies to improve these parameters.

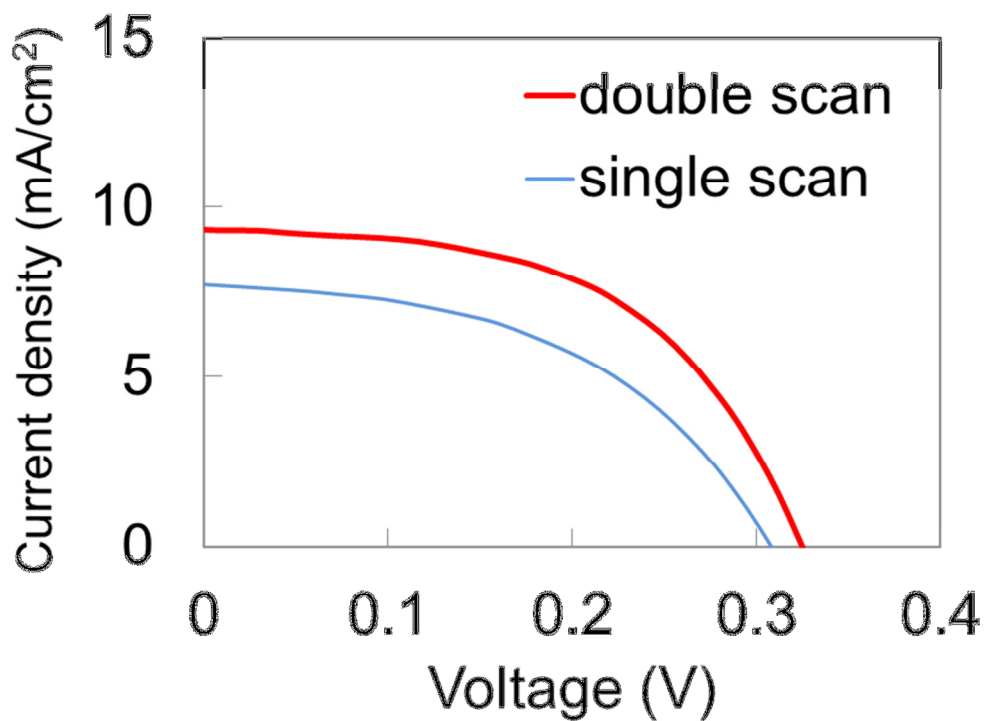


Figure 2.19 Illuminated I–V curves after single- and double-scan LD

Table 2.5 Photovoltaic characteristics extracted from Figure 2.15

	V_{oc} (mV)	J_{sc} (mA/cm ²)	FF (%)	Eff (%)
Single scan	306	7.7	47.9	1.1
Double scan	327	9.4	53.8	1.7

2.5 Summary

Emitter structures were generated by LD for c-Si solar cell fabrication. The relationship between surface structure and emitter quality after LD was evaluated. First, the surface structure was improved by additional chemical etching, suggesting that surface voids appeared after LD because of the existence of voids at the PSG–silicon interface. In addition, electric properties of LD-processed emitters were assessed. Photovoltaic characteristics of chemically etched and as-cut samples were compared. EBIC measurements demonstrated that surface voids caused electric defects. Dark I–V characteristics revealed that surface structure improvements achieved by chemical etching decreased the series resistance and increased the shunt resistance. Illuminated I–V characteristics showed that these improvements enhanced J_{sc} , V_{oc} , and FF. Overall, the surface structure significantly affected photovoltaic properties in c-Si solar cell fabrication using LD.

Furthermore, surface electric properties of LD-processed textured c-Si substrates were determined, and surface structure improvement was attempted by double-scan LD. Irregular rough surfaces were formed after single-scan LD, whereas homogenous surfaces were obtained after the second LD scan. Rough surfaces obtained by single-scan LD showed numerous electric defects, which became minority carrier recombination centers. Double-scan LD reduced these electric defects and produced heavy doping. Specifically, it increased the phosphorous concentration and the depth of the doped region. This heavy doping depends on

Chapter 2. Emitter Quality Improvement after Laser Doping by Surface Structure Control

the improvement of interface adhesion during the first laser scan and the migration of dopant atoms toward deeper regions at high concentration during the second laser scan. Illuminated I–V characteristics indicated that double-scan LD increased J_{sc} and FF values by homogenizing surfaces and reducing minority carrier recombination centers.

References of Chapter 2

- 1) K. Hirata, T. Saitou, A. Ogane, E. Sugimura, and T. Fuyuki, *Applied Physics Express* **5** (2012), p. 016501.
- 2) M. Hasegawa, K. Hirata, T. Saitoh, T. Takayama, T. Funatani, E. Sugimura, S. Tsujii, A. Tani, and T. Fuyuki: *Proc. 35th IEEE PVSC* (2010), p. 3154.
- 3) Operator's Manual, Verdi TMV-2/V-5/V-6 Diode-Pumped-Lasers (Coherent, USA, 2002).
- 4) K. Hirata, A. Ogane, A. Kitiyanan, E. Sugimura, and T. Fuyuki, *24th European Photovoltaic Solar Energy Conf.* (2009), p. 1708.
- 5) J. Acker, T. Koschwitz, B. Meinel, R. Heinemann, and C. Blocks: *Energy Procedia* **38** (2013), pp. 223–233.
- 6) H. J. Leamy: *J. Appl. Phys.* **53** (1982), R51.
- 7) H. Takahashi: *Journal of the Surface Science Society of Japan* **25** (2004) 224. (in Japanese).
- 8) S. M. Sze and K. K. Ng: *Physics of Semiconductor Devices* (Wiley, New Jersey, 2007) 3rd ed., p. 97.
- 9) A. Goetzberger, J. Knobloch, and B. Vob: *Crystalline Silicon Solar Cells* (Wiley, Chichester, 1998) 1st ed., p. 69.
- 10) I. H. Malitson: *Journal of the Optical Society of America* **55** (1965), p. 1205.
- 11) M. Hirose: *Advanced ULSI Process Technology* (Realize Inc., Tokyo, 2000) 1st ed., p. 319.

Chapter 2. Emitter Quality Improvement after Laser Doping by Surface Structure Control

12) I. Brynjulfsen, L. Arnberg, and A. Austruﬀe: *Journal of Crystal Growth* **361** (2012), p. 206.

13) G. Zhong, Q. Yu, X. Huang, L. Liu: *Solar Energy* **111** (2015), p. 218.

14) K. Nakamura, T. Saishoji, J. Tomioka: *Journal of Crystal Growth* **237** (2002), p. 1678.

Chapter 3

Interface Control by Chemical Surface Modification

3.1 Introduction

In previous chapters, spin-coated PSG was used as a doping precursor because of its low cost and high throughput. Consequently, surface defects were reduced by chemically etching substrate surfaces, improving photovoltaic characteristics. Voids may appear at PSG–substrate interfaces in LD-processed crystalline silicon (c-Si) substrates exhibiting rough surfaces, affecting heat conduction and impurity diffusion. Phosphorus diffusion is caused by thermal conduction from the substrate. Therefore, interfaces between PSG and c-Si substrate play a crucial role in this doping method. However, textured surfaces are necessary to increase light absorption in c-Si solar cells. Here, textured c-Si substrates were processed by LD using a diode-pumped solid-state (DPSS) laser and spin-coated PSG as a doping precursor. Before spin coating, the hydrophobic substrate surface was chemically turned hydrophilic to reinforce its interface with PSG. Substrate surface structures were evaluated before and after LD. In addition to doping profiles, photovoltaic characteristics were evaluated using a solar simulator after metallization.

3.2 Experimental Procedure

3.2.1 Laser Doping Set Up

The laser system comprised a 355 nm Q-switched Nd:YVO₄ laser (Coherent, MATRIX-355), reflective mirrors, and a collective lens. Samples were mounted on an x–y stage operating using a controller unit (Mark-202, SIGMA KOKI) connected to a personal computer (Fig. 3.1). The laser spot was a circle and presented a Gaussian distribution (TEM₀₀-mode). Laser pulses lasted approximately 25 ns.¹⁾

3.2.2 Sample Preparation

Experiments were performed using 180- μ m-thick p-type (100) alkali-textured c-Si wafers showing a resistivity of 1–10 Ω cm. These wafers were cleaved into 1.1 cm \times 1.1 cm squares to fabricate solar cells. All samples were subjected to RCA cleaning. Some samples were dipped into a 1:1 H₂SO₄ (96%)/H₂O₂ (30%) mixture for 10 min to change their surfaces from hydrophobic to hydrophilic.²⁾ Subsequent sample preparation steps are shown in Fig. 3.2. PSG was formed by spin coating and prebake. The dopant precursor, which contained ethanol as the main solvent, was deposited dropwise on the substrates, spread by spinning at

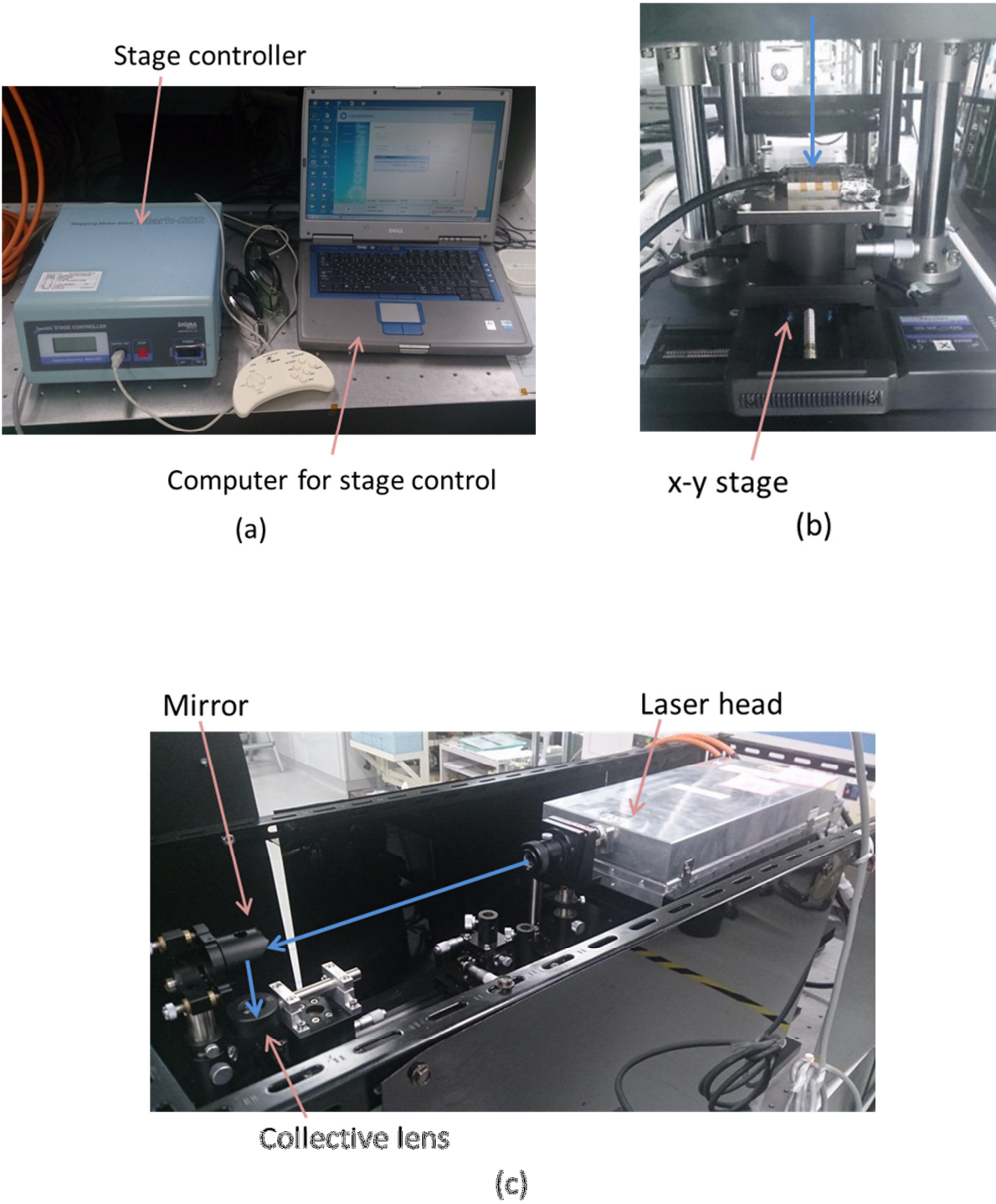


Figure 3.1 Laser doping system. (a) Stage control system, (b) x-y stage, and (c) laser system overview

3000 rpm for 30 s and baked at 300 °C for 15 min to evaporate the organic solvent. Schematic representations of PSG–substrate interfaces are shown in Fig. 3.3. PSG adhered to hydrophilic surfaces more tightly than their hydrophobic analogues because of the hydrophilicity of ethanol. Next, the entire surface was irradiated using the 355 nm Nd:YVO₄ pulsed laser under ambient atmosphere at room temperature (Fig. 3.4). Laser beams were mechanically scanned by moving the x–y sample stage from edge to edge in the x-direction at a scanning speed of 3 cm/s before a 30-μm shift in the y-direction. This cycle was repeated until the entire surface was irradiated, and residual PSG was removed by dipping the sample into a 1:10 HF/water mixture for 3 min. Ti/Ag and Al contacts were deposited by thermal evaporation to front and back sides of the substrate, respectively. Surface morphologies were examined by SEM after LD. Doping profiles were measured by SIMS. Photovoltaic characteristics were evaluated using a solar simulator (AM 1.5) after metallization.

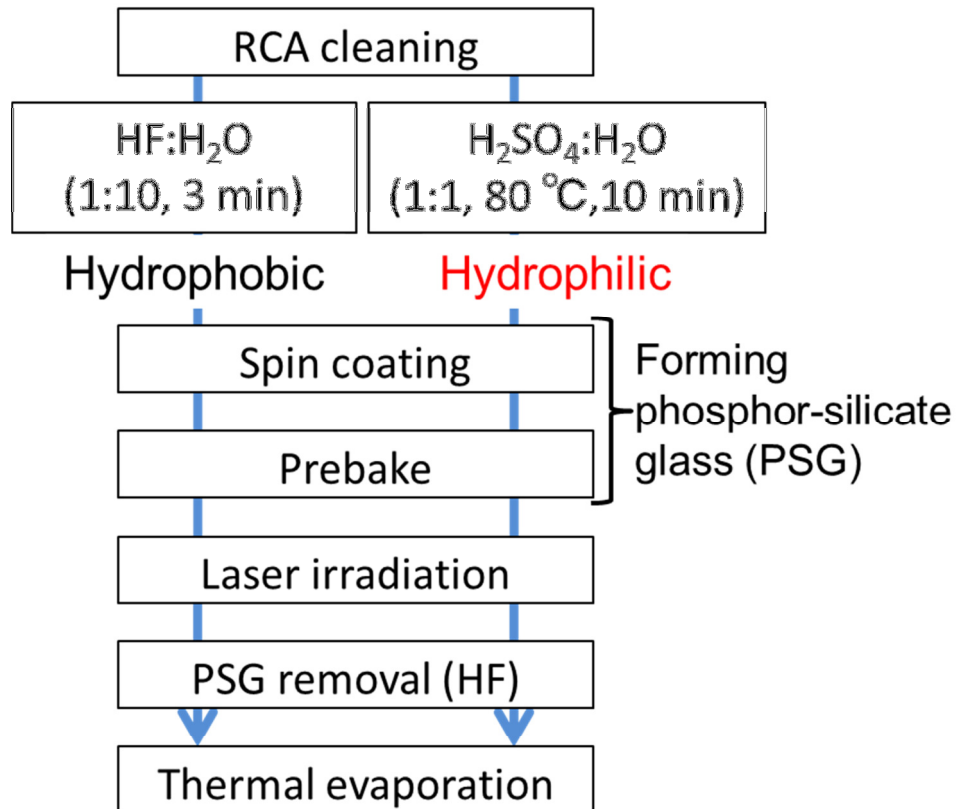


Figure 3.2 Chemical surface modification for PSG–substrate interface control

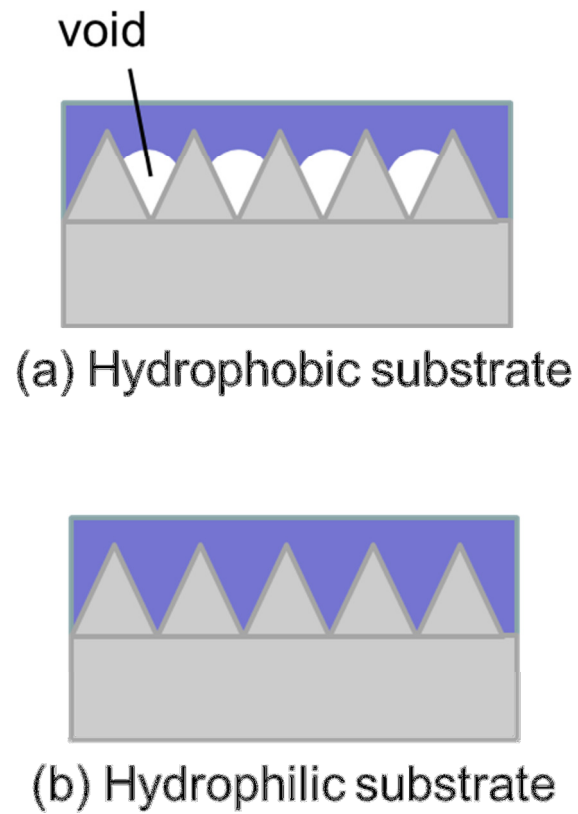


Figure 3.3 Schematic representations of PSG–substrate interfaces involving (a) hydrophobic and (b) hydrophilic substrates

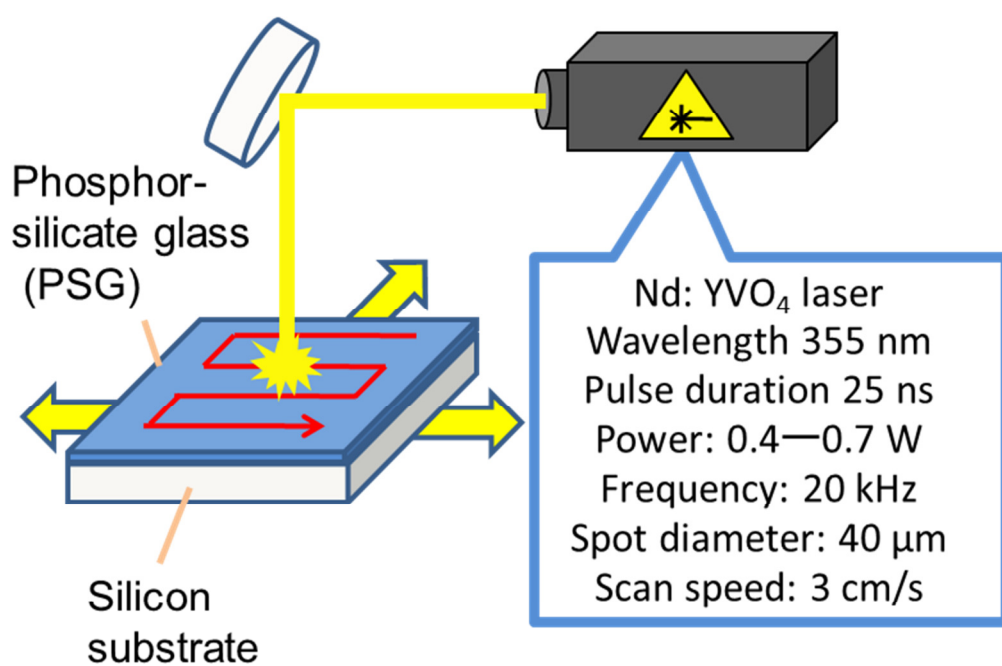


Figure 3.4 Laser doping conditions and process

3.3 Emitter Quality Improvement by Chemical Modification

Textured p-type c-Si substrate surfaces were turned hydrophilic by chemical treatment to improve emitter properties. These hydrophilic surfaces strongly adhered to PSG because the dopant solvent was also hydrophilic. The PSG–substrate interface and the LD-processed surface structure were analyzed by SEM and reflectivity measurements. Next, emitter properties were evaluated by SIMS as well as dark and illuminated I–V measurements.

3.3.1 Surface Structure Improvement after Laser Doping

Figure 3.5 shows SEM images of the PSG–substrate interface (Figs. 3.5a) and the surface formed by LD at a laser power of 0.7 W (Fig. 3.5b) using hydrophobic substrates. The white line appearing near the bottom of Fig. 3.5a was formed when the substrate was cut. Hydrophobic c-Si substrates were dipped into HF before spin coating. Because interface adhesion was poor during the spin-coating step, PSG shrunk when the organic solvent was evaporated, generating many spaces, such as cracks, in the PSG–substrate interface (Fig. 3.5a). Several holes were formed on the substrate surface after LD (Fig. 3.5b). Laser irradiation melted the textured surface, and the substrate supplied heat to PSG by thermal conduction. Dopant atoms were produced by photolysis or pyrolysis of the solid PSG phase. These

Chapter 3. Interface Control by Chemical Surface Modification

phosphorus impurities are incorporated into molten Si during laser irradiation by liquid phase diffusion.³⁾ When the laser beam was moved away, the substrate containing phosphorus impurities recrystallized by natural cooling.⁴⁾ Samples exhibiting inhomogeneous adhesion at the PSG–substrate interface displayed many superficial holes by LD after recrystallization, as discussed in Section 2.3.4.

Figure 3.6 shows SEM images of the PSG–substrate interface (Figs. 3.6a) and the surface formed by LD at a laser power of 0.7 W (Figs. 3.6b) using hydrophilic substrates. The PSG–substrate interface displayed a homogeneous adhesion and no cracks were detected (Fig. 3.6a). These surfaces were chemically turned hydrophilic before spin coating, and the PSG precursor also presented a hydrophilic dipole moment. Therefore, these hydrophilic substrate surfaces strongly adhered to the dopant precursor, resulting in uniform PSG layers after spin coating and prebake. Consequently, fewer surface holes formed during LD compared with samples with hydrophobic surfaces (Fig. 3.6b). The homogeneous PSG–substrate interface generated uniform heat transfer and allowed the substrate to recrystallize at a uniform speed over the entire surface. The textured surface was smoothed to some extent, but the textured structure was preserved even after LD.

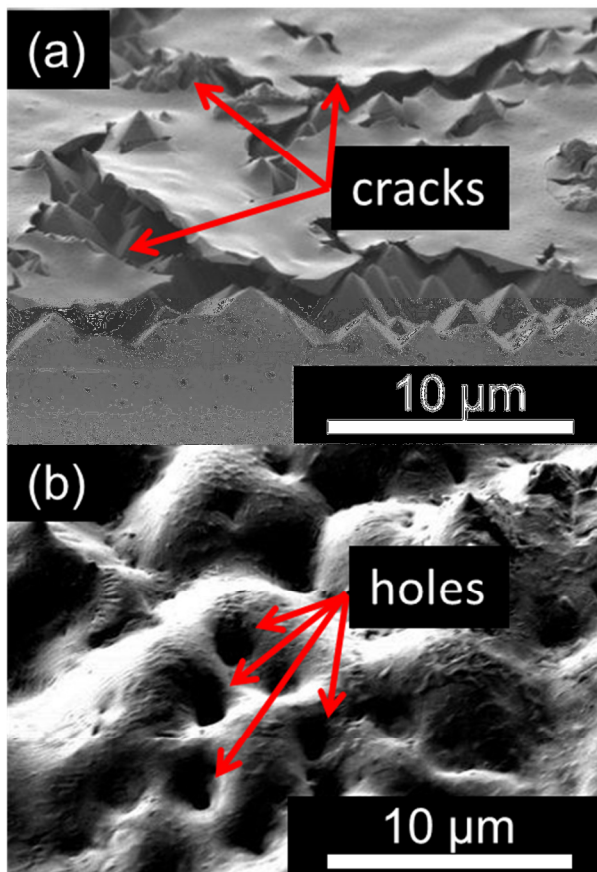


Figure 3.5 PSG–substrate interface (a) and surface morphologies obtained after LD (b) for samples exhibiting hydrophobic surfaces

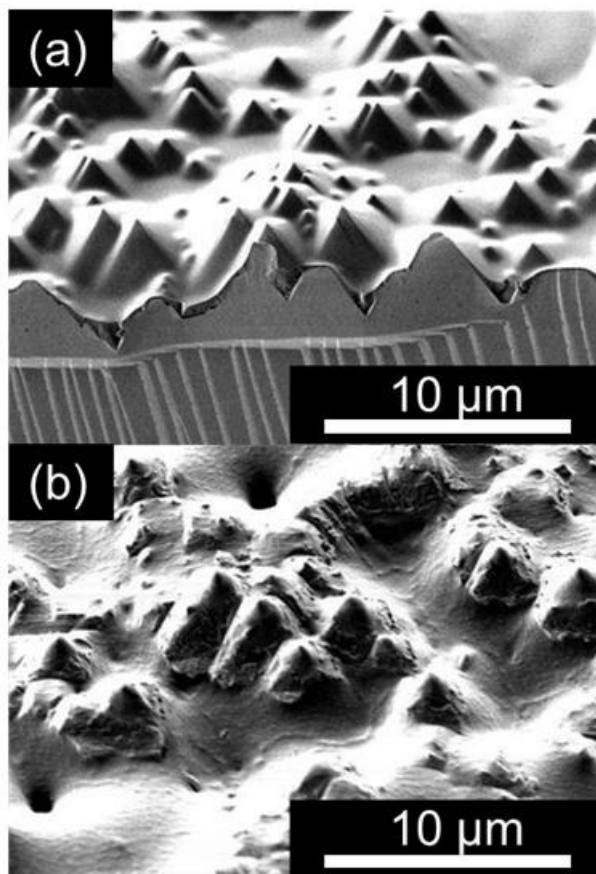


Figure 3.6 PSG–substrate interface (a) and surface morphologies obtained by LD (b) for samples exhibiting hydrophilic surfaces

The reflectivity was measured through two different experiments at laser outputs varying from 0.4 to 0.7 W. Figures 3.7 and 3.8 show the reflectivity of LD-processed hydrophobic and hydrophilic textured surfaces, respectively. The reflectivity increased with increasing laser output power for hydrophobic silicon substrates (Fig. 3.7). The surface melting depth was shallow and the surface texture remained intact during low energy LD. Surfaces were melted more deeply and the surface texture was destroyed during high energy LD. Hydrophilic substrates exhibited similar reflectivity trend to their hydrophobic counterparts (Fig. 3.8). However, the reflectivity increased monotonously with increasing laser energy, suggesting that the melting depth changed more uniformly with respect to laser energies in these samples.

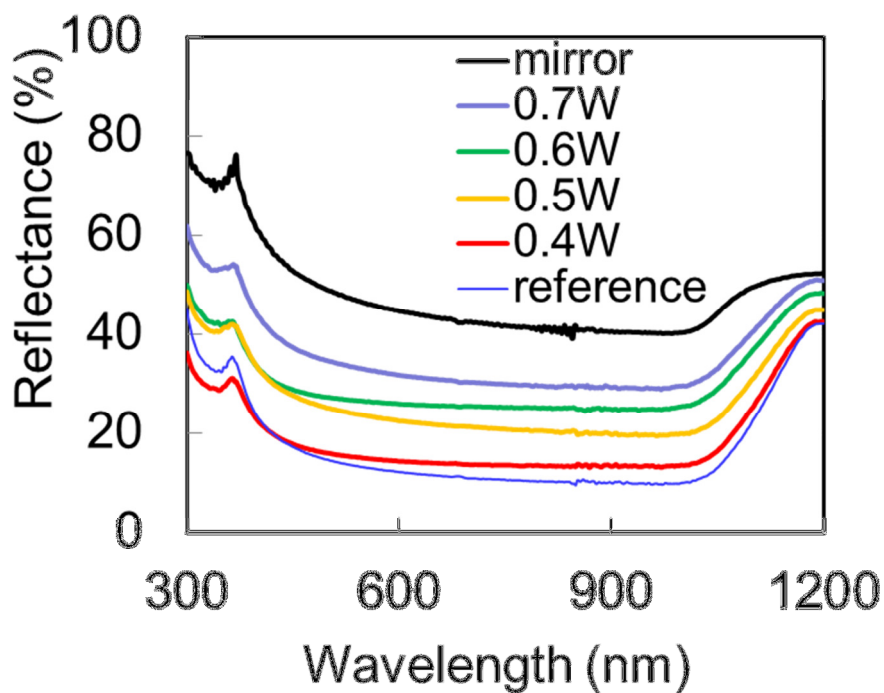


Figure 3.7 Reflectivity of hydrophobic surfaces processed at various LD energies

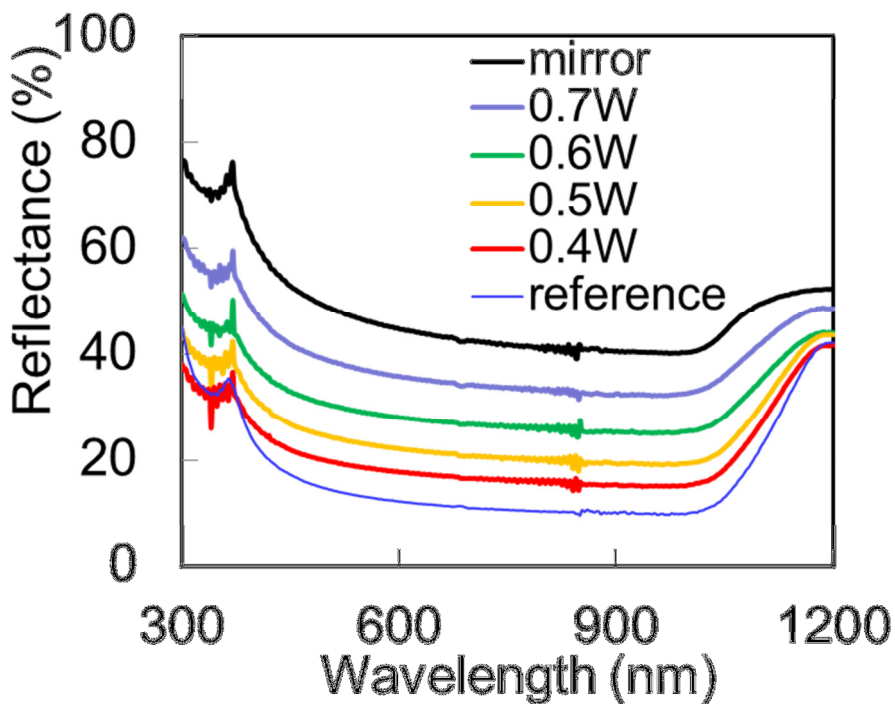


Figure 3.8 Reflectivity of hydrophilic surfaces processed at various LD energies

3.3.2 Emitter Property Improvement by Control of Interface Chemical State

SIMS phosphorus distributions are shown in Figs. 3.9 and 3.10 for hydrophobic and hydrophilic surfaces, respectively. SIMS measurements were conducted during LD at different laser outputs. Actual doping depths were not calculated because of the textured surfaces. Hence, the horizontal axis shows the measurement time, which is proportional to the doping depth. However, doping depths can be estimated by comparing these phosphorus profiles to SIMS data for smooth surfaces. A SIMS measurement of 1,000 s is nearly equivalent to a doping depth of approximately 500 nm. SIMS phosphorus profiles were determined at the same time as hydrogen distributions but were not affected by these measurements. Figure 3.8 shows phosphorus doping profiles of LD-processed hydrophobic substrates. Phosphorus concentration and doping depth increased with increasing laser output power, suggesting that melting depth and doping concentration depend on the laser energy density in LD. However, these increases were relatively small in hydrophobic samples. Surface phosphorus concentrations exceeded 10^{20} cm^{-3} for all samples (Fig. 3.9), but the doping depth only doubled when the laser energy increased from 0.4 to 0.7 W at a phosphorus concentration of 10^{19} cm^{-3} . On the other hand, phosphorus concentration and doping depth increased considerably with increasing laser energy density in hydrophilic samples (Fig. 3.10). Moreover, the number of phosphorus atoms in hydrophilic substrates surpassed that in their

Chapter 3. Interface Control by Chemical Surface Modification

hydrophobic counterparts at high laser energies. The surface phosphorus concentration amounted to approximately $5 \times 10^{19} \text{ cm}^{-3}$ at 0.4 W and increased beyond 10^{20} cm^{-3} at higher laser energies (Fig. 3.10). The doping depth at a phosphorus concentration of 10^{19} cm^{-3} approximately quadrupled when the laser energy increased from 0.4 to 0.7 W. These SIMS results can be used to predict the interfacial nanostructure between PSG and the substrate. Here, thermal energy caused phosphorus to diffuse from PSG to the substrate. The laser energy penetrated the PSG layer before being absorbed by the c-Si substrate. In turn, PSG was heated by thermal conduction from the c-Si substrate. These results suggest that the interface nanostructure plays an important role for phosphorus diffusion. The presence of voids at the PSG–substrate interface prevents thermal conduction and phosphorus diffusion, resulting in inhomogeneous melting and doping during laser irradiation. Figures 3.9 and 3.10 do not provide the actual phosphorus profiles because they were acquired over a large area of the textured surface. Deteriorated I–V characteristics suggested that the actual doping profiles were inhomogeneous (see below). The PSG–substrate interface displayed uniform adhesion at the nanoscale in hydrophilic samples, facilitating phosphorus diffusion. Therefore, laser-induced melting and doping became deep and homogeneous. The doping depth was successfully controlled by the laser power.

The deep and homogeneous doping observed in hydrophilic samples improved I–V characteristics. Photovoltaic characteristics were evaluated by I–V measurements in the dark

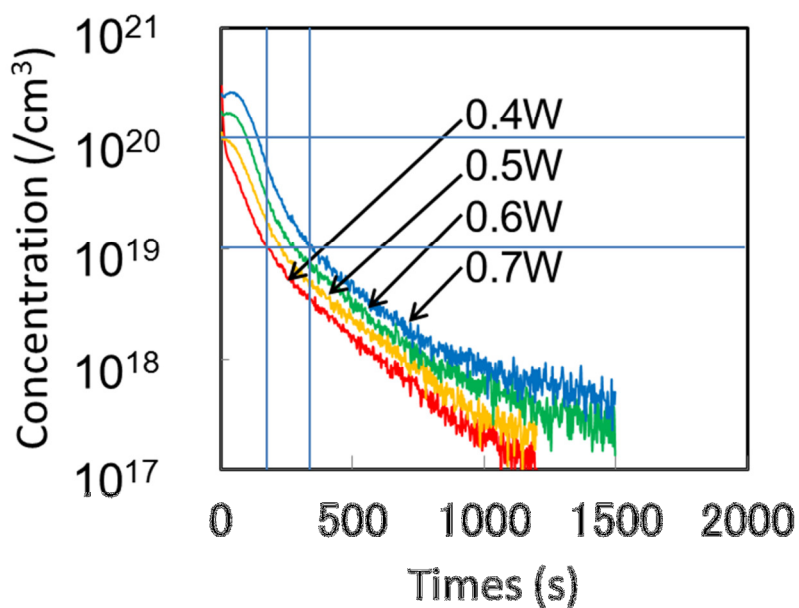


Figure 3.9 Phosphorus profiles of hydrophobic substrates processed at various LD energies

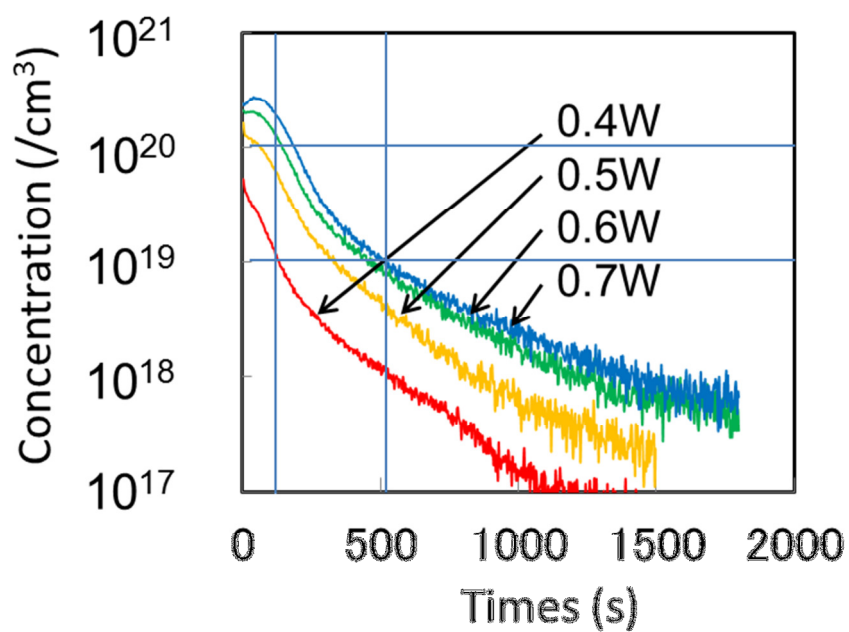


Figure 3.10 Phosphorus profiles of hydrophilic substrates processed at various LD energies

Chapter 3. Interface Control by Chemical Surface Modification

and using a solar simulator. Dark I–V characteristics of hydrophobic and hydrophilic samples are shown in Figs. 3.11 and 3.12, respectively. All hydrophobic samples presented similar dark I–V characteristics (Fig. 3.11), in which no trend was detected with respect to the laser output power. Reverse currents were quite high and the emitter region exhibited significant leakage, indicating that phosphorus doping was inhomogeneous on hydrophobic textured substrates. Hydrophilic samples showed different I–V characteristics in the 0.4–0.7 W LD energy range (Fig. 3.12). Their reverse current was higher than for hydrophobic samples at low energy before decreasing at higher energies. This indicates that emitter leakage was higher at low energy because of inhomogeneous phosphorus doping. This leakage decreased at higher energy because strong PSG–substrate interface adhesion provided homogeneous phosphorus doping.⁵⁾

Photovoltaic characteristics were measured using the solar simulator. Figures 3.13–3.15 show V_{oc} , J_{sc} , and FF plots, respectively, for hydrophobic and hydrophilic surfaces. Open-circuit voltage values slightly increased with rather large fluctuations when the laser energy increased for hydrophobic samples. This suggests that the phosphorus concentration depends on the laser energy and PSG adhesiveness to the textured substrate surface. On the other hand, V_{oc} values increased monotonically with increasing laser energy for hydrophilic samples, implying that strong interface adhesion allows each local point of the textured surface to uniformly absorb laser energy. In general, J_{sc} decreases with increasing surface reflectivity for solar cells.⁶⁾ Hydrophobic and hydrophilic samples exhibited decreasing J_{sc}

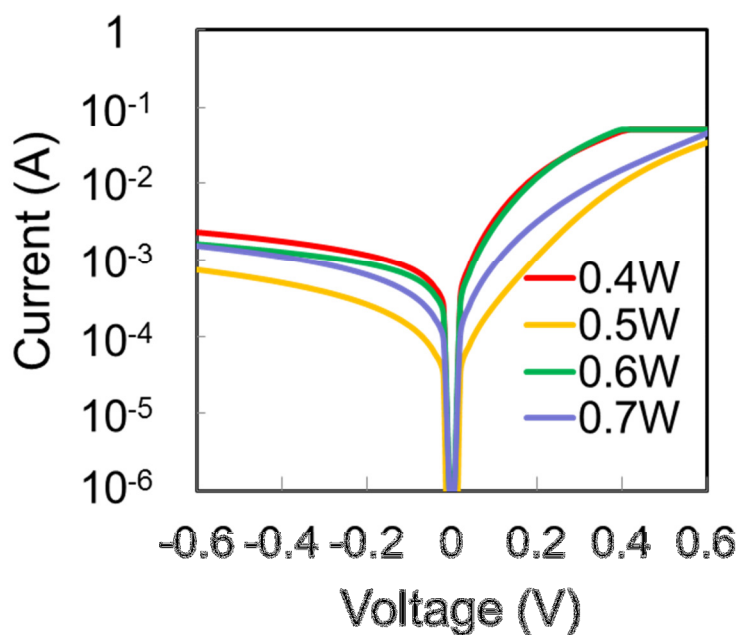


Figure 3.11 Dark I-V characteristics of hydrophobic samples processed at different LD energies

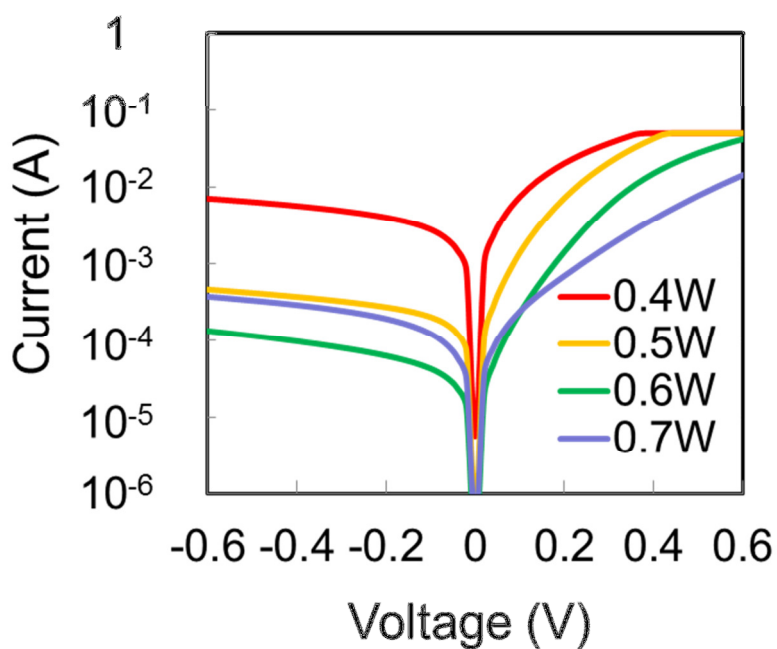


Figure 3.12 Dark I-V characteristics of hydrophilic samples processed at different LD energies

Chapter 3. Interface Control by Chemical Surface Modification

values when the laser energy increased, showing a high correlation with surface reflectivity. This decrease may result from the destruction of the textured structure at high energy. However, ARC may reduce the reflectivity,⁷⁾ lowering J_{sc} by depositing on the substrate. The FF displayed a similar trend to that of V_{oc} (Fig.3.15). This result may stem from the homogeneity of doping in the laser-doped region. Inhomogeneous doping region caused high leakage current and decreased the parallel resistance, reducing FF.⁸⁾ I-V curves of LD-processed hydrophobic and hydrophilic surfaces were compared to a sample fabricated by conventional thermal diffusion (Fig. 3.16). Photovoltaic characteristics (Table 3.1) were evaluated at a laser output power of 0.7 W to maximize efficiency for hydrophobic and hydrophilic substrates. Hydrophilic samples exhibited higher V_{oc} values than hydrophobic samples, which presented comparable values to those of the sample fabricated by thermal diffusion. The reduction of LD-generated surface voids improved V_{oc} values. Laser-doped hydrophobic surfaces displayed numerous holes (Fig. 3.5), acting as minority carrier recombination centers that reduce V_{oc} (Chapter 2). The number of surface electric defects diminished because of the reduction in surface voids in hydrophilic samples. Furthermore, hydrophilic samples showed higher J_{sc} values than hydrophobic samples but lower values than that obtained by thermal diffusion. Therefore, in addition to increasing minority carrier lifetime, the reduction in surface voids prevented the formation of discontinuous metal contacts on the textured surface. However, textured surfaces inevitably melt during LD and suffer damage to some extent. Consequently, surface reflectivity was increased and J_{sc} was

decreased in LD-processed samples compared to the sample fabricated by thermal diffusion. Finally, the solar cell efficiency increased by approximately 2% in hydrophilic samples compared to their hydrophobic counterparts. However, this efficiency remained lower than that of samples manufactured by thermal diffusion, suggesting that laser conditions need to be optimized more precisely.

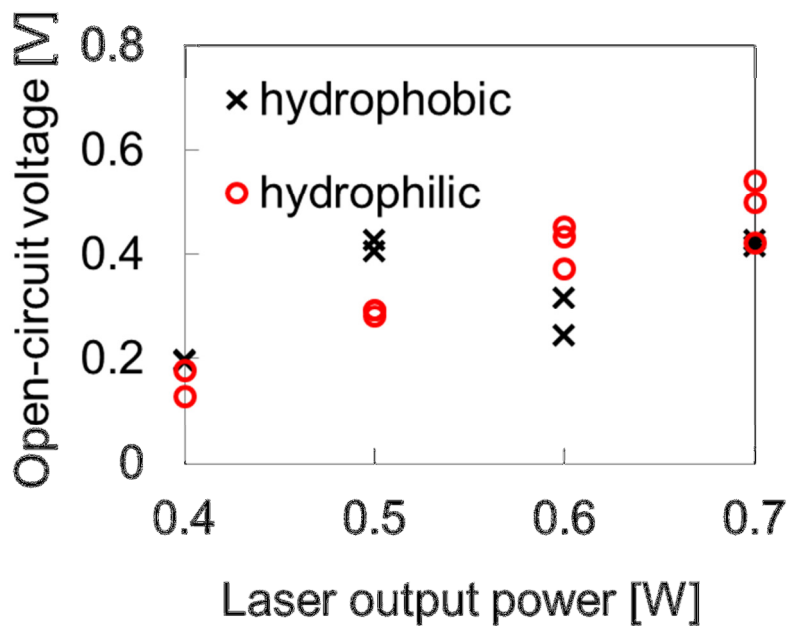


Figure 3.13 Open-circuit voltages of hydrophobic and hydrophilic samples at various LD energies

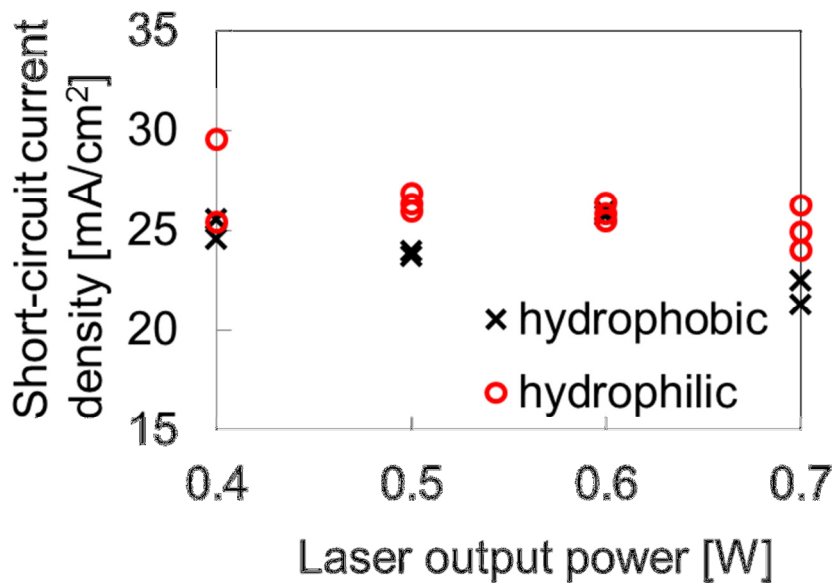


Figure 3.14 Short-circuit current densities of hydrophobic and hydrophilic samples at various LD energies

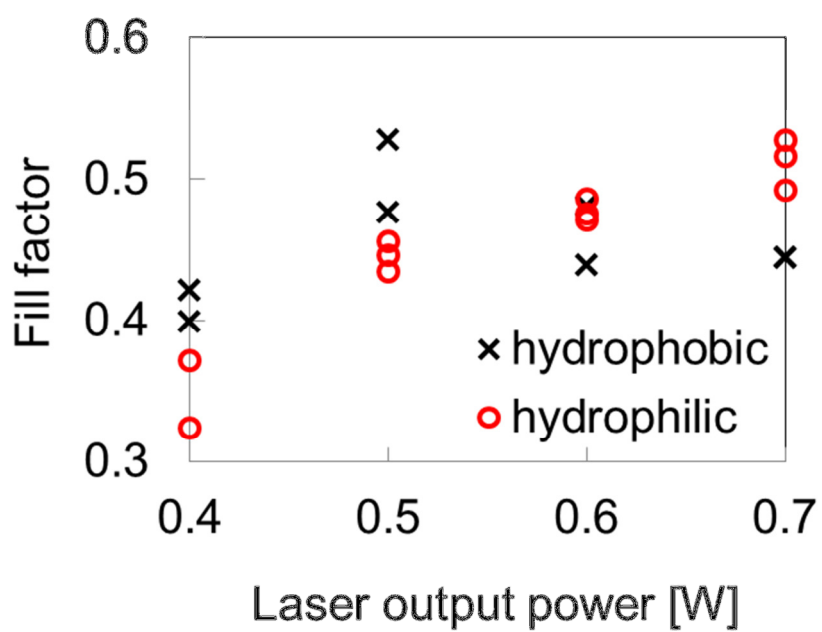


Figure 3.15 Fill factor of hydrophobic and hydrophilic samples at various LD energies

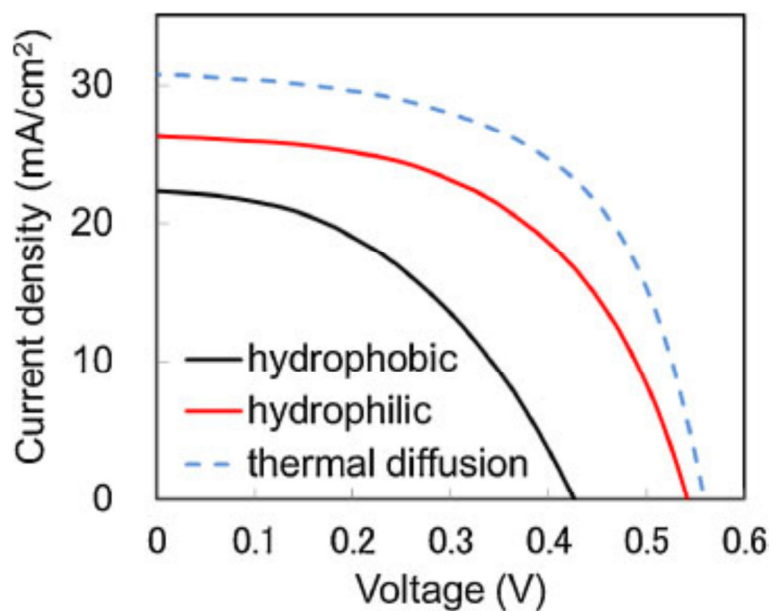


Figure 3.16 Illuminated I–V curves of LD-processed hydrophobic and hydrophilic samples compared with that of a sample fabricated by thermal diffusion

Table 3.1 Photovoltaic characteristics obtained from individual I–V curves shown in Fig. 3.15

	V _{oc} (mV)	J _{sc} (mA/cm ²)	FF (%)	Eff (%)
Hydrophobic	426	22.5	44.4	4.3
Hydrophilic	541	26.3	52.8	7.5
Thermal diffusion	559	30.8	57.5	9.9

3.4 Summary

The interface structure between the doping precursor and substrate was addressed for LD-processed textured silicon substrates. These processes involved a spin-coated dopant and a 355 nm pulsed laser. Surface and interface topographies before and after LD, doping profiles, and photovoltaic characteristics were evaluated to clarify the interfacial influence on the properties of the doped region. The c-Si substrate was chemically changed from hydrophobic to hydrophilic, providing control over the interface nanostructure between doping precursor and substrate. The number of surface voids decreased in LD-processed hydrophilic samples compared to their hydrophobic equivalents. Moreover, SIMS phosphorus profiles showed that hydrophilic samples exhibited higher doping depth and phosphorus concentration than the hydrophobic counterparts. These results originated from the strong interfacial adhesion between PSG and hydrophilic substrate at the nanoscale. Finally, the electric properties of these samples were compared with those of a sample fabricated by conventional thermal diffusion. Hydrophilic samples showed higher V_{oc} and J_{sc} than hydrophobic samples. Overall, the control of the nanoscale interface structure significantly impact electric properties in laser-doped regions.

References of Chapter 3

- 1) Operator's Manual, MATRIX-355 Diode-Pumped Q-Switched Lasers (Coherent, USA, 2007).
- 2) M. Grundner and H. Jacob: *Appl. Phys. A* **39** (1986), p. 73.
- 3) T. Sameshima and S. Usui: *Jpn. J. Appl. Phys.*, **26** (1987), L1208.
- 4) M. Hirose: *Advanced ULSI Process Technology* (Realize Inc., Tokyo, 2000) 1st ed., p. 319.
- 5) S. Kishino: *Modern Basic of Semiconductor Device* (Ohmsha, Tokyo, 2012) 1st ed., p. 78.
- 6) M. A. Green: *Solar Cells* (Prentice-Hall, Inc., New South Wales, 1982) 1st ed., p. 86.
- 7) Y. Liu, O. J. Guy, J. Patel, H. Ashraf, and N. Knight: *Microelectronic Engineering* **110** (2013), pp. 418–421.
- 8) A. Luque and S. Hegedus: *Handbook of Photovoltaic Science and Engineering* (Wiley, Chichester, 2011) 2nd ed., p. 119.

Chapter 4

Local Impurity Doping and High-Efficiency Structures using Novel Precursor Layers

4.1 Introduction

Previous chapters demonstrated that the doping precursor–substrate interface played an important role in LD. However, if silicon particles are used as doping precursor for LD, this influence of interface is low because these particles directly absorb laser energy and melt. The fabrication of high-efficiency structures, such as selective emitters and back contact solar cells, requires two-dimensional patterning processes. Printing offers a cost-effective alternative to spin coating and vacuum processes such as chemical vapor deposition because it enables material savings. Silicon nano-ink consists of silicon nanoparticles dispersed in an organic solvent. NanoGram® nano-ink has been applied to printing processes, such as ink-jet and screen printing. This study was performed with collaboration with Teijin Corporation which produces NanoGram.

On the other hand, interface adhesion can be improved using organic polymer-based doping precursors. Strong interface adhesion may facilitate the homogeneous introduction of

impurities and produce high-quality doped regions. Therefore, PBF was used as a precursor layer in the fabrication of selective emitter solar cells. Selective emitters are attractive high-efficiency crystalline silicon (c-Si) solar cell structures. Conventional homogeneous emitters present problems regarding the trade-off between Auger recombination and series resistance. Heavily doped emitters increase the Auger recombination and aggravate short-wavelength light absorption, whereas their shallow-doped analogues decrease the Auger recombination but increase series resistance. A selective emitter structure can solve these issues by formation of a heavily doped area underneath metal contacts and shallow-doped area on other area which absorbs incident light. However, selective emitter fabrication by conventional thermal processes needs additional heating and a photolithography process comprising a chemical step. These processes involve elevated additional costs and decrease yields, especially in the case of thin substrates. LD provides selective emitters in a single step in ambient air at room temperature, enabling the high-throughput fabrication of high-efficiency solar cells at low cost and high yield.

4.2 Experimental Procedures

NanoGram® (Teijin Corporation), which contained a phosphorus concentration of 1×10^{21} atoms/cm³, and PBF (Tokyo Ohka Kogyo) were used as precursor layers for LD. The laser system which was used in Section 4.2 was equipped with a 532-nm Q-switched

Nd:YVO₄ laser, which were installed in Kataoka Corporation. Another laser system which was used in Section 4.3 was equipped with a 355-nm Q-switched Nd:YVO₄ laser, as detailed in Section 3.2. A schematic model of the LD set up is shown in Fig. 3.3 along with laser conditions. The laser output power varied from 0.4 to 1.0 W (1.25–3.13 J/cm²).

4.2.1 Laser Doping Procedure using Silicon Nanoparticles

Experiments were performed on 280- μ m-thick p-type mirror polished Cz c-Si wafers presenting a resistivity of 1–5 Ω /cm. Wafers were cleaved into 1 cm \times 1 cm squares and subjected to RCA cleaning. Silicon nano-ink was deposited on the wafers by spin coating and prebake at 85 °C for 5 min to form 200-nm-thick silicon nanoparticle layers. SEM images of silicon nanoparticles are shown in Fig. 4.1. Next, local silicon nanoparticle-coated areas under the metal contacts were irradiated using a 532-nm Nd:YVO₄ pulsed laser. Silicon nanoparticles underwent laser-induced melt–recrystallization and were absorbed through the substrate (Fig. 4.2). Remaining silicon nanoparticles were removed by dipping the substrate into a 1:10 HF/water mixture for 3 min. Al and Ti/Ag metal contacts were deposited by thermal evaporation on front and rear sides of the substrate, respectively. Samples were not subjected to any surface passivation or ARC. Surface structures after LD were observed by SEM. Phosphorus doped regions were evaluated by SIMS. Electronic characteristics were determined by dark I–V measurements. Photovoltaic characteristic were assessed using a

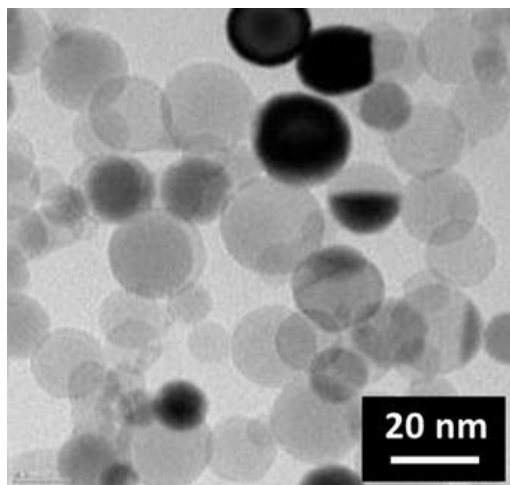


Figure 4.1 SEM image of silicon nanoparticles

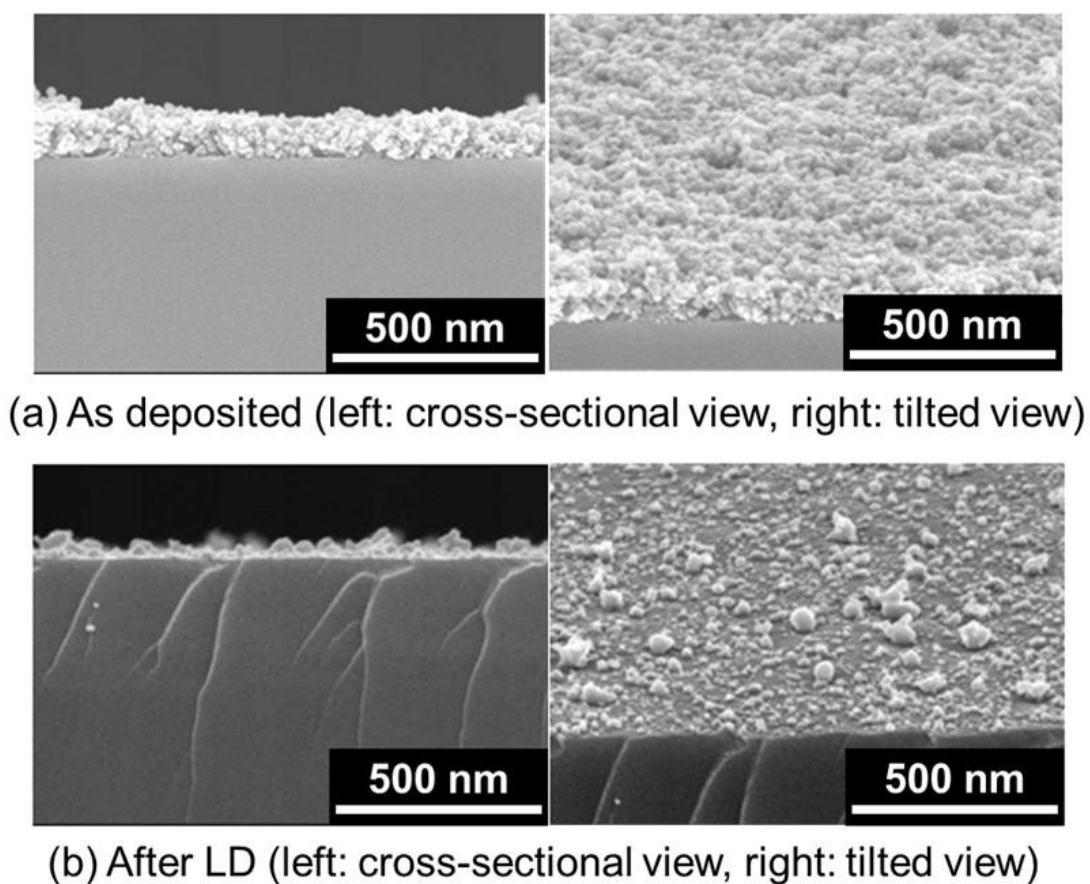


Figure 4.2 SEM images of silicon nanoparticles deposited on c-Si substrates before (a) and after LD (b)

solar simulator (AM 1.5).

4.2.2 Selective Emitter Fabrication using Polyboron Films

Selective emitters were produced using 200- μm -thick n-type alkali textured c-Si wafers displaying a resistivity of 1–10 Ω/cm . Wafers were cleaved into 1.1 cm \times 1.1 cm squares and subjected to RCA cleaning. Schematic models depicting selective emitter fabrication processes are shown in Fig. 4.3. The SoD PBF was generated on these samples by spin coating and prebake at 100 °C for 15 min. Homogeneous p+ emitters were formed on all samples by thermal diffusion at 900 °C for 30 min. Next, local PBF-covered surface areas under the metal contacts were irradiated using a 355-nm Nd:YVO₄ pulsed laser. Residual PBF and boron rich layer (BRL) were removed by oxidization using a furnace at 600 °C for 60 min and subsequent acid treatment in a 1:10 HF/water mixture for 10 min to decrease the minority carrier recombination rate at emitters.¹⁾ The Al and Ti/Ag metal contacts were deposited by evaporation on front and rear sides of the substrates. These samples did not undergo any surface passivation or ARC. Interfaces between PBF and substrate and LD-processed surface structures were examined by SEM. Boron doped regions were evaluated by SIMS. Electronic characteristics were assessed by dark I–V measurements. Photovoltaic characteristic were determined using a solar simulator (AM 1.5).

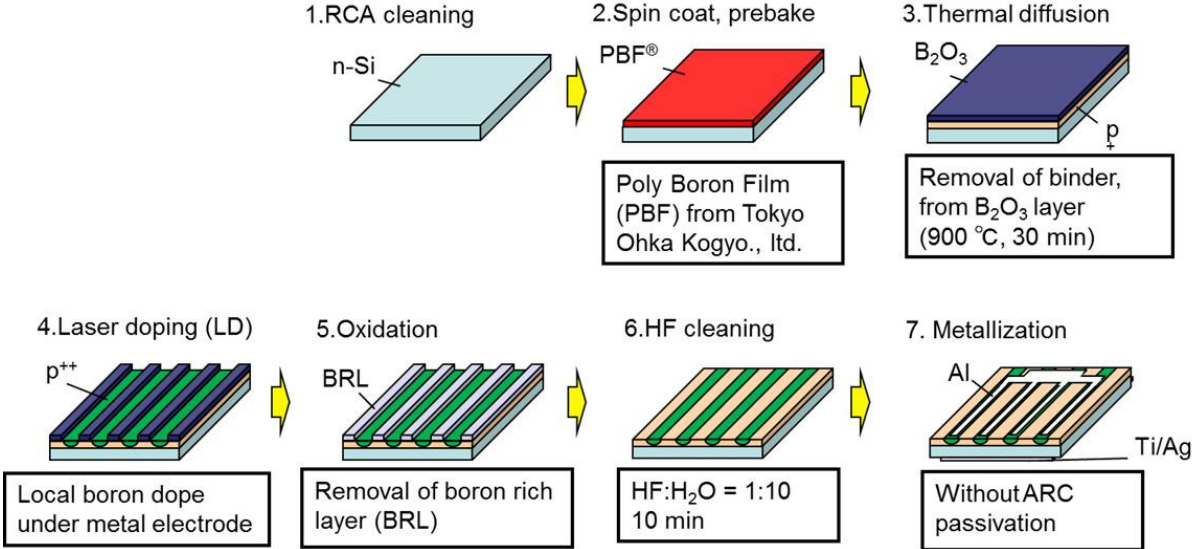


Figure 4.3 Schematic representation of selective emitter fabrication processes

4.3 Laser Doping using Silicon Nanoparticles

LD was conducted using silicon nanoparticles as doping precursors and a 532 nm pulsed laser. Figures 4.4a–c show SEM images of surface structures processed with laser power outputs of 0.4, 0.6, and 0.8 W, respectively. Droplet-like silicon clusters appeared on the surface at low energy. At low energy, the laser melted the silicon nanoparticles but not the substrates. While a portion of molten silicon nanoparticles recrystallized with the substrate, the other portion formed droplets and crystallized in this form. In contrast, a high energy laser melted substrates, causing nanoparticles to completely fuse with substrates. Theoretically, a large part of incident beam with 532 nm in wavelength is absorbed into silicon within 1 μm .²⁾ Silicon nanoparticles absorb incident beam with a high absorption coefficient at 532 nm. Therefore, large part of the laser energy is absorbed by the precursor layer. The precursor layer and the substrate are simultaneously melted by incident beam, resulting in mixing if the laser energy is sufficiently high. If the laser energy is very low to melt the entire precursor layer, remaining nanoparticles may become crystal cores and form droplet-like silicon clusters.

Fig. 4.5 shows SIMS phosphorus doping profiles of substrates processed using silicon nanoparticles as dopant precursors. Higher surface concentration and doping depth were obtained at 0.4 W than at 0.6 W. However, a large amount of precursor remained on the

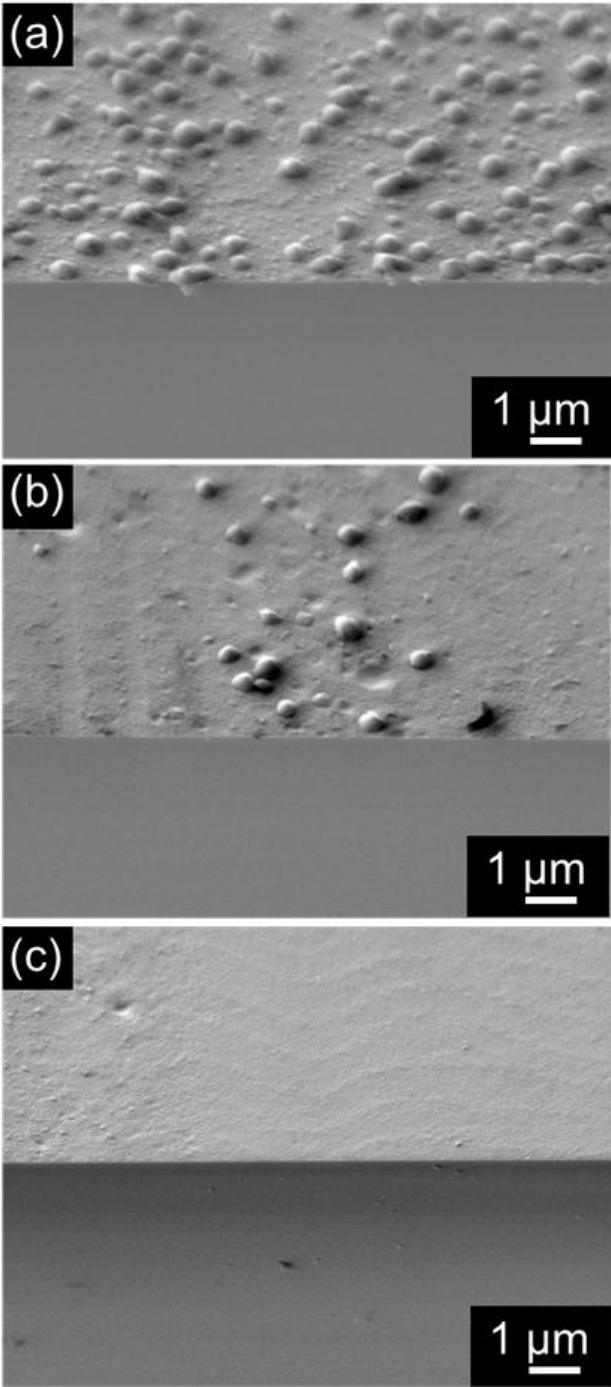


Figure 4.4 Surface morphologies of c-Si substrates processed using silicon nanoparticles as dopant precursors at laser energies of 0.4 (a), 0.6 (b), and 0.8 W (c)

surface after LD (Fig. 4.4a). SIMS measurements revealed that a large area (approximately $60 \mu\text{m} \times 60 \mu\text{m}$) contained numerous droplets. Therefore, the phosphorus doping profile was expected to be inhomogeneous, and the surface phosphorus concentration did not contribute to forming p–n-junction at 0.4 W. Droplets measured approximately 100 to 200 nm high, and SIMS surface profiles are not reliable for depths below 200 nm in the case of 0.4 W. On the other hand, similar doping profiles were observed at higher laser energies (0.6 and 0.8 W). Surface phosphorus concentrations approximated 3×10^{19} atoms/cm³, which is lower than that observed at 0.4 W. Phosphorus concentrations increased to 8×10^{19} atoms/cm³ at depths of 300 and 400 nm for energies of 0.6 and 0.8 W, respectively. The dopant pileup mechanism near the maximum melt depth was proposed by K. K. Ong et al.³⁾ Dopant pileup depends on the ratio between solid and liquid solute concentrations at the liquid–solid interface, or segregation coefficient. Therefore, phosphorus profiles revealed that silicon nanoparticles were completely melted at high laser energy. Phosphorus pileup has previously been observed using a pulsed laser at high energy density.^{4,5)} The laser energy caused silicon nanoparticles to easily blend with the substrate, producing box-like phosphorus doping profiles.

Table 4.1 shows the sheet resistances of substrates processed at different laser energies using silicon nanoparticles as doping precursors. Sheet resistances decreased with increasing laser energy, consistent with phosphorus doping profiles. At low energy, high surface concentrations did not contribute to sheet resistance because the surface was covered with silicon droplets. On the other hand, high laser energies formed homogeneous doped

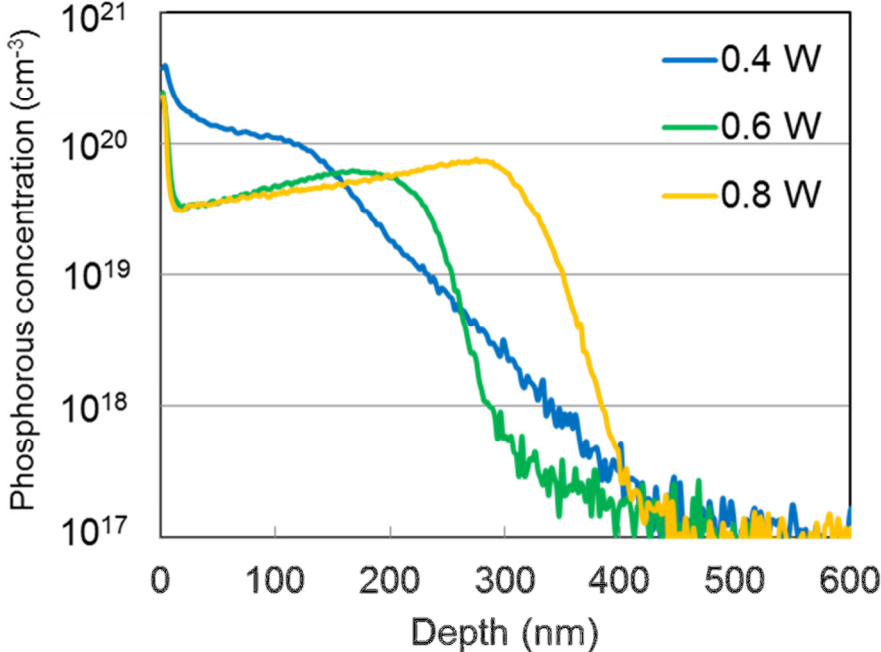


Figure 4.5 SIMS phosphorus profiles of doped regions formed at different laser energies

Table 4.1 Sheet resistances of doped regions formed at different laser energies

Laser power	Sheet resistance (Ω/cm)
0.4 W	116
0.6 W	67
0.8 W	50

regions. Therefore, phosphorus profiles contributed to sheet resistance. The highest laser energy (0.8 W) provided the lowest sheet resistance because deeper doping profiles accounted for a large number of phosphorus atoms.⁶⁾

Figure 4.6 compares dark I–V characteristics of samples processed at different laser energies. The reverse bias current and the low voltage region of the forward bias current decreased with increasing energy. These currents depend on carrier recombination at the depletion layer in solar cell devices. The reverse current was much higher at low energy than at high energy because most silicon nanoparticles formed droplet-like clusters on the surface during LD, and phosphorus atoms were insufficient to produce an appropriate p–n-junction. Diode characteristics recorded at 0.6 W improved from those measured at 0.4 W but the reverse current exceeded that obtained at 0.8 W. Although this phenomenon is unclear, shallow-doped p–n-junctions may influence diode characteristics. The doped region at 0.6 W was approximately 100 nm shallower than at 0.8 W. Therefore, laser-induced defects may readily influence depletion layers located in shallower regions. On the other hand, the sample fabricated at 0.8 W exhibited the lowest reverse current because of its deep depletion layer, which avoids laser damage at the surface.

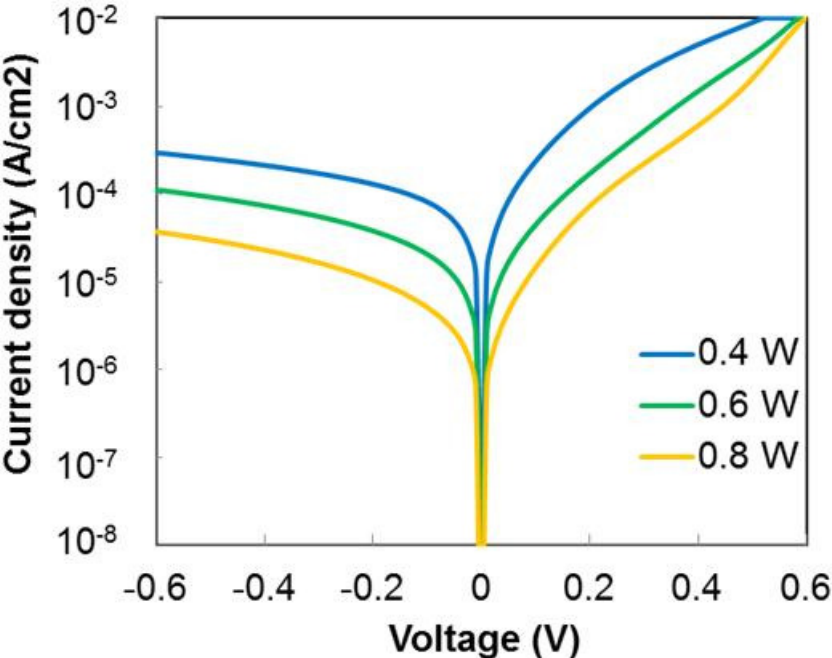


Figure 4.6 Dark I–V characteristics of solar cells processed at various laser energies

Figure 4.7 shows illuminated I–V curves of samples fabricated at different laser energies, and Table 4.2 list the corresponding photovoltaic characteristics. Samples fabricated at 0.4 W exhibited lower photovoltaic characteristics than those processed at high energy. The difference was small for J_{sc} and V_{oc} values but significant for FF. Illuminated I–V curves provide insight into the degradation of FF at low energy. The current gradient corresponds to parallel (R_p) and series resistances (R_s) near the vertical and horizontal axes, respectively.⁷⁾ High FF values require high R_p and low R_s . The sample obtained at 0.4 W exhibited lower R_p and higher R_s than those manufacture at 0.6 and 0.8 W, explaining its low FF. A large portion of silicon nanoparticles did not fuse with the substrate and remained on the surface in droplet-like configuration (Fig. 4.4a), suggesting that the number of phosphorus atoms contributing to the p–n-junction is lower than observed by SIMS and the p–n-junction was inhomogeneous. The lack of phosphorus impurities enhanced R_s . The inhomogeneity of the p–n-junction caused leak current generation and reduced R_p , contributing to the degradation of FF. On the other hand, samples obtained at 0.6 and 0.8 W presented higher FF values. Dark I–V measurements suggested that high laser energies produced appropriate p–n-junctions and the resulting samples exhibited high R_p and low R_s . Consequently, the conversion efficiency of solar cells fabricated at 0.8 W reached 7.0%, which is comparable to p–n-junctions formed by conventional thermal diffusion.

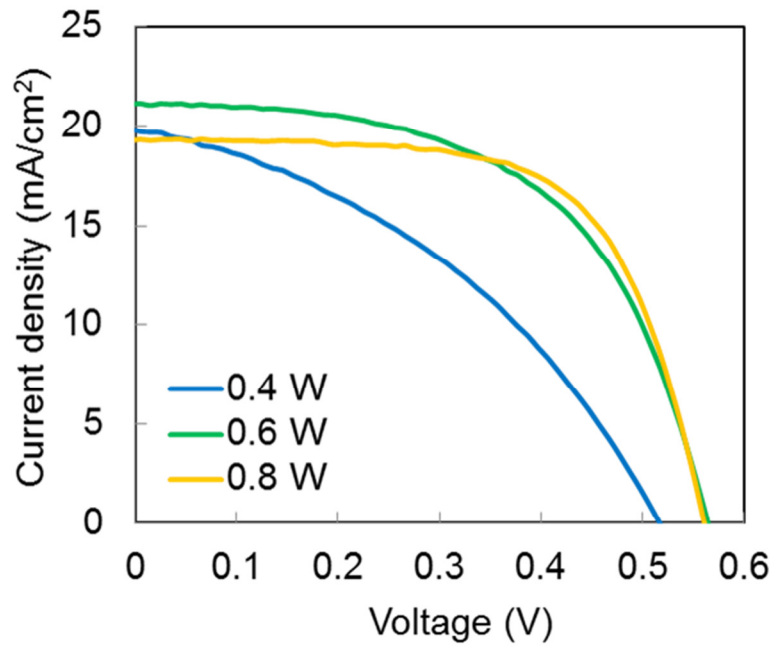


Figure 4.7 Illuminated I–V characteristics of solar cells manufactured at different laser energies

Table 4.2 Photovoltaic characteristics extracted from illuminated I–V curves shown in Fig. 4.7

Laser power	V_{oc} (mV)	J_{sc} (mA/cm ²)	FF (%)	Eff. (%)
0.4 W	518	19.7	39.5	4.0
0.6 W	568	21.1	55.7	6.7
0.8 W	568	19.3	64.2	7.0

4.4 Selective Emitter Formation by Laser Doping using Textured Substrates

Selective emitters were manufactured by LD on n-type textured c-Si substrates using a polymer-based SoD and a DPSS laser. Dopant–substrate interface, LD-processed surface structure, doping profiles, and photovoltaic characteristics were evaluated. As comparison to the sample fabricated by thermal diffusion, Dark I–V characteristics showed that the reverse saturation current decreased and illuminated I–V characteristics revealed improved V_{oc} and FF, which is consistent with the formation of selective emitters by laser irradiation. The LD process generated a homogeneous boron-doped region under the metal contacts and stopped the current leakage.

Figures 4.8 and 4.9 shows the interface adhesion between PBF and the textured substrate and an angled top view image of the textured surface after LD. The polymer-based dopant tightly adhered to the substrate and no void was observed at the interface. The polymer-coated textured surface was homogeneous and exhibited no detectable defect. The surface structure showed no marked change upon processing. In contrast, the surface structure of samples using PSG as a doping precursor changed dramatically and displayed voids after laser irradiation because of poor precursor–substrate adhesion (Fig. 3.6b). Moreover, the dopant profile became inhomogeneous because of the presence of numerous voids.

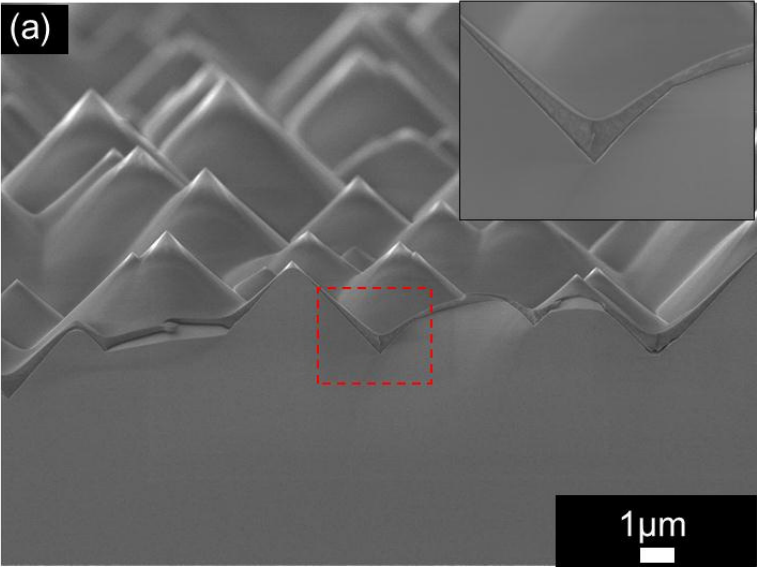


Figure 4.8 Interface adhesion between PBF and the textured substrate

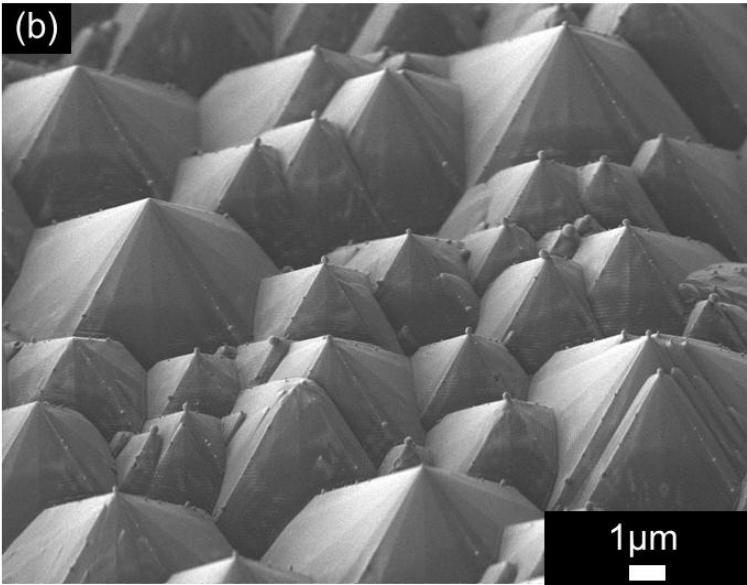


Figure 4.9 Surface morphology after LD using PBF as a dopant

When PBF acted as a dopant, the strong interface adhesion facilitated a homogeneous absorption of the laser energy by the textured surface, which melted shallowly and recrystallized by incorporating boron atoms. Consequently, boron atoms doped the substrate without damaging the textured structure, which may produce a homogeneous doping profile.

The reflectivity of doped regions formed on textured surfaces by thermal diffusion and additional LD was measured for laser outputs varying from 0.4 to 1.0 W (Fig. 4.10). The reflectivity remained low at high energy. Samples using PBF as a precursor layer exhibited significantly lower reflectivity than those using PSG (Fig. 3.8) for the same energy. The silicon present in PSG may be sintered into the substrate during the melt–recrystallization process, whereas the PBF precursor layer does not contain any silicon. Therefore, textured structures were not smoothed by melt–recrystallization during the LD procedure.

Boron doping profiles were measured by SIMS using flat substrates. Figure 4.11 compares SIMS boron profile of samples fabricated by thermal diffusion and LD at different energies. Thermal diffusion produced a specific gradient in the boron profile, which displayed a surface concentration exceeding 10^{20} atoms/cm³ at a junction depth of 600 nm. Unexpectedly, the surface boron concentration increased with increasing energy in LD-processed samples, reaching 10^{21} atoms/cm³ at the highest laser energy density. At 0.4 W, boron distribution profiles showed similar surface concentration and gradient for samples produced by LD and thermal diffusion. The laser fluence did not reach the threshold at which the c-Si substrate temperature increases to the melting point. In this study, BRL was removed

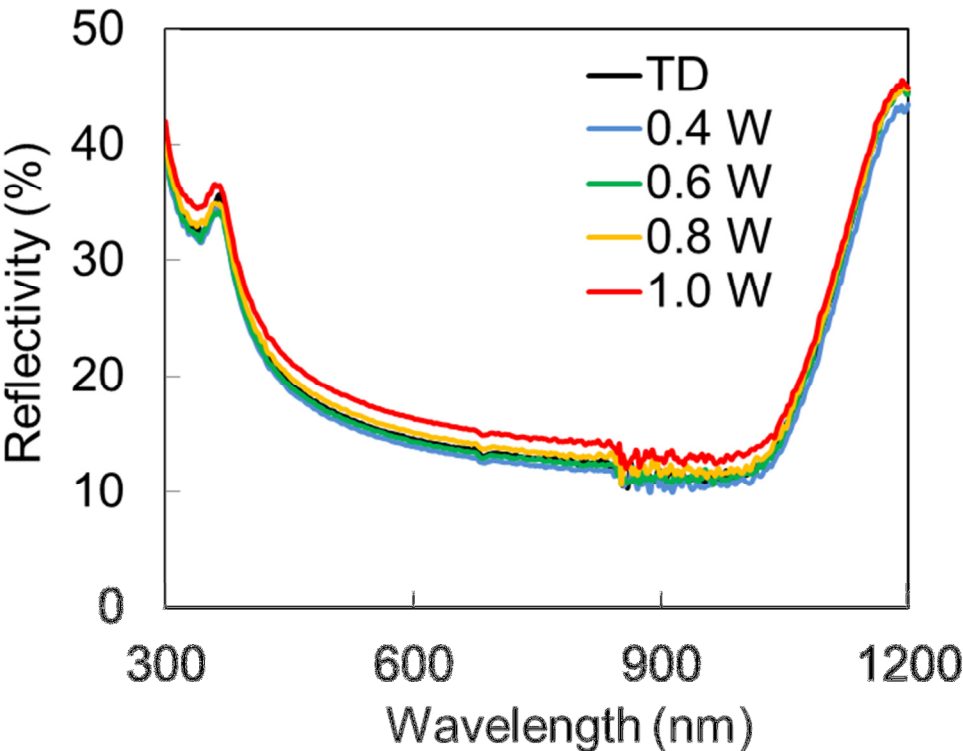


Figure 4.10 Reflectivity of doped region formed by thermal diffusion (TD) and additional LD with different laser energy

from the substrate surface by oxidation and HF cleaning before SIMS measurements. The thermally diffused area was exposed to the laser before BRL removal. Therefore, high dopant concentrations in laser doped samples were attributed to the redistribution of BRL boron atoms. While a laser pulse lasted 25 ns, surfaces underwent melt–recrystallization within 100 ns.⁸⁾ The boron diffusion coefficient is below 10^{-10} and 2.4×10^{-4} cm²/s in solid and liquid silicon, respectively.⁹⁾ The boron doping profile (Fig. 4.11) that was obtained within a short time using the diffusion coefficient of the liquid phase confirmed that LD redistributed the BRL boron atoms by liquid phase diffusion. Higher dopant concentrations reduced the series resistance while enhancing FF and conversion efficiency, as discussed for illuminated I–V characteristics.

Sheet resistances of doped regions formed by thermal diffusion and additional LD at laser energies ranging from 0.4 to 1.0 W are shown in Fig. 4.12. These resistances were measured by the four-point probe method.¹⁰⁾ At low energy, the sheet resistance was the same as after thermal diffusion because the number of boron atoms did not change from that observed after thermal diffusion. At 0.6 and 0.8 W, sheet resistances decreased from the values obtained by thermal diffusion because of LD-induced additional boron doping (Fig. 4.11). However, samples processed at 1.0 W exhibited higher sheet resistance than at 0.8 W. Sheet resistances measured by the four-point probe method strongly depend on surface features, such as crystal defects and surface roughness.¹¹⁾ High laser energies may cause substantial damage, increasing the sheet resistance.

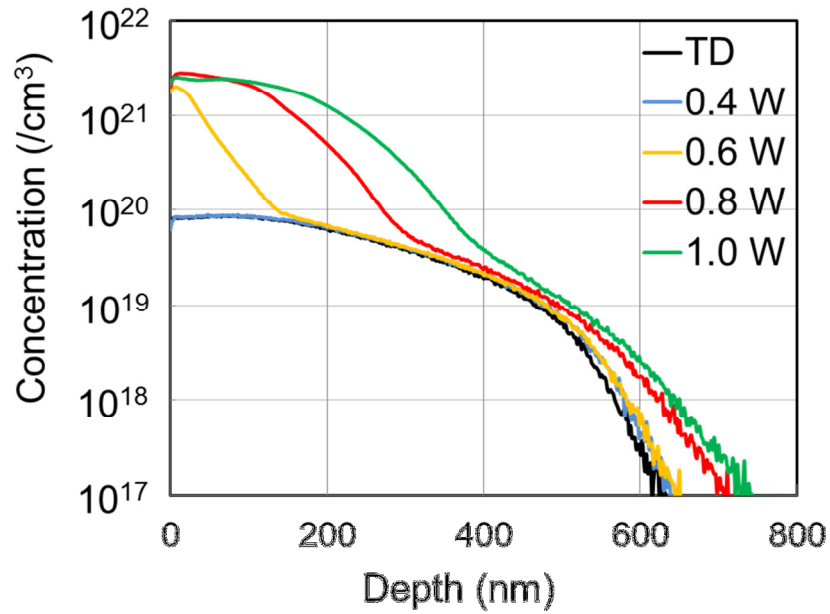


Figure 4.11 SIMS boron profiles of doped regions formed by thermal diffusion (TD) and additional LD at different energies

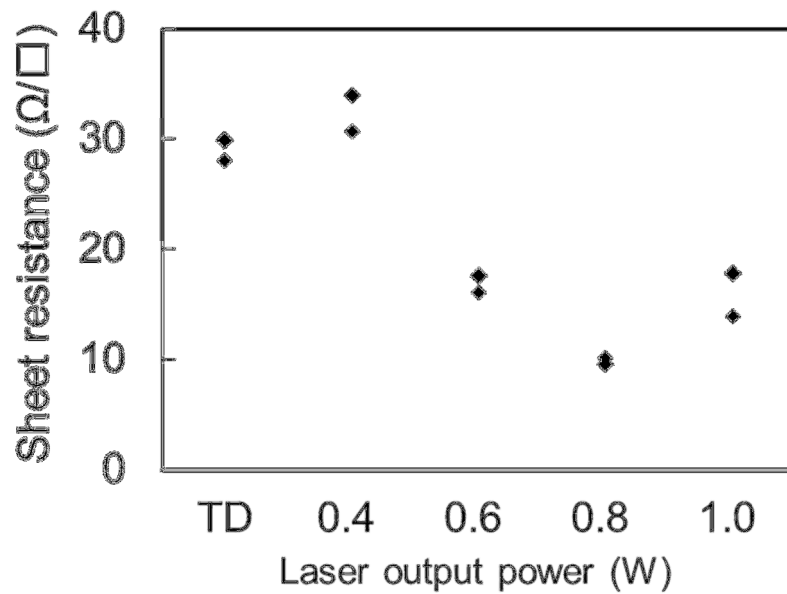


Figure 4.12 Sheet resistances of doped regions formed by thermal diffusion (TD) and additional LD at different energies

Figure 4.13 shows dark I–V curves of samples fabricated by thermal diffusion and additional LD at different energy densities. Laser irradiation reduced the saturation current under the reverse voltage at 0.6 W. It induces additional boron doping from BRL (Fig. 4.11), which may improve the homogeneity of the p–n-junction. In addition, PBF tightly adhered to the substrate (Fig. 4.8), facilitating a homogeneous absorption of the laser energy over the entire substrate surface. Diode characteristics were also evaluated by Suns–Voc measurements. Parallel resistance losses were calculated using V_{oc} and pseudo fill factor (pFF) measured by Suns–Voc.¹²⁾ The difference between the ideal fill factor (FF_0) determined from V_{oc} and pFF provides the ratio of R_p losses in the reduction of FF relative to FF_0 .¹³⁾ Figure 4.14 compares R_p losses in FF for samples fabricated by thermal diffusion and selective emitters obtained by LD at different laser power outputs. Solar cells fabricated by thermal diffusion displayed considerably high R_p losses because of the difficult formation of homogeneous boron-doped regions on textured surfaces. Additional boron-doped regions underneath metal contacts formed by LD at 0.6 W decreased the emitter leak current, suggesting that PBF induce boron doping by LD without extensive photo-damage at optimum laser power.

Illuminated I–V characteristics were measured for homogeneous emitters obtained by thermal diffusion and selective emitter formed by additional LD at different energies (Fig. 4.15). Resulting photovoltaic characteristics of best-performing samples were compared with averages acquired for all samples (Table 4.3). The selective emitter formed by LD at 0.6 W showed higher V_{oc} and FF values than its homogeneous counterpart fabricated by thermal

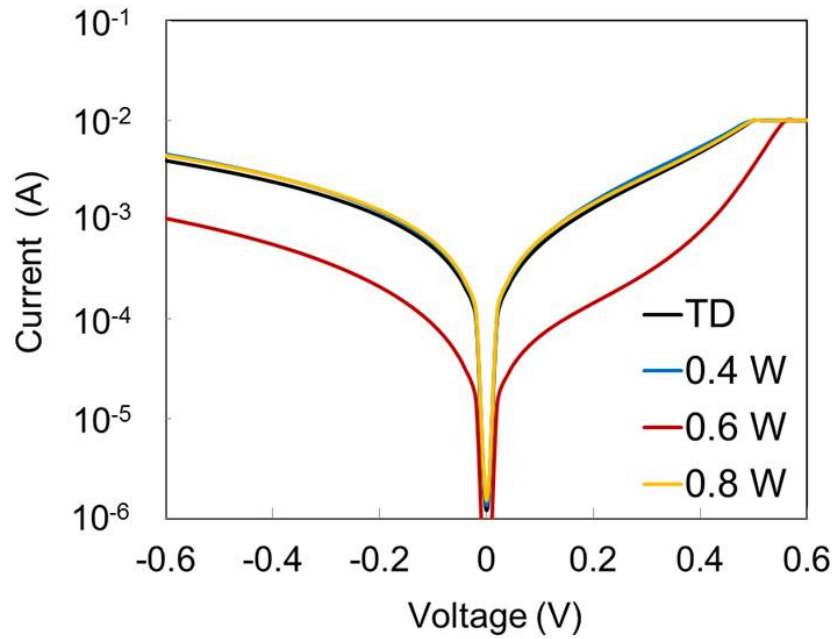


Figure 4.13 Dark I-V characteristics of homogeneous emitters formed by thermal diffusion (TD) and selective emitters processed by additional LD at different energies

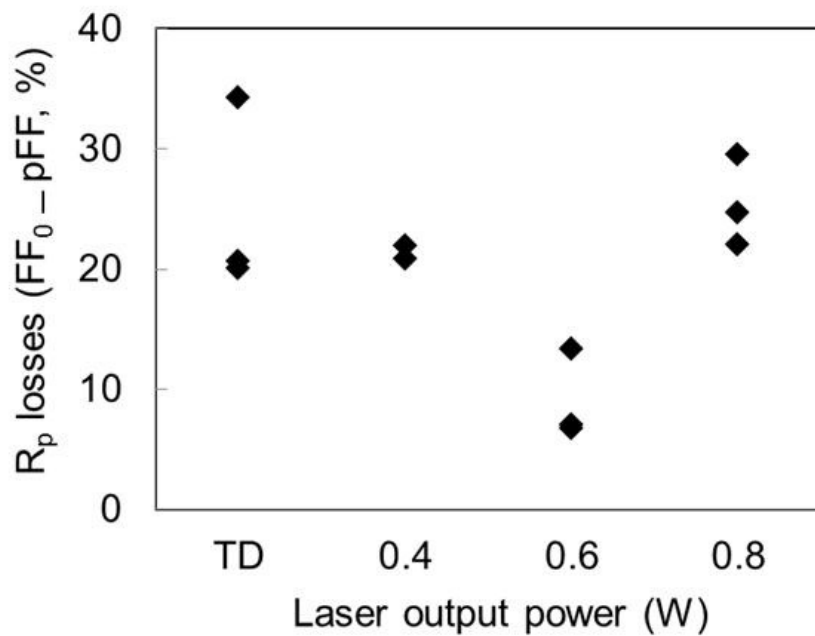


Figure 4.14 R_p losses calculated from Suns-Voc measurements of homogeneous emitters obtained by thermal diffusion (TD) and selective emitters formed by additional LD at various energies

diffusion. This V_{oc} increase originated from the reduction of reverse saturation currents in the dark I–V measurements (Fig. 4.13), while FF enhancement resulted from the reduction of series resistance and increase of shunt resistance caused by additional boron doping. Dark and illuminated I–V measurements revealed the existence of a critical optimum of laser energy value for selective emitter formation. At low energy, the number of boron atoms did not increase because of the lack of heat energy. At high energy, the laser produced severe damage on the substrates. Additional LD processing did not improve the photovoltaic characteristics of the sample fabricated by thermal diffusion only.

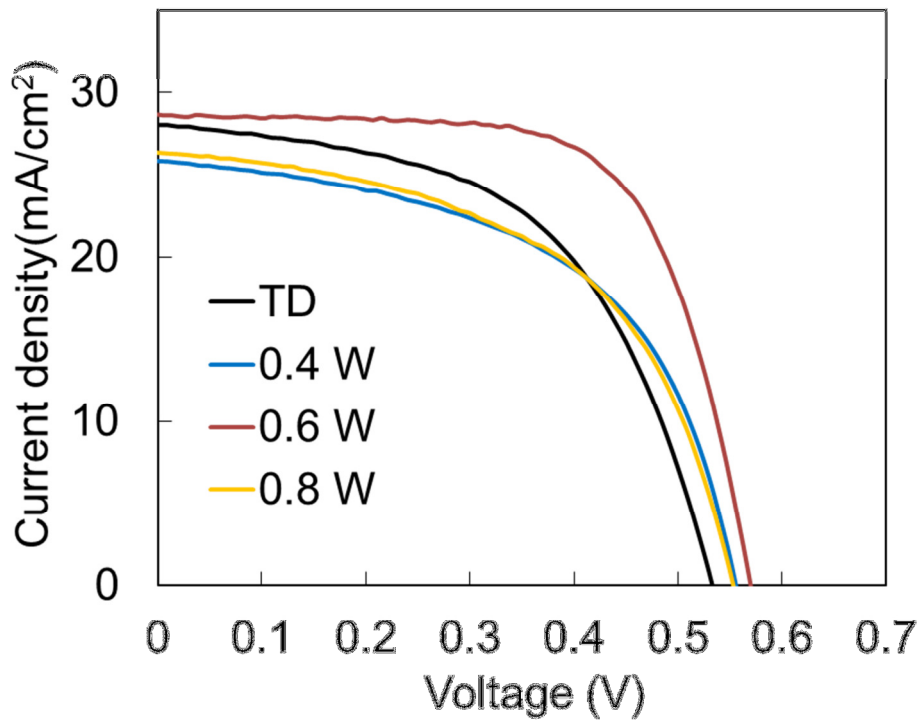


Figure 4.15 Illuminated I–V characteristics of homogeneous emitters produced by thermal diffusion (TD) and selective emitters formed by additional LD at different energies

Table 4.3 Photovoltaic characteristics extracted from illuminated I–V curves comparing best-performing samples with averages obtained for all samples

	V_{oc} (mV)	av. V_{oc} (mV)	J_{sc} (mA/cm ²)	av. J_{sc} (mA/cm ²)	FF (%)	av. FF (%)	η (%)	av. η (%)
TD	534	548	27.9	25.5	53.9	48.9	8.0	6.9
0.4 W	555	530	25.7	25.9	54.3	53.4	7.7	7.3
0.6 W	563	563	28.6	28.4	67.7	64.5	10.9	10.3
0.8 W	553	546	26.2	24.7	53.6	49.9	7.8	6.7

4.5 Summary

Local impurity doping and high-efficiency solar cell structures were achieved by LD using silicon nanoparticles and PBF as new precursor layers to achieve repeatability. Photovoltaic property evaluations exhibited high-quality results.

Silicon nanoparticles were deposited on silicon substrates as a doping precursor layer for LD. Surface structures after LD and boron doping profiles were determined along with dark and illuminated I–V characteristics. Samples formed by LD at high energy exhibited high photovoltaic characteristics. High energies enabled the nanoparticles to completely fuse with the substrates. Nanoparticles absorbed the laser energy and subsequently melted. At high energy, heat conduction from these nanoparticles also melted the substrates. Molten silicon nanoparticles and substrates mixed in the liquid phase and phosphorus impurities doped the substrate by recrystallization. Consequently, silicon nanoparticles produced high-quality p–n-junctions. A conversion efficiency of 7.0% was achieved without any additional structure, back surface field, passivation, or ARC, comparable to data obtained for p–n-junction obtained by conventional thermal processes.

Moreover, the fabrication of n-type c-Si solar cells consisting of a LD-generated selective emitter structure was addressed using PBF as SoD. PBF–substrate interface and surface topography were examined in addition to boron doping profiles and dark and

Chapter 4. Local Impurity Doping and High-Efficiency Structures using Novel Precursor Layers

illuminated I–V characteristics. Selective emitter formation at an optimum laser energy enhanced the photovoltaic characteristics of the samples. Interfaces between PBF and hydrophobic substrates adhered tightly, and surface structures mostly remained intact after LD. Additional boron doping from the laser irradiated BRL was detected by SIMS measurements. Dark I–V characteristics suggested that additional boron doping under the metal contacts reduced the reverse saturation current. LD formed homogeneous boron-doped regions on the textured surfaces. Photovoltaic characteristics of selective emitters formed at different laser energies were compared. Selective emitters formed at 0.6 W showed higher values in V_{oc} and FF than the sample without selective emitters, which represents approximately 3% improvement in solar cell efficiency.

References of Chapter 4

- 1) S. P. Phang, W. Liang, B. Wolpensinger, M. A. Kessler, and D. Macdonald: IEEE Journal of Photovoltaics **3** (2013), p. 261.
- 2) P. Würfel: Physics of Solar Cells (Wiley, Germany, 2009) 2nd ed., p. 71.
- 3) K. K. Ong, K. L. Pey, P. S. Lee, A. T. S. Wee, X. C. Wang, Y. F. Chong: Appl. Phys. Lett. **89** (2006), p. 172111.
- 4) A. Safiei, R. Bleidiessel, R. Khandelwal, T. M. Pletzer, H. Windgasse, and H. Kurz: Proc. of 26th European Photovoltaic Solar Energy Conf. (2011), p. 1229.
- 5) A. Ogane, K. Hirata, K. Horiuchi, Y. Nishihara, Y. Takahashi, A. Kitiyanan, and T. Fuyuki: Jpn. J. Appl. Phys. **48** (2009), p. 0721201.
- 6) M. A. Green: Solar Cells (Prentice-Hall, Inc., New South Wales, 1982) 1st ed., p. 145.
- 7) Y. Hamakawa: Solar Energy Engineering (Baifukan, Tokyo, 1997) 4th ed., p. 46.
- 8) G. Poulain, D. Blanc, B. Semmache, Y. Plégrin, and M. Letimi: Energy Procedia **8** (2011), p. 587.
- 9) H. Kodera: Jpn. J. Appl. Phys. **2** (1963), p. 212.
- 10) M. Yamashita, S. Yamaguchi, and H. Enjoji: Jpn. J. Appl. Phys. **27** (1988), p. 869.
- 11) K. S. Wang, B. S. Tjahjono, J. Wong, A. Uddin, and S. R. Wenham: Sol. Energy Mater. Sol. Cells **95** (2011), p. 974.
- 12) S. Bowden, V. Yelundur, and A. Rohatgi: Proc. of 29th IEEE Photovoltaic Specialist Conf.

Chapter 4. Local Impurity Doping and High-Efficiency Structures using Novel Precursor Layers

(2002), p. 371.

13) U. Jäger, F. Fertig, P. Oesterlin, A. Büchel, R. Ullmann, H. U. Zühlke, and R. Preu: Proc.

of 26th European Photovoltaic Solar Energy Conf. (2011), p. 1377.

Chapter 5

Summary and Outlook

5.1 Summary

This study applied LD to the fabrication of high-efficiency solar cell structures, such as textured surfaces and selective emitters. LD readily enables impurity doping by two-dimensional patterning in a single step at room temperature under ambient atmosphere. However, emitter properties after LD depend on substrate surface structure and doping precursor conditions. Therefore, several approaches were proposed to form high-quality doped regions.

Chapter 2 describes the investigations of the influence of surface roughness on emitter properties. Moreover, double-scan LD improved the reproducibility of homogeneously doped regions in textured substrates. Surface appearance and electric properties after LD were evaluated along with phosphorus doping profiles and I–V characteristics.

The influence of surface unevenness was determined using unpolished and flat surfaces formed by additional chemical etching. Laser doped surface appearance suggested

Chapter 5. Summary and Outlook

that surface unevenness generated voids at the PSG–substrate interface during spin coating, leading to crater-like surface defects. These defects were controlled by additional surface chemical etching, improving photovoltaic characteristics, especially V_{oc} . As expected, LD of textured surfaces produced electric defects on the surfaces. Doping homogeneity improvement and electric defect control were attempted using double-scan LD on textured surfaces. The resulting surface structure appeared smooth but covered by ARC. In addition, surface electric properties were improved, as indicated by EBIC measurements, and higher phosphorus doping concentration and depth were observed because of the enhanced doping homogeneity. Consequently, double-scan LD increased the photovoltaic characteristics (J_{sc} , V_{oc} , and FF).

In Chapter 3, the influence of PSG–substrate interface adhesion on emitter properties was investigated in LD-processed textured c-Si substrates. Interface adhesion among PSG and substrate, surface structure after LD, doping profiles, and photovoltaic characteristics were evaluated. Before spin coating, the hydrophobic substrate surface was chemically turned hydrophilic to reinforce interface adhesion. Photovoltaic characteristics were determined using a solar simulator after metallization.

The hydrophobic-to-hydrophilic change in surface wettability provided control over the interface nanostructure between doping precursors and substrates. Laser doped hydrophilic samples displayed a reduction in surface voids compared to their hydrophobic counterparts. They also exhibited a greater doping depth and a higher phosphorus

concentration by SIMS. These observations originated from the strong interface adhesion between PSG and substrates at the nanoscale. Hydrophilic samples showed higher V_{oc} and J_{sc} than their hydrophobic equivalents. Overall, interface structure control at the nanoscale influences electric properties in laser-doped regions to a great extent.

In Chapter 4, the LD process was conducted using a silicon nanoparticle and PBF as doping precursor layers for the first time. Locally doping was also applied to manufacture high-efficiency solar cell structures such as selective emitters. The doping precursor–substrate interface adhesion may be ignored when silicon nanoparticles act as doping precursors because nanoparticles absorb laser energy directly and melt. On the other hand, it may be improved using organic polymer-based doping precursors such as PBF. Strong interface adhesion may result in the homogeneous introduction of impurities and high-quality doping. Therefore, PBF was exploited for the fabrication of selective emitter solar cells.

When silicon nanoparticles were deposited as a doping precursor layer in the LD process, they absorbed the laser energy and melted. Heat conduction from these nanoparticles also melted the substrates at high laser energy. Molten nanoparticles and substrates fused in the liquid phase and phosphorus impurities doped the substrates by recrystallization. Consequently, silicon nanoparticles provided high-quality p–n-junctions. A conversion efficiency of 7.0% was achieved, comparable to that of p–n-junctions manufactured by conventional thermal processes.

Next, n-type c-Si solar cells presenting a selective emitter structure were fabricated

Chapter 5. Summary and Outlook

by LD using PBF as SoD. Photovoltaic characteristics improved when selective emitters were formed at optimum laser energy. The dopant tightly adhered to hydrophobic substrates, and surface structures remained almost intact after LD. Laser irradiation induced additional boron doping from BRL, as shown by SIMS measurements. Dark I–V characteristics suggested that additional boron doping under the metal contacts reduced the reverse saturation current. LD provided homogeneous boron-doped regions on the textured surface. The selective emitter formed by LD at 0.6 W showed increased V_{oc} and FF values, which corresponds to approximately 3% improvement in solar cell efficiency.

5.2 Outlook

The application of LD to industrial c-Si solar cell fabrication processes hinges on further research as described below.

1. Laser irradiation conditions, such as laser pulse duration and number irradiating the c-Si substrate surface, require more precise optimization in order to fabricate high-quality p–n-junction and achieve reproducibility. In this thesis, the irradiation was performed using nanosecond pulses but shorter pulses of the order of picosecond or femtosecond may be used. Peak laser power is inversely proportional to pulse duration. Therefore, the peak power-dependent melt–recrystallization process needs to be investigated using various pulse durations.
2. A spatially controlled laser is necessary to optimize the doping profile for textured surface LD. This study was conducted using a Gaussian-profile laser. However, laser irradiation conditions were not fully optimized because of the textured surface. The top-hat laser, which provides a spot exhibiting a homogeneous energy density, may enable a more precise laser condition optimization on textured surfaces.
3. In this thesis, all doping precursors were formed by the cost-effective and high-throughput spin-coating method. However, all precursor materials required organic solvents as

Chapter 5. Summary and Outlook

dispersants. Therefore, organic contamination of the precursor layer may occur. Several vacuum processes, such as chemical vapor deposition, produce amorphous silicon (a-Si) exclusively comprising phosphorus or boron dopant without any contamination. The influence of contamination in SoD sources may be evaluated by comparison with a-Si.

4. Microscale optical analysis is necessary to further understand the LD processing of textured surfaces. The laser spot diameter ranges from 10 to 50 μm . A typical textured surface called random pyramid structure consists of micron-sized pyramids. Therefore, the laser spot spreads over several pyramids in one pulse, and the energy absorbed by the substrate may differ at each part of pyramid. This absorption needs to be analyzed by optical simulation.
5. Cost reduction is a critical issue in industry. Many studies have addressed the low-cost production of substrates, such as solar-grade, monocrystalline-like, and high-performance multicrystalline silicon. However, low-cost processes cannot avoid contamination by impurities, such as metal precipitation from casting molds. The influence of impurities, except dopants, needs to be investigated for the application of LD to low-cost substrates.
6. In situ observation is necessary to understand the laser-induced melt–recrystallization process. The LD process generally comprises epitaxial growth during recrystallization. However, such a growth requires LD processing of a smooth surface using an ultraviolet

pulse laser. Industrial application involves various laser conditions (such as CW laser and longer wavelength) and textured surfaces. Therefore, the melt–recrystallization process must be analyzed under various conditions by in situ observation using instruments, such as an ultra-high-speed camera.

7. High-efficiency structures, such as PERL cells, are expected to benefit from the ability of LD to easily form locally doped regions in a single step. The application of LD to PERL cells rely on the analysis of minority carrier lifetime after surface passivation. Therefore, passivation layer deposition and laser irradiation need to be optimized. The quasi-steady-state photoconductance decay approach can evaluate minority carrier lifetime and facilitate condition optimization.

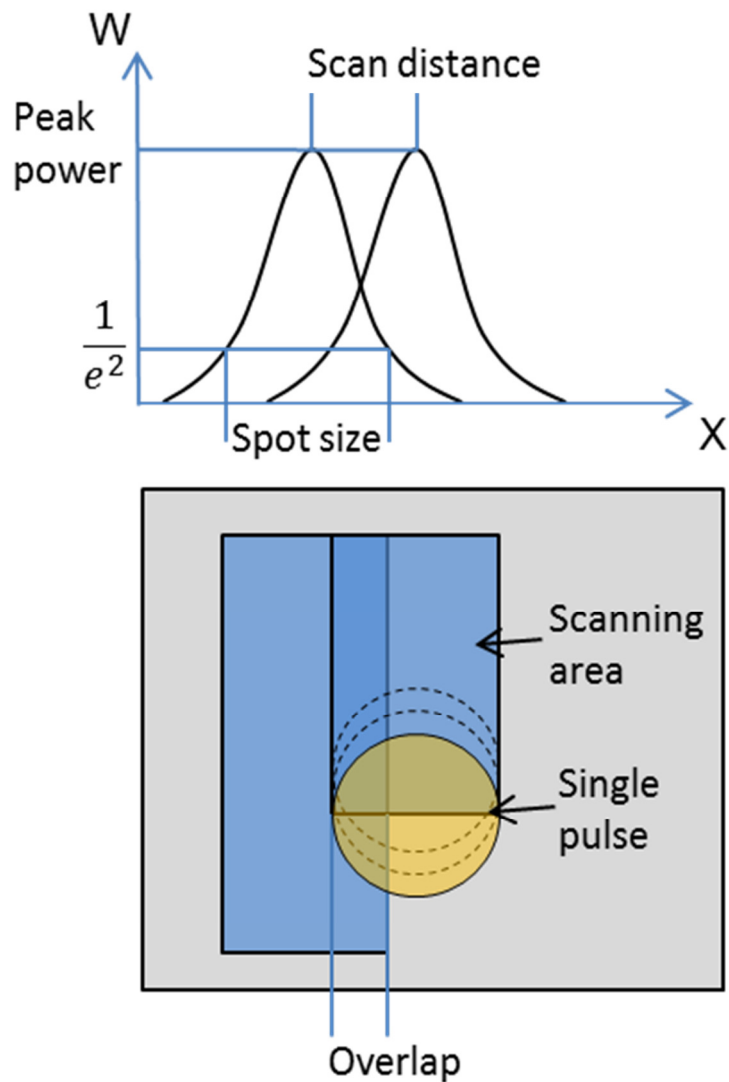
Appendix A

Influence of Gaussian Profile to Inhomogeneity of Doping

It is expected that the special Gaussian intensity beam profile which leads to an inhomogeneous intensity distribution on the substrate¹⁾ forms inhomogeneous doping profile²⁾. Thus, influence of overlap rate between laser-scans to solar cell efficiency fabricated by LD using the laser with Gaussian beam was discussed in this section. The overlap rate can be calculated as shown in Fig. A.1. As depicted in Fig. A.1, in the case of Gaussian beam, the low overlap rate leads to lower the energy at near the edge of laser scan. The enough energy needed for melt-recrystallization process is not given to substrate at the edge of laser scan. LD was conducted with different overlap rates and solar cell efficiencies were evaluated. Fig. A.2 shows solar cell efficiencies compared with the samples fabricated by LD with different overlap rates. The tendency of efficiency shown in Fig. A.2 revealed that efficiency was getting lower with overlap rate under 20 % of overlap rate but it shows constant value in efficiency over 20 % of overlap rate. In the LD with fewer than 20% of overlap rate, inadequate regions of impurity doping might appear at the edge of laser scan. The reason of the constant value of efficiency of the samples with over 20 % of overlap rate is contemplated that the homogeneous doping profile needed for the fabrication of solar cell was formed by

Appendix A: Influence of Gaussian Profile to Inhomogeneity of Doping

LD with 20 % of overlap rate. It also would appear that increase of the number of laser pulse with overlap rate did not aggravate emitter quality after LD. In this thesis, overlap rates are 37.5 % and it can be considered adequate value for the resolution of inhomogeneity of impurity doping caused by Gaussian beam profile.



$$\text{Overlap rate} = \frac{\text{spot size} - \text{scan distance}}{\text{spot size}} \times 100 (\%)$$

Figure A.1 Schematic viewing of calculation of overlap rate

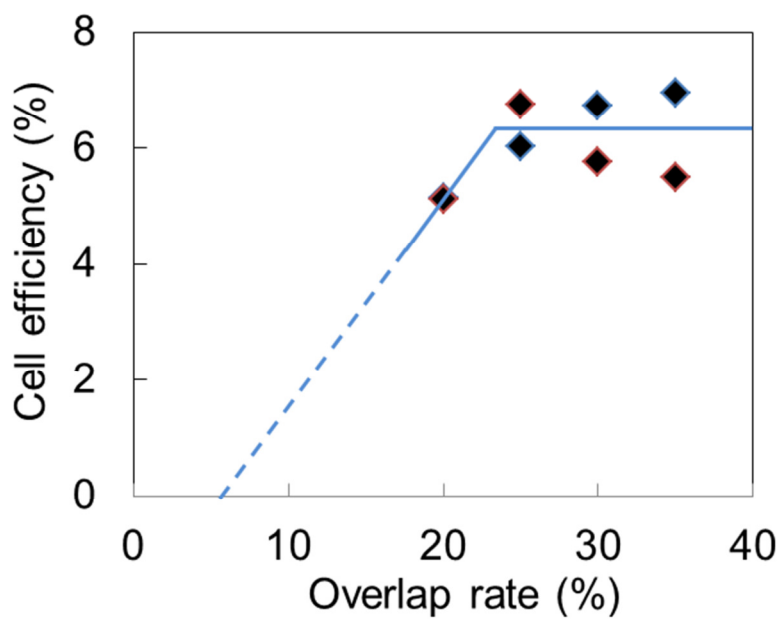


Figure A.2 Solar cell efficiency of the samples with different overlap rate

References of Appendix A.

- 1) U. Jäger, P. Oesterlin, A. Kimmerle, and R. Preu: Proc.35th IEEE PVSC, 2010, p1401.
- 2) S. Tanaka, Master thesis, Nara Institute of Science and Technology (in Japanese)

List of Publications

Academic journals

- [1] “IMPROVED ELECTRONIC PROPERTIES OF LASER DOPED EMITTERS BY REDUCING SURFACE ROUGHNESS”

Hideki Nishimura, Kenji Hirata, Mitsuhiro Hasegawa, Takuya Katagiri, and Takashi Fuyuki

Japanese Journal of Applied Physics, Vol. 51, 10NA15 (2012)

- [2] “Surface Polarity Control to Reinforce Dopant Adhesion in Laser Doping for Textured Silicon”

Hideki Nishimura, Takanori Okamura, Yuki Yamamoto, and Takashi Fuyuki

Japanese Journal of Applied Physics, Vol. 53, 056501 (2014)

International conferences

- [1] “Improvement of multi-crystalline silicon solar cell fabricated by Laser Doping Technique Using Continuous Wave Laser”

List of Publications

Hideki Nishimura, Kenji Hirata, Mitsuhiro Hasegawa, Tomohiro Funatani, Tamaki Takayama, and Takashi Fuyuki

37th IEEE Photovoltaic Specialist Conference, (Seattle, USA), 2011

- [2] “IMPROVED ELECTRONIC PROPERTIES OF LASER DOPED EMITTERS BY REDUCING SURFACE ROUGHNESS”

Hideki Nishimura, Kenji Hirata, Mitsuhiro Hasegawa, Takuya Katagiri and Takashi Fuyuki

21st International Photovoltaic Science and Engineering Conference, (Fukuoka, Japan), 2011

- [3] “IMPROVED ELECTRONIC PROPERTIES OF LASER DOPED EMITTERS BY REDUCING SURFACE ROUGHNESS”

Hideki Nishimura, Kenji Hirata, Mitsuhiro Hasegawa, Takuya Katagiri and Takashi Fuyuki

International Photovoltaic Young Scientist Symposium, (Nara, Japan), 2011

- [4] “SPATIAL HOMOGENIZATION OF THE DOPANT PROFILE USING DOUBLE SCAN LASER DOPING FOR TEXTURED MONO-CRYSTALLINE SILICON SOLAR CELL”

Hideki Nishimura, Kenji Hirata, Emi Sugimura, and Takashi Fuyuki

27th European Photovoltaic Solar Energy Conference and Exhibition, (Frankfurt, Germany), 2012

- [5] “Reduction of Minority Carrier Defects by Surface Homogenization Using Double Scan Laser Doping for Textured mc-Si Solar Cell”

Hideki Nishimura, Kenji Hirata, Emi Sugimura, and Takashi Fuyuki

2012 GIST-NAIST-NCTU Joint Symposium on Interdisciplinary Nanoscience and Beyond, (Hsinchu, Taiwan), 2012

- [6] “Improvement of the Emitter properties by Controlling the Interface Between Dopant and Substrate in Laser Doping for Textured Silicon”

Hideki Nishimura, Shigeaki Tanaka, Shota Morisaki, Shingo Yumoto, and Takashi Fuyuki

39th IEEE Photovoltaic Specialist Conference, (Tampa, USA), 2013

- [7] “POLARITY CONTROL TO REINFORCE INTERFACES BETWEEN DOPANT AND SI TEXTURED SURFACES FOR JUNCTION IMPROVEMENT IN LASER DOPING”

Hideki Nishimura, Shigeaki Tanaka, Emi Sugimura, and Takashi Fuyuki

28th European Photovoltaic Solar Energy Conference and Exhibition, (Paris, France), 2013

List of Publications

- [8] “Boron Laser Doping for n-type Si Back Contact Silicon Solar Cell”

Hideki Nishimura, Takanori Okamura, Yuki Yamamoto, and Takashi Fuyuki

2013 GIST-NAIST-NCTU International Joint Symposium on Innovative Materials for Future Technology, (Nara, Japan), 2013

- [9] “REDUCTION OF EMITTER LEAK CURRENT BY SELECTIVE BORON LASER DOPING FOR TEXTURED CRYSTALLINE SILICON SOLAR CELL”

Hideki Nishimura, Mitsuaki Manabe, and Takashi Fuyuki

The 29th European Photovoltaic Solar Energy Conference and Exhibition, (Amsterdam, Netherlands), 2014

- [10] “Boron Laser Doping Using Spin-on Dopant for Textured Crystalline Silicon”

Hideki Nishimura, Mitsuaki Manabe, Yoshifumi Kudamatsu and Takashi Fuyuki

The 6th World Conference Photovoltaic Energy Conversion, (Kyoto, Japan), 2014

Domestic conferences

- [1] “Laser doping process in multi-crystalline silicon solar cells”

Hideki Nishimura, Kenji Hirata, Mitsuhiro Hasegawa, Tomohiro Funatani, Tamaki

Takayama, and Takashi Fuyuki

Abstracts of the 58th Spring Meeting of the Japan Society of Applied Physics and Related Societies, (Kanagawa), 2011 in Japanese

- [2] “Correlation between Surface Roughness and Electrical Properties of Laser Doped Emitter in Multicrystalline Silicon Solar Cells”

Hideki Nishimura, Kenji Hirata, Mitsuhiro Hasegawa, Takuya Katagiri, and Takashi Fuyuki

Abstracts of 8th Next Generation Photovoltaic System Symposium, (Gifu), 2011 in Japanese

- [3] “Improvement of emitter properties by control of surface roughness in laser doping process”

Hideki Nishimura, Kenji Hirata, Mitsuhiro Hasegawa, Takuya Katagiri, and Takashi Fuyuki

Abstracts of the 59th Spring Meeting of the Japan Society of Applied Physics and Related Societies, (Tokyo), 2012 in Japanese

- [4] “Improvement of surface formation by double scan laser doping for textured crystalline silicon”

List of Publications

Hideki Nishimura, Kenji Hirata, Emi Sugimura, and Takashi Fuyuki

Abstracts of 9th Next Generation Photovoltaic System Symposium, (Kyoto), 2012 in

Japanese

- [5] “Improvement of the Electronic States by Controlling the Interface Between Dopant and Substrate in Laser Doping for Textured Silicon”

Hideki Nishimura, Shigeaki Tanaka, Shota Morisaki, Shingo Yumoto, and Takashi Fuyuki

Proceedings of IEICE SDM, (Kyoto), 2012 in Japanese

- [6] “Polarity Chemical Control of Si surface for Improvement of p-n Junction properties fabricated by Laser Doping”

Hideki Nishimura, Takanori Okamura, Yuki Yamamoto, and Takashi Fuyuki

Abstracts of 2013 Second Meeting of Kansai department of the Japan Society of Applied Physics, (Ikoma), 2013 in Japanese

- [7] “Formation of Selective by Laser Doping for Crystalline Silicon Solar Cell using n-type textured substrates”

Hideki Nishimura, Mitsuaki Manabe, Yoshifumi Kudamatsu and Takashi Fuyuki

Abstracts of 11th Next Generation Photovoltaic System Symposium, (Miyazaki), 2014 in Japanese

Related academic journals

[1] “High-Precision Transfer-Printing and Integration of Vertically Oriented Semiconductor

Arrays for Flexible Device Fabrication”

Mark Triplett, Hideki Nishimura, Matthew Ombaba, V.J. Logeeswarren, Matthew Yee,

Kazim G. Polat, Jin Y. Oh, Takashi Fuyuki, François Léonard, and M. Saif Islam

Nano Research, DOI 10.1007/s12274-014-0462-7 (2014)

Related international conferences

[1] “Investigation of Precursor Layer for Laser Doping Technique in Crystalline Silicon Solar

Cell”

Takuya Katagiri, Tomohiro Funatani, Kenji Hirata, Hideki Nishimura and Takashi Fuyuki

The 26th European Photovoltaic Solar Energy Conference and Exhibition, (Hamburg,

Germany), 2011

[2] “Prescription of Precursor film Deposition for Laser Doping in Crystalline Silicon Solar

Cell Process”

Takuya Katagiri, Tomohiro Funatani, Kenji Hirata, Hideki Nishimura and Takashi Fuyuki

List of Publications

21st International Photovoltaic Science and Engineering Conference, (Fukuoka, Japan),
2011

- [3] “OPTIMIZATION OF SELECTIVE EMITTER PROFILES BY LASER DOPING IN
CRYSTALLINE SILICON SOLAR CELLS”

Kenji Hirata, Hideki Nishimura, Takuya Katagiri, Sohichiroh Takamoto, Emi Sugimura,
and Takashi Fuyuki

21st International Photovoltaic Science and Engineering Conference, (Fukuoka, Japan),
2011

- [4] “Prescription of Precursor film Deposition for Laser Doping in Crystalline Silicon Solar
Cell Process”

Takuya Katagiri, Tomohiro Funatani, Kenji Hirata, Hideki Nishimura and Takashi Fuyuki

International Photovoltaic Young Scientist Symposium, (Nara, Japan), 2011

- [5] “Fabrication of N-type Mono Crystalline Silicon Solar Cells under Optimal Conditions of
P-type Solar Cells”

Shota Morisaki, Kenji Hirata, Takuya Katagiri, Hideki Nishimura, Shigeaki Tanaka and
Takashi Fuyuki

International Photovoltaic Young Scientist Symposium, (Ikoma, Japan), 2011

[6] “Depth Controlled Laser Doping Using Silicon Nano Ink for Novel Crystalline Silicon Cell Structures”

Takanori Okamura, Hideki Nishimura, Takashi Fuyuki, Yuka Tomizawa, and Yoshinori Ikeda

The 28th European Photovoltaic Solar Energy Conference and Exhibition, (Paris, France), 2013

[7] “LASER CHEMICAL PROCESSING (LCP) DOPING FORMED THROUGH DIFFERENT DIELECTRIC LAYERS”

Xinbo Yang, Andreas Fell, Lujia Xu, Evan Franklin, Sachin Surve, Daniel Macdonald, Klaus Weber, Hideki Nishimura, and Takashi Fuyuki

The 28th European Photovoltaic Solar Energy Conference and Exhibition, (Paris, France), 2013

[8] “BOX PROFILING OF BORON BY LASER DOPING WITH SILICON NANO INK”

Mitsuaki Manabe, Takanori Okamura, Hideki Nishimura, Yuka Tomizawa, Yoshinori Ikeda, and Takashi Fuyuki

The 29th European Photovoltaic Solar Energy Conference and Exhibition, (Amsterdam, Netherlands), 2014

List of Publications

- [9] “Room Temperature Boron Doping Using UV Pulse Laser with Boron-doped Silicon Nano Ink”

Mitsuaki Manabe, Hideki Nishimura, Yuka Tomizawa, Yoshinori Ikeda, and Takashi Fuyuki

The 6th World Conference Photovoltaic Energy Conversion, (Kyoto, Japan), 2014

Related domestic conferences

- [1] “Development of Laser Doping for Crystalline Silicon Solar Cell Process”

Kenji Hirata, Tamaki Takayama, Mitsuhiro Hasegawa, Tomohiro Funatani, Hideki Nishimura, and Takashi Fuyuki

Abstracts of the 58th Spring Meeting of the Japan Society of Applied Physics and Related Societies, (Kanagawa), 2011 in Japanese

- [2] “Formation and Optimization of Selective Emitter Structure by Laser Doping in Crystalline Silicon Solar Cells”

Kenji Hirata, Tamaki Takayama, Hideki Nishimura, Takuya Katagiri, Sohichiroh Takamoto, Emi Sugimura, and Takashi Fuyuki

Abstracts of 8th Next Generation Photovoltaic System Symposium, (Gifu), 2011

in Japanese

- [3] “Influence of Phosphorus Concentration in PSG Layer in Laser Doping for Crystalline Silicon Solar Cells”

Takuya Katagiri, Tomohiro Funatani, Kenji Hirata, Hideki Nishimura and Takashi Fuyuki

Abstracts of 8th Next Generation Photovoltaic System Symposium, (Gifu), 2011

in Japanese

- [4] “Boron Laser Doping in n-type crystalline Silicon”

Shota Morisaki, Kenji Hirata, Hideki Nishimura, Takuya Katagiri, Shigeaki Tanaka and

Takashi Fuyuki

Abstracts of 9th Next Generation Photovoltaic System Symposium, (Kyoto), 2012 in

Japanese

- [5] “Optimization of Selective Emitter Fabricated by Laser Doping”

Shingo Yumoto, Kenji Hirata, Emi Sugimura, Hideki Nishimura, and Takashi Fuyuki

Abstracts of 9th Next Generation Photovoltaic System Symposium, (Kyoto), 2012 in

Japanese

- [6] “Analysis of Laser Doping Changing Over Rap Rate in Beam Scanning”

List of Publications

Shigeaki Tanaka, Hideki Nishimura, and Takashi Fuyuki

Abstracts of 9th Next Generation Photovoltaic System Symposium, (Kyoto), 2012 in

Japanese

- [7] “Fabrication of High Efficiency n-type Crystalline Silicon Solar Cell using Laser Doping Technique”

Shota Morisaki, Hideki Nishimura, Emi Sugimura, and Takashi Fuyuki_

Proceedings of IEICE SDM, (Kyoto), 2012 in Japanese

- [8] “Optimization of Crystalline Silicon Solar Cell with Selective Emitter Formed by CW Laser”

Shingo Yumoto, Kenji Hirata, Emi Sugimura, Hideki Nishimura, and Takashi Fuyuki

Proceedings of IEICE SDM, (Kyoto), 2012 in Japanese

- [9] “Control of Depth of Emitter and Selective Emitter Formed by Laser Doping and Photovoltaic Characteristics”

Shigeaki Tanaka, Hideki Nishimura, and Takashi Fuyuki_

Proceedings of IEICE SDM, (Kyoto), 2012 in Japanese

- [10] “Fabrication of Crystalline Silicon Solar Cell by Laser Doping using Silicon Nano Ink”

Takanori Okamura, Hideki Nishimura, Takashi Fuyuki, Yuka Tomizawa, and Yoshinori

Ikeda

Abstracts of 10th Next Generation Photovoltaic System Symposium, (Ishikawa), 2013 in

Japanese

- [11] “Fabrication of Solar Cell by Laser Doping Using Silicon Nano-Ink as Doping Precursor”

Takanori Okamura, Hideki Nishimura, Takashi Fuyuki, Yuka Tomizawa, and Yoshinori

Ikeda

Abstracts of 2013 Second Meeting of Kansai department of the Japan Society of Applied

Physics, (Ikoma), 2013 in Japanese

- [12] “Fabrication of n-type Crystalline Silicon Solar Cell by Boron Doping using Laser Process”

Yuki Yamamoto, Hideki Nishimura, Takanori Okamura, Keigo Fukunaga, and Takashi

Fuyuki

Proceedings of IEICE SDM, (Ikoma), 2013 in Japanese

- [13] “Fabrication of Crystalline Silicon Solar Cell by Laser Doping using Phosphorus Doped Silicon Nano-Ink”

List of Publications

Takanori Okamura, Hideki Nishimura, Takashi Fuyuki, Yuka Tomizawa, and Yoshinori Ikeda

Proceedings of IEICE SDM, (Ikoma), 2013 in Japanese

[14] “Fabrication of n-type Silicon Solar Cell using Boron Doped Silicon Nano-Ink for Laser Doping”

Mitsuaki Manabe, Hideki Nishimura, Yuka Tomizawa, Yoshinori Ikeda, and Takashi Fuyuki

Abstracts of 10th Next Generation Photovoltaic System Symposium, (Miyazaki), 2014 in Japanese

[15] “Fabrication of Silicon Solar Cell by Pulsed Laser Doping using Silicon Nano-ink”

Mitsuaki Manabe, Hideki Nishimura, Yuka Tomizawa, Yoshinori Ikeda, and Takashi Fuyuki

Abstracts of the 75th Fall Meeting of the Japan Society of Applied Physics, (Sapporo), 2014 in Japanese

[16] “Application of Laser Doping using Boron Doped Silicon Nano-Ink to High Efficiency Silicon Solar Cell”

Mitsuaki Manabe, Hideki Sakagawa, Hideki Nishimura, Yuka Tomizawa, Yoshinori Ikeda,

and Takashi Fuyuki

Proceedings of IEICE SDM, (Kyoto), 2014 in Japanese

About the Author

Personal Data

Name: Hideki Nishimura

Data of birth: June 20th in 1986, Innoshima city in Hiroshima prefecture, Japan

Nationality: Japan

E-mail: n-hideki@ms.naist.jp

Education

2006-2010 Bachelor course study at Department of Electric and Electronic Engineering Science, Faculty of Science and Engineering, Kinki University
Bachelor thesis on *Development of $Bi_{2-x}Sb_xTe_3$ thermoelectric devices*

2010-2012 Master course study at Graduate school of Materials Science in Nara Institute of Science and Technology (NAIST)
Master thesis on *Surface Chemical Modification and Evaluation in Laser Doping at Room Temperature for Fabrication of Crystalline Silicon Solar Cell*

2012-2015 Doctor course study at Graduate School of Materials Science in Nara Institute of Science and Technology (NAIST)
Ph. D. thesis on *Development of Laser Doping Process at Room Temperature for High Efficiency Crystalline Silicon Solar Cell Fabrication*

2013 Overseas study at Integrated Nanodevices and Nanosystems Research (iNano),
University of California Davis, USA

Research Interests

- Engineering of solar cell fabrication process and strategy aimed at high efficiency
- Laser processing for micro and nano device fabrication focused on solar cell
- Physical analysis of semiconductor material and device characteristics

Language

Japanese, English

Financial Support Acquirement

- Exemption from returning of scholarship during master course from Japan Student Services Organization (2010-2012)
- Exemption from returning of scholarship during doctor course from Japan Student Services Organization (2012-2015)
- International research activity support by Foundation of Nara Institute of Science and Technology (2013)
- Competitive research support by Graduate school GP program (2011), (2012), (2013), (2014)